

TOYOTA Technical Review

2022/3 237

SPECIAL FEATURE

Toyota's initiatives for building a society through sports in which everyone can participate in peace and equality, and for realizing a sustainable society through mobility



Cover design:

The special feature of this issue of the *Toyota Technical Review* focuses on the mobility solutions and robots (mobility groups) developed by Toyota to support the running of the Olympic and Paralympic Games Tokyo 2020.

The cover shows a mosaic of images depicting possible usage scenarios for these mobility groups. In addition to expressing the diversity of freedom of movement, this mosaic and the prominent use of the word “sustainability” symbolize Toyota’s desire to help realize a sustainable society through mobility.

Accessible People Mover (APM): developed for the Paralympic Village of the Tokyo 2020 Paralympic Games. The photo shows an artist’s impression of the APM in use.

Tokyo 2020 Mascot Robots: jointly developed with the Tokyo 2020 Organising Committee.

Contents

Preface

- Transforming Our Home Planet
Hiroaki Okuchi, Fellow, Advanced R&D and Engineering Company 2

▷ Special Feature: Toyota's initiatives for building a society through sports in which everyone can participate in peace and equality, and for realizing a sustainable society through mobility

- Field Operational Tests of Automated Driving Using the Sora Fuel Cell Electric Bus
Takuya Kagawa 4
- Development of the Accessible People Mover (APM)
Hiroyuki Kato/Akihiro Yanaka/Masashi Otoyoy 9
- Development of Walking Area Electric Vehicles
Masashi Yamada/Akihiro Yanaka/Makoto Mori/Yoshiyuki Senba 14
- The Toyota LQ
Daisuke Ido/Tatsuya Takei/Yoichi Iwata/Shogo Sekizawa/Satoshi Nakagawa 19
- Support for Spectators in Wheelchairs at the Olympic and Paralympic Games Tokyo 2020 Using Human Support Robots (HSRs)
Takahiro Toda/Kazuhito Tanaka/Yuka Iwanaga/Keisuke Takeshita/Yuji Onuma/Takemitsu Mori 25
- Development of the T-TR2 Telepresence Robot
Takahiro Nakayama/Yusuke Kida 30
- Development of Field Support Robot (FSR)
Takeshi Kuwabara/Satsuki Yamane/Takeshi Shigemoto 34
- Development of Tokyo 2020 Mascot Robots
Tomohisa Moridaira/Hirohito Hattori/Masahiro Doi/Hiroyuki Iyama/Hiroyuki Kondo/Kazuya Yamamoto 41
- Development of the CUE5 AI Basketball Robot
Takayoshi Tsujimoto/Masazumi Yagi/Ryo Takizawa/Masahiro Doi/Tetsushi Harada/Yuya Yasui/Hikaru Sano 48

▷ Technical Papers/Technical Articles

- Development of Peer-to-Peer Energy Trading System Including Plug-in Hybrid Electric Vehicles
Kazuki Obata/Yuki Kudo/Satoshi Kikuchi/Hiromitsu Kigure/Kazutaka Kimura 55
- The TRI Approach to Advanced Automated Driving in Complex Urban Environments
Ryan Eustice/Wolfram Burgard/John J. Leonard/Ryan W. Wolcott/Robert Zidek/Gill Pratt 62

▷ Technical Award News 70

Transforming Our Home Planet

H. Okuchi

**Hiroaki Okuchi,
Fellow, Advanced R&D and Engineering Company**



Due to the global coronavirus pandemic, the Olympic and Paralympic Games Tokyo 2020 was the first Games in history to be postponed for a year and was held mostly without spectators. After everything that has happened, I wonder how many people know the reasons given by Akio Toyoda, the president of Toyota, in 2015 for deciding to become a worldwide partner.

We became a worldwide partner because we shared the concept and values of the Olympic and Paralympic Games, namely to challenge our limits and realize a more inclusive society. Our aim was to help build a society through sports in which everyone can participate in peace and equality, and to help realize a sustainable society through mobility.

In particular, we believe that mobility goes beyond cars. Mobility is about overcoming challenges and making dreams come true, something that might be possible if we can realize mobility for everyone in society.

Therefore, rather than being a sponsor responsible simply for providing vehicles, as has been the case in previous games, we actively took on the challenge of providing a comprehensive mobility solution for the Games as the first ever worldwide mobility partner.

This comprehensive mobility solution was built from three pillars that express the essence of our sustainable development goals (SDGs): sustainability, mobility for all, and the Toyota Production System (TPS). We developed and deployed a whole range of advanced technologies at the Tokyo 2020 Games based on these pillars.

For sustainability, we provided a whole fleet of hydrogen-powered mobility for the Games, including operational vehicles such as buses and forklifts, in addition to passenger vehicles. As well as helping to realize the most environmentally friendly Games in history, these actions and the use of hydrogen for the Olympic and Paralympic flames also helped to show the way toward the carbon-neutral hydrogen energy based society of the future and demonstrated how we can leave a beautiful planet for the next generations.

Tokyo is the first city in the world to host the summer Paralympic Games twice. We supported the running of the Games by providing technologies with the potential to become the ultimate solutions for realizing the concept of mobility for all. We also enabled virtual mobility for people in far-away places via the T-TR1 and T-TR2 telepresence robots to help bring the Torch Relays closer to as many people as possible. These technologies embody the potential for what mobility for all could mean in the future.

In addition, through a TPS- and IoT-driven Olympic and Paralympic Games transport management system, we helped to realize safe, secure, and comfortable mobility in Tokyo, which is one of the major challenges for transportation in densely populated cities.

We also helped to reduce the number of officials needed for throwing events through the development of a field support robot (FSR), enhanced the spirit of welcome of the Games through the development of mascot robots, and provided excitement through the superhuman performance of the CUE basketball robot. Our efforts brought happiness to athletes, the people who watched the Games, and every other stakeholder. Behind all these accomplishments are powerful stories about the remarkable development progress that was achieved after the Games were postponed.

Simultaneously, as we face the challenge of living with the coronavirus and with new emphasis being placed on the value of space and mobility, growing attention is being focused on mobility technologies that have a particular significance for current times, such as the LQ, which is the ultimate example of a personally owned vehicle (POV), and non-contact robot technologies such as human support robots (HSRs).

Through these projects, Toyota's development teams at the Olympic and Paralympic Games have taken on challenges in a wide range of new fields. I believe that this was the perfect opportunity to accelerate advanced technical development while working seriously toward our SDGs as we transform into a mobility company.

This is because the Olympic and Paralympic Games form a varied and vibrant real-world community made up of athletes and background staff from around the world, as well as volunteers and other supporters. Realizing technology for this community is an excellent opportunity to communicate our vision for the mobility society of the future to as many people as possible.

Finally, it will be important for our development teams to continue their tireless work to provide ever-better solutions that fit the characteristics of each host city and demonstrate their progress as we move from Tokyo to Beijing, and then to Paris.

With the Olympic and Paralympic Games being held every two years, I believe that this cycle can provide a spark for Toyota's rebirth as a mobility company and act as a catalyst for us to transform our home planet.

Field Operational Tests of Automated Driving Using the Sora Fuel Cell Electric Bus

Takuya Kagawa*1

Abstract

Toyota participated in the automated driving field operational tests (FOTs) carried out in the Tokyo waterfront area as part of phase 2 of the Cross-Ministerial Strategic Innovation Promotion Program (SIP) using an automated bus, which was jointly developed by Hino Motors, Ltd. and based on the Sora, Japan's first mass-produced fuel cell electric bus. These automated driving tests were carried out on public roads in the area around Haneda Airport and involved coordination with infrastructure such as traffic signals and bus lanes, localization technology using magnetic markers, automated acceleration, deceleration and steering, detection of the surrounding traffic environment, and so on. A wide range of knowledge was obtained with regard to the future social implementation of fixed-route bus services on public roads using automated driving.

Keywords: *automated driving, fuel cell, public transportation, fixed route bus, infrastructure, social implementation, precise docking control system, public acceptance*

1. Introduction

Research and development into the practical application of automated driving is being promoted as a way of helping to address social issues such as traffic accidents and congestion.

Public transportation, which plays a vital role in supporting people's everyday lives, is also facing a wide range of issues, including ongoing cutbacks in local train and bus routes as Japan's population declines, and reduced service even on some routes with sufficient demand due to shortages of drivers. The adoption of automated buses is regarded as a promising way of introducing new means of transportation for vulnerable road users, while also helping to maintain unprofitable routes and addressing the scarcity of drivers.

This article describes the knowledge obtained through automated driving field operational tests (FOTs) carried out using fixed-route buses capable of communicating with traffic signals and other intelligent transportation systems (ITS).

2. Test Vehicle Outline

An automated bus based on the Sora fuel cell electric bus was developed for the tests. A fuel cell electric bus combines highly environmentally friendly performance with excellent ride comfort since it emits no CO₂ or other environmental pollutants while in operation and generates little noise or vibration. The characteristic smooth acceleration of electrified vehicles and the uniform power demand that can be realized by the high-performance artificial intelligence (AI) system adopted on automated

vehicles means that fuel cell electric buses are highly suited for automated driving.

Fig. 1 shows the functions installed on the test vehicle. In these FOTs, the location of the bus was identified using magnetic sensors installed under the bus in front and behind the rear axle to detect magnetic markers embedded along the bus route. This magnetic marker system is capable of obtaining accurate position information in poor weather (such as when the road is covered by snow, in thick fog, or the like), as well as in tunnels and other locations with poor global positioning system (GPS) radio wave reception. For these reasons, a magnetic marker system is well suited for public buses that run along fixed routes.

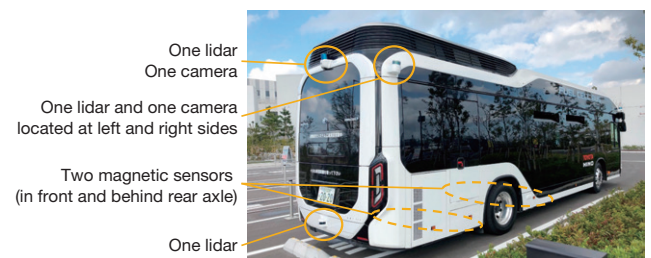
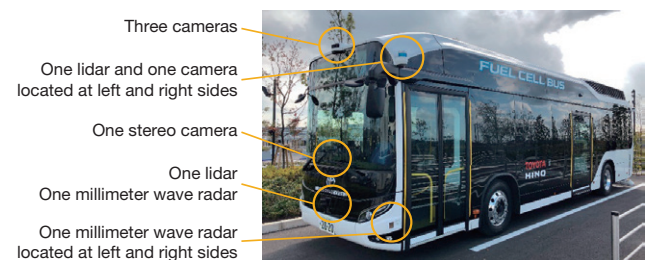


Fig. 1 Vehicle Used in FOTs of Automated Driving

*1 CVZ, CV Company

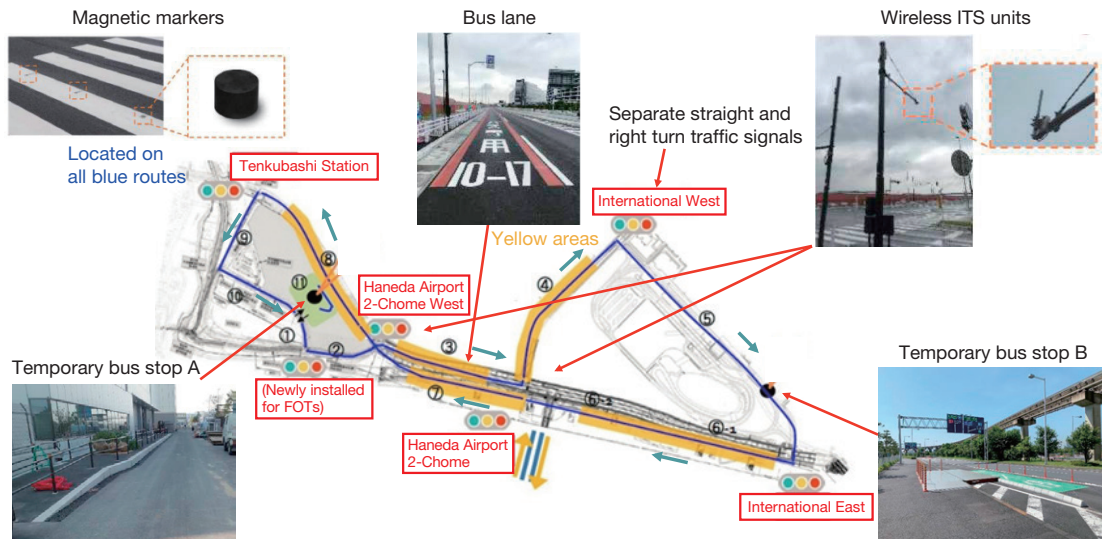


Fig. 2 Test Route and Prepared Infrastructure

Automated driving is realized through cameras and light detection and ranging (lidar) systems installed at the front and rear of the bus to detect objects, oncoming vehicles, pedestrians, and the like around the vehicle, in combination with automated acceleration, deceleration, and steering functions.

One of the characteristics of a fixed-route bus is the presence of standing passengers inside the bus. Therefore, an upper limit deceleration target of 0.15 G was set to help prevent passengers falling over due to sudden braking.

The top speed of the bus was also limited to 35 km/h to help ensure that the bus is not caught in the so-called dilemma zone (the area in front of a traffic signal in which, when the traffic signal changes from green to yellow, the vehicle cannot cross the stop line safely while the traffic signal remains yellow, but also cannot stop at the stop line without braking suddenly).

3. Test Route and Prepared Infrastructure

These FOTs were mainly carried out on public roads in the area around Haneda Airport. Various items of infrastructure were prepared in advance on these roads in collaboration with the relevant government ministries. Fig. 2 shows the test route and infrastructure that was prepared for the tests.

Magnetic markers were embedded in all the roads along the route. The creation of bus-only roads or dedicated bus lanes is regarded as an effective way of realizing early social implementation of automated driving systems by helping to lower the frequency of control activation to avoid interactions with ordinary vehicles. Therefore, bus lanes (bus-only restrictions in place from 10:00 to 17:00) were created within intersections and, excluding some short sections, along one lane of the roads along the route for the test.

In addition, vehicle to infrastructure (V2I) communication using wireless ITS units was established to transmit traffic signal color information (green/yellow/red) from traffic signals to the bus. This information was used in the starting and stopping controls.

4. Results of FOTs

4.1 Driving using magnetic markers

Magnetic markers are capable of estimating the position of the vehicle and are less affected by the weather and surrounding environment. The results of the tests underlined the effectiveness of using magnetic markers with public fixed-route buses.

However, although the target lateral deviation of less than ± 200 mm with respect to the driving path in normal driving was achieved, it was difficult to realize a driving path that did not contact the road shoulder boundary line when turning left or zebra markings when turning right (Photo 1).



Photo 1 Zebra Markings before Right-Turn Lane

In addition, cases occurred in which the front right corner of the bus came into close proximity with vehicles in the opposite lane when turning left (**Photo 2**). Because of its width, the large test bus also came close to large trucks in the next lane because of the narrowness of the bus lane (**Photo 3**).



Photo 2 Vehicle in Opposite Lane when Turning Left



Photo 3 Driving Next to Large Truck in Neighboring Lane

As these are issues related to vehicle size, it would be preferable to widen lanes for automated vehicles, and to establish road shoulder boundary lines, zebra markings, and stop lines in consideration of automated vehicles. It will also be important to develop autonomous driving systems with greater detection accuracy than systems used by passenger vehicles, as well as prediction technology for vehicles driving close to automated vehicles (to predict dangerous driving).

4.2 Precise bus stop docking control system using magnetic markers

A precise docking control system designed to help elderly passengers, wheelchair users, and passengers with strollers embark and disembark the bus more easily (i.e., barrier-free embarkation and disembarkation) was evaluated. Since the maximum gap that can be crossed by a wheelchair user when boarding a bus without assistance is 60 mm, the target for the gap between the bus and the bus stop was set to 45 ± 15 mm. Two temporary bus stops (A and B, **Photos 4** and **5**) with different approach paths were set up. The test results showed that the target gap

was achieved with a deviation of approximately 4 mm (**Fig. 3**).



Photo 4 Approach Path to Temporary Bus Stop A



Photo 5 Approach Path to Temporary Bus Stop B

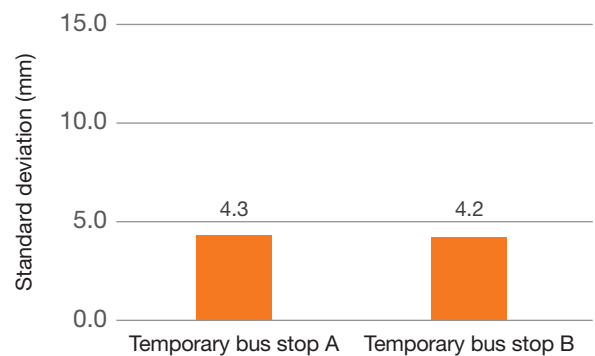


Fig. 3 Deviation of Gap between Bus and Temporary Bus Stops

However, it was necessary to lower the speed of the bus to around 5 km/h at the entrance to temporary bus stop B, which had a more difficult and sharper-angled approach path. From the standpoint of the punctuality of the bus service, it would be preferable to set a shallower approach path angle, i.e., ensure that there is sufficient space before the bus stop.

4.3 Stopping and starting control based on traffic signal information

The traffic signal information transmitted from the wireless ITS units was received by the bus without any major delays. The stopping and starting control based on

this information also functioned without any issues (Photo 6). In addition, limiting the top speed of the bus to 35 km/h also prevented the bus from entering the dilemma zone.

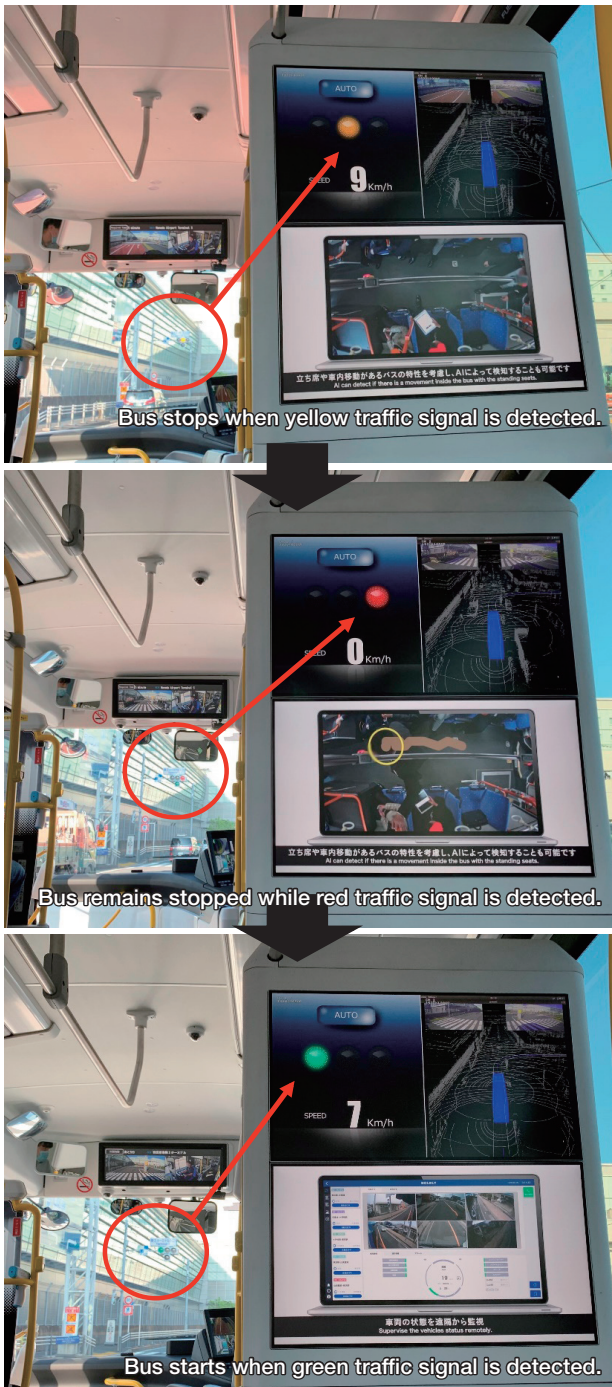


Photo 6 Received Traffic Signal Information (Onboard Monitor)

4.4 Operation of automated bus using bus lanes

Bus lanes can help to create a low-disturbance driving environment suitable for automated vehicles.

However, on some roads along the route, vehicles parked in the bus lane during the restricted hours (10:00

to 17:00), and some incidents of vehicles suddenly cutting in front of the bus occurred. In these cases, the standby bus driver was forced to intervene and avoid the potential danger manually (Fig. 7). It may only be possible to address these cases by creating completely dedicated bus lanes free from external disturbances caused by ordinary vehicles and the like, or to require passengers to be seated.

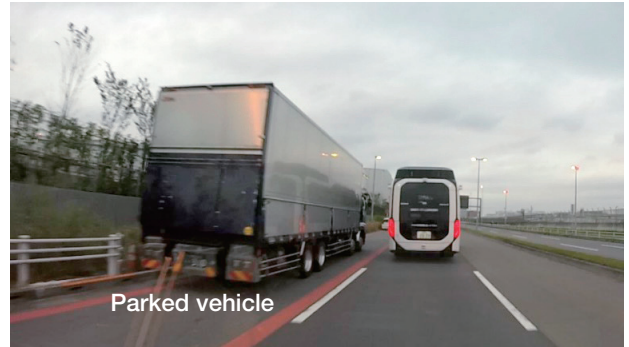


Photo 7 Vehicle Parked in Bus Lane

5. Conclusions

Tests were carried out to verify the feasibility of an automated fixed-route bus service using magnetic markers, bus lanes, bus stops, wireless ITS units, and the like. The following issues related to the early practical application of this service were identified.

- 1) It is difficult to completely prevent vehicles parking in bus lanes and vehicles suddenly cutting in front of buses. This means that it will be necessary to, for example, develop automated buses with an automatic lane change function or functions capable of responding to external disturbances that require the passengers to be seated.
- 2) Large buses have little margin for error when driving in narrow lanes, which makes it difficult to ensure a safe distance to large trucks driving next to the bus. For this reason, wider lanes will be required.
- 3) It is difficult to ensure a safe distance to vehicles waiting at stop lines in the opposite lane when turning left. This means that the positions of stop lines should be moved backward and public awareness of the importance of stopping at stop lines encouraged.
- 4) Since it is difficult to design driving paths that do not cross road boundary lines or zebra markings, it will be necessary to revise the positions of road markings.
- 5) It is difficult to secure sufficient space for bus stops that enable precise docking controls while also ensuring service punctuality. For this reason, a large enough space must be secured for the target stop position, while also creating an approach angle to the bus stop that factors in the surrounding traffic flow.

This FOT was carried out with invaluable cooperation from the relevant government ministries in preparing the infrastructure and Hino Motors, Ltd. in developing the

test vehicle. The author would like to extend his sincere gratitude to everyone that contributed to this development.

Author



T. KAGAWA

Development of the Accessible People Mover (APM)

Hiroyuki Kato*¹
 Akihiro Yanaka*¹
 Masashi Otoyō*²

Special Feature

Abstract

This article describes the development of a dedicated battery electric vehicle for the Olympic and Paralympic Games Tokyo 2020 under the concept of facilitating last-mile transportation and providing comfortable, safe, confident, and natural mobility for all.

Keywords: mobility for all, last-mile transportation, C⁺pod, signage

1. Introduction

Toyota is promoting product development projects and a wide range of other initiatives to help realize its vision of mobility for all. In its role as a worldwide partner of the Olympic and Paralympic Games Tokyo 2020 (abbreviated below as “the Games”), Toyota applied this vision by developing a dedicated mobility solution called the Accessible People Mover (APM) to support the running of the Games. This article describes the details of the APM.

2. Development Concept

In the initial phase of development, the Tokyo 2020 Organising Committee specified the wide ranging transportation requirements of people and goods under the accessibility guidelines defined for the Games. After being presented with various mobility options and the lineup of vehicles made available by Toyota for the Games, the Committee selected the optimum vehicles for each transportation requirement. This process served to underline the importance of providing short-distance transportation solutions, and prompted the start of development of the APM under the concept of facilitating last-mile transportation and providing comfortable, safe, confident, and natural mobility for all (**Fig. 1**).

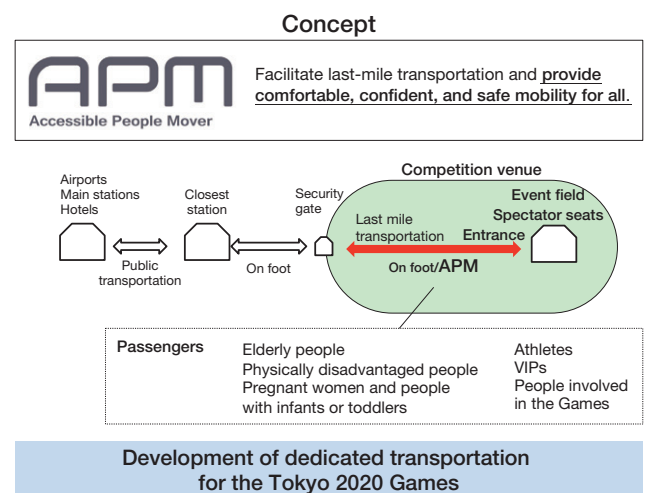


Fig. 1 APM Development Concept

The specific concept assumed that, when moving to a final destination such as the National Olympic Stadium or another event venue, people would first travel by public transportation from an airport, mainline station, hotel, or the like to the station nearest the venue, before walking or taking another means of transportation to the security gate. The APM was conceived to facilitate last-mile transportation to a final target space inside the venue.

In addition to athletes, VIPs, and people involved in the Games, the development also assumed that the APM would be used by elderly and physically disadvantaged people, pregnant women, and people with infants or toddlers.

3. Distinguishing Features of the APM

The targeted key points for developing a last mile mobility solution for a sporting event were defined as follows in cooperation with the Organising Committee and other relevant institutions.

- Simple access (including for wheelchairs)
- Consideration to both passengers and people moving alongside the APM

*¹ ZEV B&D Lab., Toyota ZEV Factory

*² Toyoda Gosei Co., Ltd.

- Packaging that enables smooth operation
 - Easy-to-drive compact battery electric vehicle (BEV)
- Three vehicle variations were developed, as described in detail below (**Table 1**).

Table 1 Vehicle Variations

Type	Purpose and distinguishing features	Number
Standard type*	Maximum passenger capacity: 5 (wheelchair accessible)	144
First aid type*	For transporting people in need of first aid	40
Bullpen cart	Used to transport relief pitchers in baseball games	2

* Permitted to be driven on public roads

The main specifications of the APM are as follows (**Fig. 2**).

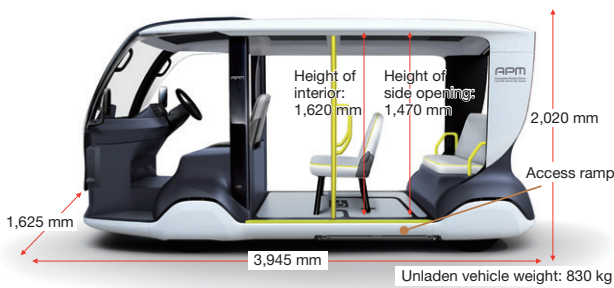


Fig. 2 Main Specifications

The distinguishing features of the APM are as follows.

- (1) Compact dimensions
⇒ To make the vehicle easy to steer
- (2) Elevated driver's seat positioned in center of vehicle
⇒ To facilitate assistance to passengers entering or leaving vehicle at the left or right sides and to ensure excellent visibility from a raised position
- (3) Low and flat floor for passengers (batteries installed under the floor)
⇒ To facilitate access and to secure a spacious interior
- (4) Retractable under-floor access ramp
⇒ To facilitate wheelchair access (standard type only)
- (5) Top speed of 19 km/h (high enough to comply with regulations for driving on public roads)
⇒ So that it can be driven between venues

The APM was designed to enable comfortable last-mile transportation for all. The open-sided design provides an excellent field of view and the wheels were covered to prevent contact with pedestrians and passengers. The result is a user-friendly advanced-looking vehicle that also incorporates design cues from Toyota's electrified vehicles. To ensure clear forward visibility and allow the driver to see all the passengers by looking back, the driver's seat is located in an elevated position above a floor step at the center of the APM. The front of the vehicle tapers inward to ensure good visibility to the left and right when driving, and to help present an accessible

and friendly image. In addition, to facilitate smooth movement in and out of the APM, the passenger seats were designed to be flat with a slightly high hip point. Highly visible yellow piping was also adopted to match the hand rails of the same color. Dirt-resistant and water-repellent seat covering materials were adopted. The cushions were designed to facilitate sideways movement and a mesh was adopted for the seatbacks to help prevent the accumulation of heat (**Fig. 3**).



Fig. 3 Exterior Styling

The underbody, chassis, and driving/battery system made maximum use of the components developed for the C⁺pod launched at the end of 2020 to help reduce development costs (**Fig. 4**).

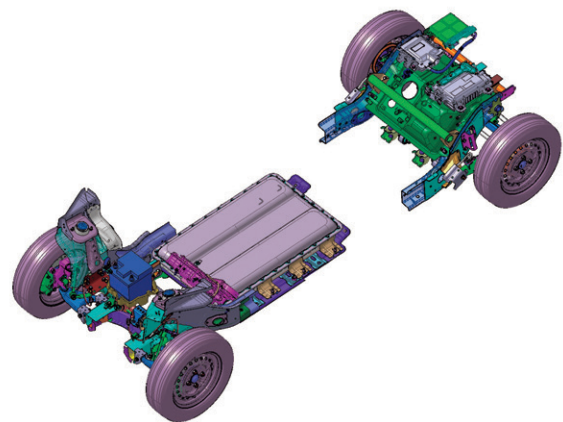


Fig. 4 Components Carried Over from the C⁺pod

3.1 Standard type

- Interior arrangements

The maximum capacity of the standard APM is five passengers. However, the second row of seats can be folded down for wheelchair access or cargo. The standard APM is also equipped with a retractable under-floor ramp for smooth access. For even easier wheelchair access, guides that are both easy-to-understand and stylish are provided on the ramp and floor (**Figs. 5 and 6**).

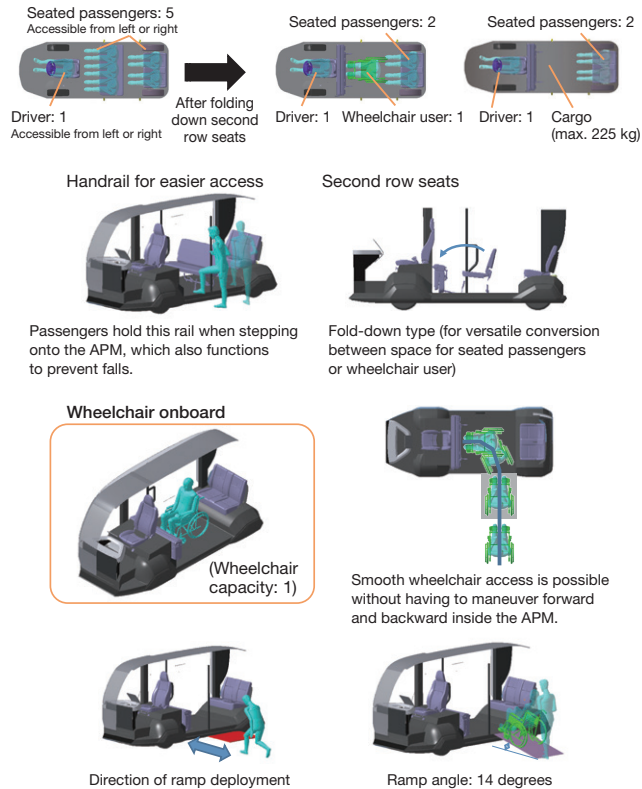


Fig. 5 Interior Arrangements



Fig. 6 Usage Scenario (Wheelchair Access)

- Measures for rainy weather

The APM was designed without side doors to create an open and airy design for use in the summer and to facilitate access. The APM is equipped with curtains for use in the rain.

For consistency with the exterior styling, the curtains were integrated into the front and rear pillars, and can be pulled out when required and fixed to the center handrail. The front and rear curtains can be opened and closed independently to minimize the open area when accessing the APM. A user-friendly curtain that rolls down from the roof is also provided at the rear. The curtains are made from a semi-transparent material that shuts out the rain while still providing visibility to the inside and outside of the APM (**Figs. 7 and 8**).

Finally, to prevent rain from blowing into the driver's seat area, large side visors and a transparent plastic panel are provided at the sides of the seat.

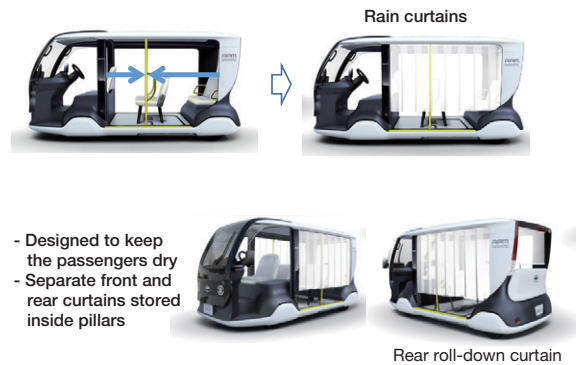


Fig. 7 Rain Curtains

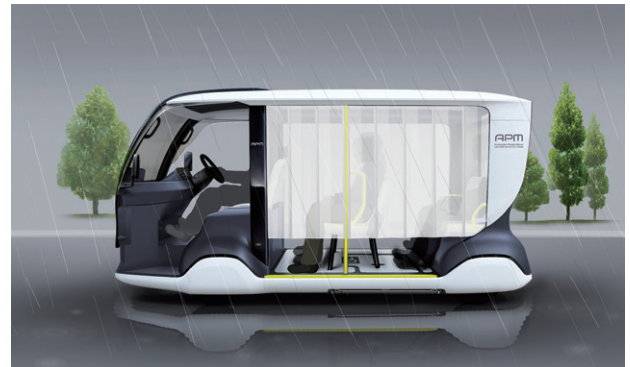


Fig. 8 Usage Scenario (Rain)

3.2 First-aid type

This version of the APM was developed to transport people requiring first aid to the first-aid center (**Fig. 9**).



Fig. 9 First-Aid Type

The first-aid type APM was designed assuming the use of a basket stretcher. This APM is also equipped with a flexible hose air conditioner to help people suffering from heatstroke and the like. The air conditioner is positioned to deliver cool air to the patient's face and upper body. This APM has enough space for two medical personnel and is equipped with interior lighting for operation after dark. The curtains can also be used to protect the privacy of the patient (**Fig. 10**).

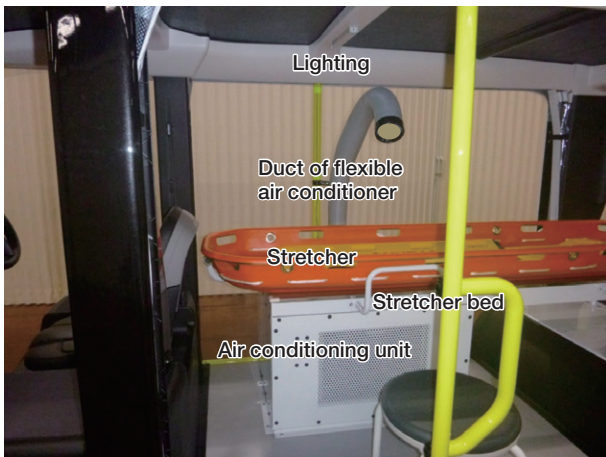
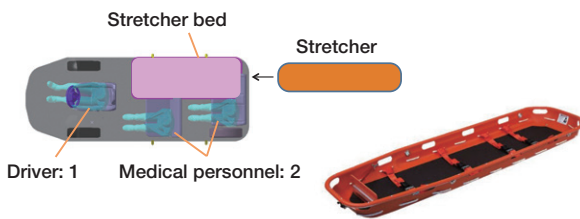


Fig. 10 First-Aid Type

3.3 Bullpen cart

A special bullpen cart to transport relief pitchers inside the baseball stadium was developed.

This version of the APM has an open design with no roof so that spectators in the stands can see the pitcher clearly. The pitcher's seat is shaped like a baseball glove and artificial turf is set on the floor in consideration of the

spiked shoes worn by pitchers. The outline of a baseball diamond is displayed on the artificial turf to further appeal to fans at the stadium (**Fig. 11**).



Fig. 11 Bullpen Cart

In addition, Toyota worked with Toyoda Gosei Co., Ltd. to provide special signage panels at the front and rear of the APM. These panels use LEDs and bright colors to display messages for fans that are visible even from far away (**Fig. 12**).

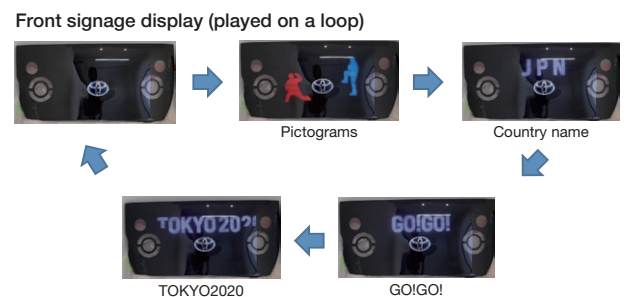


Fig. 12 Signage

4. Conclusions

Although designed as a dedicated mobility solution for the Tokyo 2020 Games, the APM is an excellent embodiment of the mobility for all vision. Toyota intends to continue delivering appealing products to provide comfortable, confident, and safe mobility for everyone.

The development of the APM was affected by various issues, including the impact of the coronavirus pandemic, delays in the production schedule due to the postponement

of the Games, and suppliers backing out of the project. The APM was only developed in time for the Games thanks to the invaluable cooperation of the companies and people involved in the project. The authors would like to express their sincere gratitude to everyone concerned.

Authors



H. KATO



A. YANAKA



M. OTOYO

Development of Walking Area Electric Vehicles

Masashi Yamada*¹
 Akihiro Yanaka*¹
 Makoto Mori*¹
 Yoshiyuki Senba*¹

Abstract

This article describes the development of personal mobility vehicles capable of being operated in pedestrian spaces with the aim of providing confident and natural mobility to people at all stages of life under the concept of mobility for all.

Keywords: *mobility for all, walking area*

1. Introduction

Under its vision of mobility for all, Toyota is aiming to provide safe, confident, and natural transportation to people at all stages of life through a range of services and mobility products.

Toyota also supported the mobility of organizers and security staff at the Olympic and Paralympic Games Tokyo 2020, with the aim of examining how mobility can coexist with people in new areas.

This article describes the walking area electric vehicles (EVs) that were developed to help realize these objectives.

2. Significance of Walking Area EVs

As people's physical capabilities and needs change with age, and as the issues and requirements of areas such as urban and semi-urban spaces continue to diversify, there is increasing demand for mobility solutions for specific purposes and scenarios.

In addition to these age-related changes in physical capabilities, people are moving away from conventional means of transportation in response to family pressure and the risk of accidents. This creates a gap between the desire for mobility and people's actual sphere of activity.

One important turning point in this process is when driving licenses are returned by elderly drivers. This act can dramatically increase this gap and result in a complete loss of mobility even within the range necessary for everyday life. The introduction of walking area EVs is significant because it can fill this gap, broaden the scope of people's mobility, and help them live more rewarding lifestyles (**Fig. 1**).

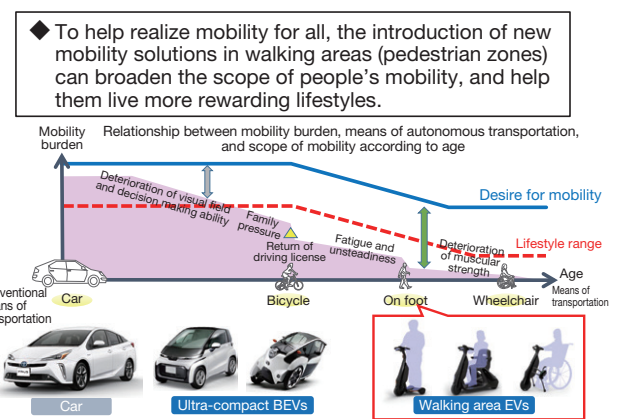


Fig. 1 Outline of Significance of Walking Area EVs

Until recently, Toyota has focused on cars as the principle means of transportation. However, it has now started to consider introducing new mobility solutions for walking areas with the aim of providing support for mobility throughout every stage of a person's life, including after that person is forced to return his or her driving license.

3. Objectives and Target Users of Walking Area EVs

Three types of walking area EVs were developed for specific purposes and usage scenarios: a standing type, a seated type, and a wheelchair-linked type EV (**Fig. 2**).



Fig. 2 Three Types of Walking Area EVs

*¹ ZEV B&D Lab., Toyota ZEV Factory

The following sections describe the objectives, target users, and packaging of each type of walking area EV.

3.1 Standing type EV

3.1.1 Objective of standing type EV

The standing type walking area EV was developed to support the lifestyles of seniors who want to continue contributing to their community. The development team envisioned this type of EV being used by elderly people engaged in patrolling or security work, or being adopted by companies wanting to reduce the workload of their employees.

Since standing type EVs cannot be ridden on public roads under current laws and regulations, the use of this type of EV is likely to be restricted to private facilities.

3.1.2 Packaging of standing type EV

To facilitate acceptance in pedestrian zones, the standing type EV was designed by factoring in the space taken up by a pedestrian. For example, the length of the EV was set to the length of stride of a pedestrian, and the width of the EV was set to the width of a person's waist. The height of the step was also set for easy boarding and alighting (**Fig. 3**). In addition, to realize a small turning circle, this EV has a steering angle of 90 degrees in either direction.

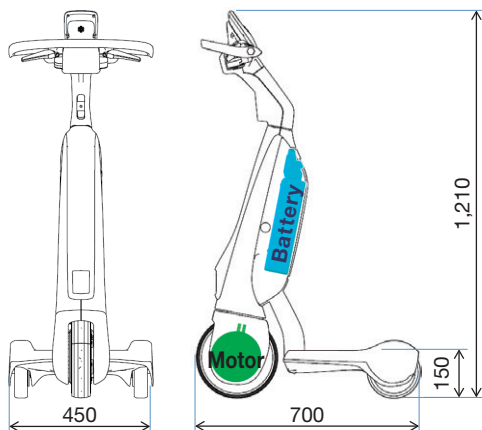


Fig. 3 Packaging of Standing Type EV

3.2 Seated type EV

3.2.1 Objective of seated type EV

The seated type walking area EV was developed to support movement from a person's home to a nearby facility. This EV was developed for users that are capable of walking by themselves, but who find long distances a challenge. Specific usage scenarios include shopping for everyday items, participation in community events, or visiting the hospital. These users want more freedom of movement to address the following issues.

- Difficulty of walking long distances

- Inability to walk faster than a certain speed
- Difficulty of walking while carrying something

Under current laws and regulations, these types of EVs can be ridden on public roads.

3.2.2 Packaging of seated type EV

The external dimensions of the seated type EV were set to comply with the Japanese Industrial Standard (JIS) definition of an electric four-wheeled cart. A three-wheeled design was selected to respond to sudden changes in road surface in the direction of movement and for greater visibility around the front wheel. To ensure a step height and hip point that facilitate boarding and alighting, the design focused on lowering the height of the step. Additionally, enough space was created in front of the seat so that the user can stand upright on the step and does not have to board or alight the EV in a half-crouched posture (**Fig. 4**).

The seat position can be adjusted forward and backward to match the physique of the user. The EV is also equipped with a compartment for shopping below the seat that does not have to be opened before use.

The design also emphasizes maneuverability with a minimum turning circle of 0.95 meters.

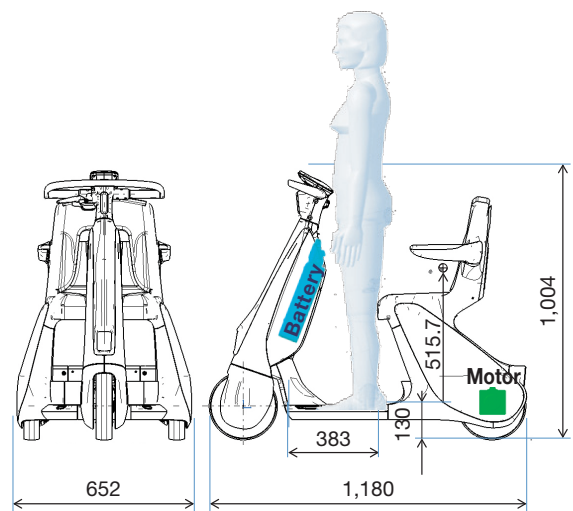


Fig. 4 Packaging of Seated Type EV

3.3 Wheelchair-linked type EV

3.3.1 Objective of wheelchair-linked type EV

The wheelchair-linked type EV was developed to help active users of manual wheelchairs travel longer distances. The development team envisioned frequent wheelchair travelers renting and attaching this EV to their wheelchairs at their travel destination to address the following issues.

- Long distances from a carpark to the destination
 - Difficulty of manually wheeling a wheelchair up a hill
 - Relying on someone else to push the wheelchair
- Therefore, the development assumed that this EV

would be adopted by public facilities or government bodies wanting to attract wheelchair users and other visitors.

Similarly to the seated type EV, this type of EV can also be operated on public roads under current laws and regulations.

3.3.2 Packaging of wheelchair-linked type EV

In the same way as the seated type EV, the external dimensions of the wheelchair-linked type EV were set to comply with the JIS standard for electric four-wheeled carts. The components of this EV are virtually the same as those used on the standing type EV, with an attached stand that is used when attaching, detaching, and storing the EV (Fig. 5).

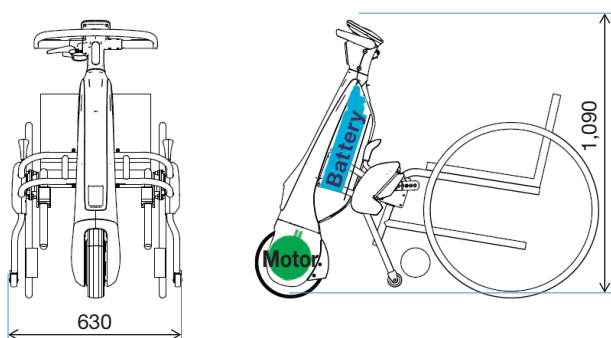


Fig. 5 Packaging of Wheelchair-Linked Type EV

4. Designed to Create Value through New Mobility Experiences

Design will play an extremely important role in popularizing new forms of mobility.

The design theme was defined as follows: the development of compact EVs capable of creating value through new mobility experiences by greater accessibility and closer connections between people, urban areas, and communities.

Although these EVs were designed to support the mobility of elderly people, the styling was developed with the aims of expressing freshness and encouraging actual use.

A sleek external form based on covered tires at the front and rear and a two-tone plastic body was adopted. The EVs were specifically designed to be operated seamlessly in busy pedestrian zones without adversely affecting other users of the same space.

5. Main Functions

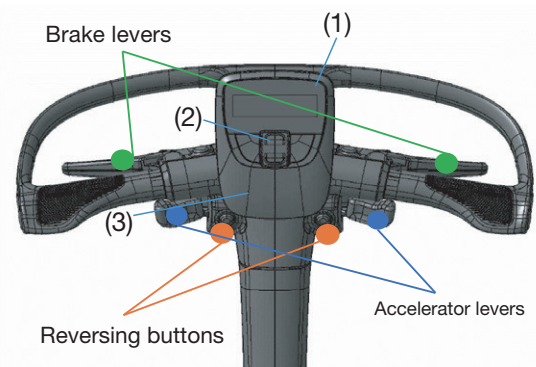
5.1 Handlebars (control system)

The EVs are targeted at elderly people that have returned their driving license. To enable these people to

ride and handle the EVs more easily, the development adopted handlebars and levers inspired from the familiar system used on bicycles.

Accelerator levers are located below the handlebars so that the user cannot operate one by mistake when gripping the handlebars. Reversing buttons are provided in different positions to the accelerator levers to help reduce the likelihood of mistaken operation.

The accelerator levers, brake levers, and reversing buttons are provided on both sides so that the EVs can be ridden by both left- and right-handed users. This dual layout allows the rider to change grip to reduce fatigue after long periods of use, and to make larger turns of the handlebars easier (Fig. 6).



- (1) Status display
- (2) Operation buttons (horn, front light, top speed setting)
- (3) NFC reader

Fig. 6 Expanded View of Handlebars: Dual Layout of Control System

5.2 Speed setting

Button (2) in Fig. 6 is used to set the top speed of the EVs. This speed can be set in 1 km/h intervals between 2 and 6 km/h. The EVs have a control that prevents this top speed from being exceeded, which enables the rider to travel easily at a constant speed or to maintain pace with an accompanying pedestrian.

The top speed of the standing type EV can be set to 10 km/h specifically for work-related scenarios.

5.3 Electronic key authentication using NFC reader

Item (3) in Fig. 6 is a near field communication (NFC) reader that allows the vehicle to be driven once an electronic key ID is authenticated.

A top speed can be set for specific electronic key IDs, which allows the people responsible for the EVs to change the speed according to the skill of the user.

5.4 Removable batteries

The EV batteries can be removed and charged. This allows people living in, for example, an apartment

building to detach and charge the batteries indoors.

Furthermore, anxiety about battery depletion can be relieved and the range of the EVs extended by preparing a second battery.

The batteries can be attached and detached easily (Fig. 7).

When attaching a battery, the user aligns the bottom of the battery with the body of the EV and locks it in place with an upward pivoting motion. The battery can then be detached by pulling a lever to unlock.

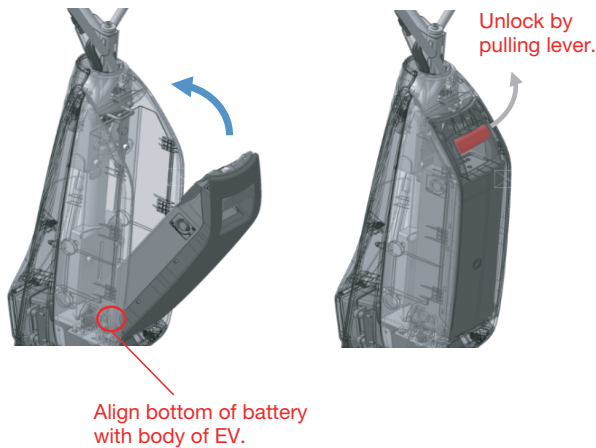


Fig. 7 Battery Attachment and Detachment Procedure

5.5 Functions for confident and natural riding

The EVs are equipped with three speed restriction functions to enable users to ride naturally and with confidence.

The first function reduces lateral acceleration while turning by automatically slowing the EV in accordance with the steering angle.




The second sounds an alarm at the start of steep hills and automatically slows the EV when going downhill.

When an object is detected in front of the EV, the third function automatically applies the brakes in accordance with the speed and distance to the object, and then notifies the rider.

6. Main Specifications and Performance

Table 1 lists the main specifications of the EVs

Table 1 Main Specifications

Type	Standing	Seated	Wheelchair-linked
Appearance			
Length	700 mm	1,180 mm	540 mm
Width	450 mm	652 mm	630 mm
Height	1,210 mm	1,002 mm	1,090 mm
Top speed	6 (10) km/h	6 km/h	6 km/h
Range without charging	Approx. 14 km	Approx. 10 km	Approx. 20 km
Charging time	2.5 hours	2.5 hours	2.5 hours
Hill climbing performance	6°	10°	6°
Weight capacity (including cargo)	100 kg	100 kg	100 kg
Applicable standard	None Cannot be ridden on public roads (For use in private facilities)	Electric four-wheeled cart Can be ridden on public roads	Electric four-wheeled cart Can be ridden on public roads
Functions for confident and natural riding (speed restriction functions)	Standard: reduces speed while turning Option: reduces speed on hills and when object is detected	Standard: reduces speed while turning and on hills Option: reduces speed when object is detected	Standard: reduces speed while turning and going downhill Option: reduces speed when object is detected

Special Feature

7. Application at Olympic and Paralympic Games Tokyo 2020

Toyota planned to deploy adopt 210 of these EVs (primarily standing type EVs) at large venues such as the Olympic stadium and Ariake Tennis Park to support the mobility of organizers as well as security and medical personnel.

8. Conclusion

Walking area EVs were developed as a key product to help realize mobility for all.

These EVs were realized by carrying out field operational tests (FOTs) using actual vehicles from an early phase in the development period, identifying issues and requirements by listening to comments from the target users, and responding to a wide range of expectations and requests for improvements. These initiatives helped to raise the level of these EVs. In this way, Toyota is aiming to help create a society in which

everyone can live active and rewarding lifestyles through the development of ever-better products by listening carefully to customers and adopting a process of continuous improvement.

Authors



M. YAMADA



A. YANAKA



M. MORI



Y. SENBA

The Toyota LQ

Daisuke Ido*1
Tatsuya Takei*2
Yoichi Iwata*3
Shogo Sekizawa*4
Satoshi Nakagawa*4

Abstract

The Toyota LQ was developed for the milestone year of 2020 under the concept of showcasing ideas for the beloved cars of the future. The LQ embodies the essence of what can make a car truly beloved in the age of Mobility as a Service (MaaS), building upon the conventional concept of cars as a possession. In addition, although not intended for general sale, a model featuring a wide range of advanced world-first and Toyota-first technologies was developed to be driven on public roads. This model was developed to give people the opportunity to test drive and experience the future at first hand, create customer feedback for development, and to help further advance and enrich the component technologies. This article focuses on the latter objective and provides a panoramic outline of the technologies used in the LQ.

Keywords: Toyota LQ, large side glass, invisible register, seat with alertness and relaxation functions, automated driving, automated valet parking system, AI agent, AR HUD, DMD-equipped headlamps

1. Introduction

The year 2020 is likely to be remembered as a year that derailed the plans of many people. This certainly applies to the Toyota LQ. Toyota wanted the LQ to be test driven by as many ordinary people as possible and form part of the memory of their visit to Tokyo. However, the risk of COVID-19 infection was too great and these plans had to be canceled.

The LQ was equipped with a wide range of new technologies to give people the opportunity to experience the future at first hand and to create technical feedback from customers for further development. Although limitations of space prevent a full exploration, this article introduces some of the main technologies that were developed for the LQ.

2. Design Development

2.1 Aims of design

While visually expressing an image of a car equipped with cutting edge technologies, the aim of the design was to project a feeling of warmth like a piece of traditional Japanese craftsmanship and eliminate any hints of coldness.

2.2 Design characteristics

- The interior and exterior of the LQ are styled with lines that flow seamlessly from the inside-out, centered on Yui, an interactive agent powered by artificial intelligence (AI) (**Fig. 1**).
- The shape and textures of the LQ combine cutting edge technologies with the warmth of a handcrafted piece of art.
- Taking advantage of the characteristics of an engine-free battery electric vehicle (BEV), the LQ features a futuristic silhouette with sleek unbroken lines that extend rearward from swept-back front pillars.
- Expansively styled door glass openings were adopted to create a completely different sensation to a conventional vehicle when boarding (**Fig. 2**).



Fig. 1 Faithful Representation of the Inside-Out Design Concept



Fig. 2 External Styling Taking Advantage of the Characteristics of a BEV

*1 ZEV B&D Lab., Toyota ZEV Factory
*2 MS Design Div., Mid-size Vehicle Company
*3 Automated Driving & Advanced Safety System Development Div., Vehicle Development Center
*4 Cockpit Electronics System Div., Vehicle Development Center

3. Body Design

3.1 Large side glass

For the design team, it was particularly important to realize an upper body structure with large side glass to enhance the openness of the interior by increasing the transparent area of the vehicle sides, and to emphasize the futuristic impression of the LQ when seen from the outside.

Practically realizing this objective presented various issues, including the adoption of large adhesive glass panels, glass that can be raised and lowered for safety and usability (such as when taking a ticket from a machine), and internal reinforcing members to ensure door rigidity.

Below the beltline, trim parts were added that extend at an angle from the top of the interior to outside the vehicle so that the legs of the occupants are not directly visible from the outside.

3.2 Invisible registers

“Register” is the technical name given to an air conditioning vent. To realize distinctive interior styling, the registers were located in locations invisible to the occupants.

Using the Coanda effect, by which airflow is forced to move along a surface, flaps were provided at the appropriate locations to separate and direct the air toward the upper bodies of the occupants, creating a design that is both stylish and comfortable (**Fig. 3**).

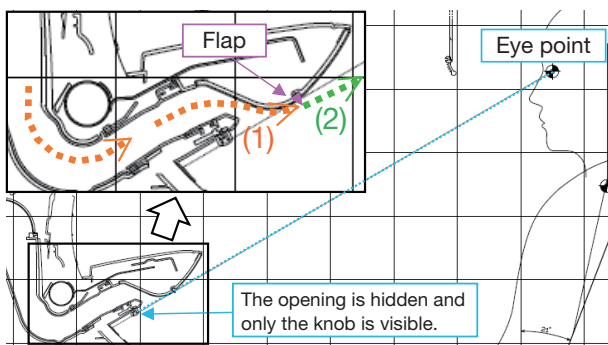


Fig. 3 Concept of Invisible Registers

3.3 Seats with alertness and relaxation functions

The seats were designed to help keep the occupants alert or relaxed. Extreme tension or drowsiness can reduce alertness and adversely affect driving. When the occupant is feeling tense, the seating system controls bladders embedded in the seats to facilitate a more relaxed posture by encouraging abdominal breathing. In contrast, when the occupant is feeling drowsy, the system helps to encourage alertness by supporting an upright seating posture.

Cameras at the front of the cabin and time of flight

(TOF) sensors are used to detect the degree of alertness of the occupants. This detection capability was extended to both the front two seats since it was assumed that people trying out the LQ would also sit in the front passenger seat.

4. Automated Driving

The LQ is equipped with two automated driving technologies. The first is called Chauffeur, a level 4-equivalent automated driving system as defined by the Society of Automotive Engineers (SAE). The other is an automated valet parking system.

4.1 Chauffeur

Japanese regulations and guidelines require the presence of a driver to take control if an emergency occurs. For this reason, the Chauffeur system is described as equivalent to SAE level 4.

The LQ is equipped with the latest automated driving technology developed by the Toyota Research Institute (TRI), which is called Platform 5 (**Fig. 4**). It was planned to demonstrate the Chauffeur system negotiating the most scenic part of the test drive route around Daiba and Toyosu in Tokyo, a distance of around 1.6 kilometers. During this stretch of the test route, the driver would be able to enjoy the experience of looking away from the road ahead (eyes-off). The development team envisioned a scenario in which all the occupants of the vehicle, including the driver, could share the enjoyment of beautiful scenery. This automated driving section of the route was also important because it would provide an opportunity to experience a practical issue of automated driving, namely the switch over between automated and manual operation.



Fig. 4 Automated LQ

The LQ is also equipped with a function called Sight-to-Sound, which uses the cameras and sensors of the Chauffeur system. This system assists the recognition of objects such as pedestrians, bicycles, and other vehicles detected by the Chauffeur system by emitting sounds corresponding to the location and speed of the object. The aim of the system is to help maintain the attention level of the driver when the automated driving system is engaged.

4.2 Automated valet parking system

A new low-speed automated parking system was developed that can be used between the loading zone of a car park and the parking space. This system has merits for both users and business operators. For example, it eliminates the need to both search for and park in a parking space, which can be a concern for the elderly and other people with accessibility requirements as well as drivers that find parking difficult. At the same time, it is also capable of parking with a gap of only 20 cm between vehicles, thereby helping to reduce the amount of space required by the car park (Fig. 5).



Fig. 5 20 cm Gap between Parked Vehicles

The onboard system combines multiple cameras, sonars, and radars with road maps to identify the current vehicle location. At the same time, the system detects pedestrians and other objects to be avoided and the target parking position between white lines, before determining the appropriate trajectory and controlling the acceleration and deceleration of the vehicle (Fig. 6).

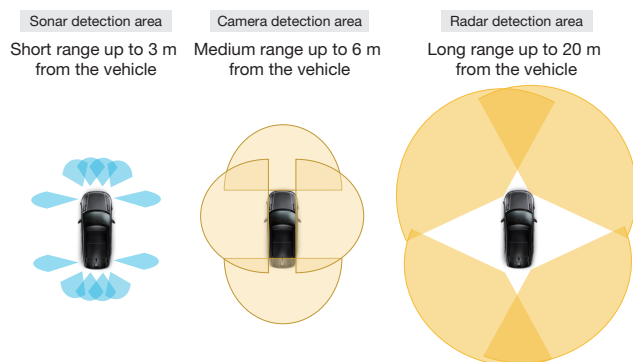


Fig. 6 Detection Range of Onboard Cameras and Sensors

The system can also communicate with the cameras and management server of the car park to guide the automated vehicle to an empty space. The system is also capable of bringing the vehicle to the loading zone automatically at the time reserved on the operation terminal (Fig. 7).

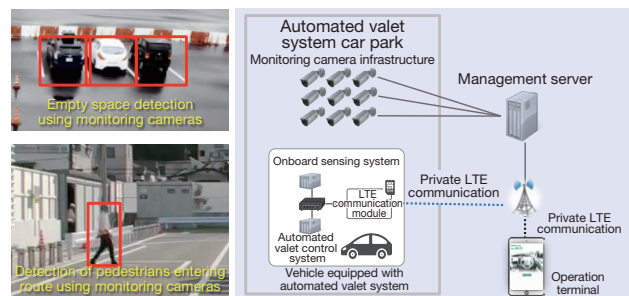
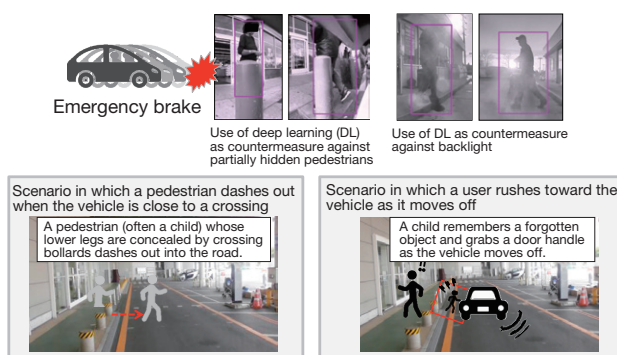


Fig. 7 System Detection and Vehicle Guidance Capabilities

The system uses both the vehicle sensor suite and car park cameras to monitor vehicles and pedestrians entering the automated driving route, and will stop the vehicle automatically if a collision risk is determined (Fig. 8).



Detection requirements for assumed dangerous scenarios at MEGA WEB

Fig. 8 Example of Pedestrian Detection at Vehicle Loading Zone

The management server can control multiple automated vehicles at the same time. Unlike sequential control that operates one vehicle at a time, this approach reduces the time required to bring vehicles in and out of the car park and enables a wait-free service for customers at the loading zone.

5. AI Agent

The LQ features an AI agent named Yui, which was developed as a mobility expert to provide a special personalized user experience (UX). Yui gauges the emotional and physical state (such as drowsiness) of the user based on facial expressions and body movements. In addition to conversation-centered communication, Yui helps to provide a safe, secure, and comfortable mobility experience via the range of human machine interfaces (HMIs) in the vehicle, including the seats equipped with alertness and relaxation functions, music, interior lighting, air conditioning, fragrances, and so on. Yui was also developed to facilitate a more enjoyable experience by selecting and playing music in accordance with the driving scenario or user preference, raising interesting topics, or providing information about relevant points on the route.

Special Feature

The system configuration is described below focusing on the controllable inputs and outputs of the agent system (Figs. 9 and 10). First, Yui is equipped with a user interface (UI) avatar located at the center of the vehicle near the driver’s seat. This avatar is the center of communication with the vehicle occupants. The onboard agent ECU is capable of controlling the microphones, camera, lighting, audio, music, and the like directed at the driver, front passenger, and rear seat occupants. For example, the four-seat digital microphone and seat separation control enables conversations with Yui via voice recognition at each seat. Alternatively, Yui is also equipped with an easy-to-understand HMI that turns on the floor lighting for only the occupant to whom it is talking. Additionally, Yui can identify the emotional state of occupants (e.g., whether the occupants are happy or not) using the image recognition function of the driver and front passenger seat monitoring system. The system can then select music in accordance with the occupants’ preferences, or help to create a more comfortable environment by operating the alertness and relaxation functions of the seats or the aroma diffuser to dispense fragrances (Fig. 11). As a result, a Yui-centered UX can be realized using an array of onboard devices through integrated control of multiple inputs and outputs, as well as effective utilization of image recognition technology. The system also connects the vehicle to the cloud and can link up with smart phone applications to teach Yui about user tastes and trends based on inputs to those applications, thereby enabling more personalized user services (Table 1).

A demonstration experience for ordinary users was prepared using three languages: Japanese, English, and Chinese. Cultural context was also factored in to help prevent conversations based on difficult-to-understand literal translations.



Fig. 9 Example of Simultaneous Automated Parking of Three Vehicles

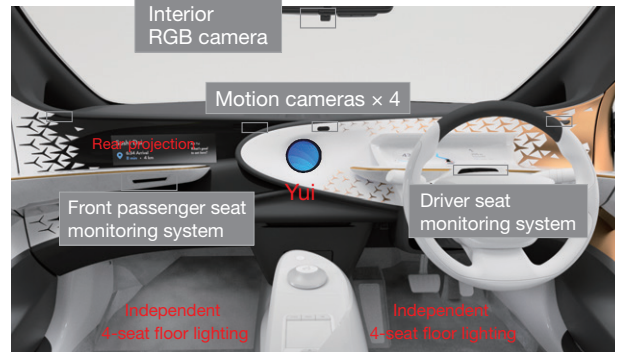


Fig. 10 AI Agent-Related Functions around Driver’s Seat

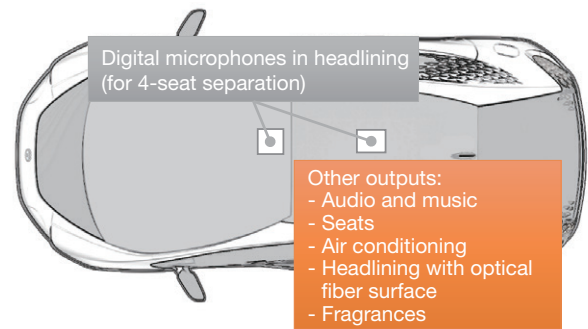


Fig. 11 Additional Inputs and Outputs inside Vehicle

Category	Applicable functions
Occupant state estimation (image recognition)	Emotional state/degree of alertness estimation
	Gaze/facial direction
Conversation control	4-seat microphone processing, automatic speech recognition (ASR)/natural-language understanding (NLU), custom text-to-speech (TTS)

Table 1 Main Recognition System Software

6. AR-HUD

The augmented reality head-up display (AR-HUD) projects necessary safety and route information on the front windshield while driving to augment the background of the actual driving environment. The HUD uses a large full-color display (width: 11.4° × height: 4.0°) to project this information in a range between 7 and 41 meters in front of the driver’s eyes, creating realistic depth perception in accordance with the distance to the actual target object (Fig. 12). The distance and height of the projection minimizes the amount of gaze movement and focus adjustment by the driver, and helps to ensure that the driver can read the safety or route information safely and comfortably. User interaction is carried out while ensuring that the forward field of view or attention of the driver is not blocked or lost. The system uses consistent graphics that take advantage of the effects of psychological depth cues to facilitate integration of the

real and virtual worlds. This approach supports the provision of accurate information and aids intuitive recognition. In addition, the AR-HUD links with the automated driving system and utilizes high-precision maps and localization information to project virtual graphical information onto road shapes or the locations of objects present in the real world (Fig. 13).

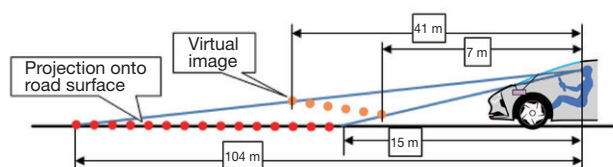


Fig. 12 AR-HUD Concept

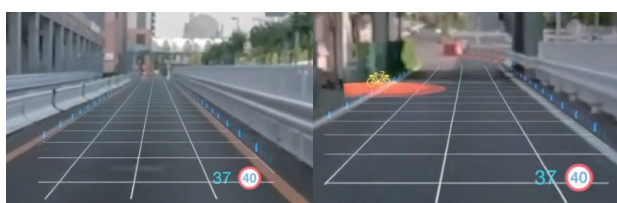


Fig. 13 Example of AR-HUD Displays
(Right Figure: Alert Display)

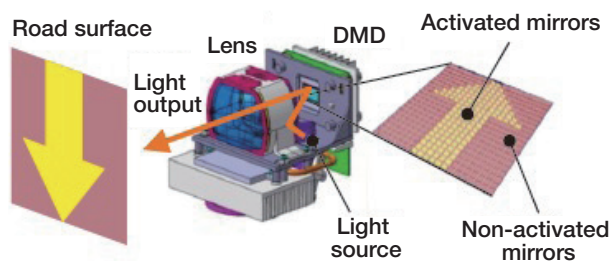
7. Road Surface Projection Headlamps

7.1 Outline

The headlamps of the LQ are equipped with digital micromirror devices (DMDs) that project images onto the road surface as a means of communication inside and outside the vehicle.

A DMD is capable of activating large numbers (a total of 1.3 million) of tiny mirrors (size: less than 10 μm per mirror) to project any image onto the surface of the road.

These DMD-equipped headlamps can project letters or symbols onto the road to convey information to the driver or people around the vehicle (Fig. 14).



The mirrors are activated to form an arrow.

Fig. 14 Details of DMD

7.2 Lamp specifications

When projecting information onto the road surface, the location and content of the projection differ greatly depending on whether the information is for the driver or people outside the vehicle. Therefore, the DMDs in the left and right headlamps of the LQ have different projection ranges.

A typical example of actual projected information is described below.

- For the driver (7 to 8 meters in front of the vehicle)
⇒ Reminder of vehicle width

The width of the vehicle is projected onto a narrow road to facilitate more confident driving.

- For people around the vehicle (2 to 3 meters in front of the vehicle)

⇒ Notification that the vehicle is going to move off (Fig. 15)

Arrows are projected to alert people when the vehicle is about to move off.



Fig. 15 Illustration of Notification when Vehicle Moves Off

7.3 Regulatory status

Practical adoption of this technology will require revision to lamp-related regulations. Discussions are currently under way about what lamp projection content will be permitted, with the aim of revising regulations defined by the United Nations (UN). Although the timing at which this system can be used on public roads is not yet clear, it has already been authorized for use inside Germany.

8. OLED Instrument Cluster

The instrument cluster of the LQ uses an organic light-emitting diode (OLED) panel. OLEDs can display deeper levels of black and achieve a higher contrast ratio than liquid crystal panels. Colors rendered using OLEDs also have smaller variation depending on the view angle and OLEDs are more suitable for curved displays. Taking advantage of these characteristics, the instrument cluster was installed in front of the styling surface, enabling the necessary driving information to

be displayed while realizing a distinctive interior design (Fig. 16).



Fig. 16 OLED Instrument Cluster

9. All-Solid-State Battery

A new all-solid state battery (ASSB) was developed for the LQ and a license plate registration number was obtained for driving on public roads (Fig. 17). An ASSB is a type of lithium-ion (Li-ion) battery that uses a solid electrolyte rather than a conventional liquid electrolyte and separator configuration. The use of a solid electrolyte increases the velocity of the Li ions in the battery, lowering resistance and enhancing its rapid charging performance. In addition to full compliance with the UN-R100 Part II safety requirements, progress was made in the development of peripheral vehicle technologies such as the support and cooling structures necessary to withstand use in actual driving.

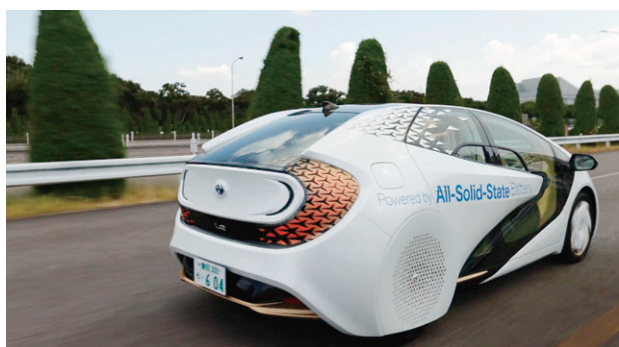


Fig. 17 LQ Equipped with ASSB and Registered License Plate

10. Conclusion

The LQ was developed for the milestone year of 2020. Although never intended for sale, the development team faced various challenges, both large and small, to achieve the goal of enabling customers to ride and drive the LQ on public roads. This article focused on describing the main distinctive features of the LQ.

The process of developing and raising the new

technologies adopted in the LQ to actual automotive quality resulted in the acquisition of a wide range of knowledge and helped to identify issues for the next generation of technological development. The same applies to the members of the development team.

In the writing of this article, valuable information was provided by Yasuyuki Kato of Koito Manufacturing Co., Ltd. about the road-surface projection lamps in Section 7.

Valuable advice related to the acquisition of the license plate registration number was also received from everyone at the Road Bureau of the Ministry of Land, Infrastructure, Transport and Tourism (MLIT) as well as everyone at the Kanto and Chubu District Transport Bureaus. Full support was also received from every member of the LQ development team and the people involved in the planning and operation of the demonstration program. The authors would like to express their sincere gratitude to everyone concerned.

Authors



D. IDO



T. TAKEI



Y. IWATA



S. SEKIZAWA



S. NAKAGAWA

Support for Spectators in Wheelchairs at the Olympic and Paralympic Games Tokyo 2020 Using Human Support Robots (HSRs)

Takahiro Toda*¹
Kazuhito Tanaka*¹
Yuka Iwanaga*¹
Keisuke Takeshita*¹
Yuji Onuma*¹
Takemitsu Mori*¹

Abstract

As part of the Tokyo 2020 Robot Project, plans were made to provide support for spectators in wheelchairs at the Japan National Stadium using human support robots (HSRs). In line with the Tokyo 2020 Games Vision of staging the most innovative Games in history and bringing a positive legacy to future generations, this project aimed to help realize a deeply caring spectator experience by combining the remote control and autonomous operation functions of HSRs. This article describes how this development aimed to enable free movement of multiple HSRs within busy environments filled with people on the move in all directions.

Keywords: *Olympic and Paralympic Games Tokyo 2020, autonomous movement, remote control, human support, human-robot collaborative control*

1. Introduction

Toyota planned a wide range of initiatives to help realize the vision of the Olympic and Paralympic Games Tokyo 2020 (abbreviated below as “the Games”), namely, to stage the most innovative Games in history and bring a positive legacy to future generations. Due to the potential of robots to fulfill useful roles in close proximity to people in various situations during the Games, Toyota teamed up with the Tokyo 2020 Organising Committee, Panasonic Corporation, and other experts in the robotics field to launch the Tokyo 2020 Robot Project. The purpose of this project was to develop support robots for different sports, the Tokyo 2020 Mascot Robots, and so on.⁽¹⁾ This project also aimed to provide support for spectators in wheelchairs using a human support robot (HSR).⁽²⁾ This HSR was developed to create a stress-free experience for spectators in wheelchairs entering and leaving the Japan National Stadium by guiding the spectators to their seats and transporting various items.⁽³⁾

To help alleviate the stress involved in maneuvering a wheelchair around the crowded environs of the Japan National Stadium, the HSR was designed to help resolve various difficulties by leading spectators in wheelchairs to their seats, picking up rubbish around the seats, taking commemorative photographs, and the like. These objectives were realized through a combination of autonomous movement technologies involving the robot automatically recognizing its surrounding environment and remote control (**Fig. 1**).

As a research platform, the HSR has previously been used for researching ways of providing support to people mainly in household environments.⁽⁴⁾ In contrast, unlike home helper robots, the HSR developed for the Tokyo

2020 Games would need to operate in spacious areas filled with people on the move in all directions, and multiple HSRs would also have to be operated at the same time through a combination of autonomous and remote controls. Therefore, for the Games, a remote control system was developed alongside technology to enable movement in crowded and busy areas. This article describes the details of this development.



Fig. 1 HSR Leading Wheelchair User

2. System Configuration

2.1 Overall image

Ten PC terminals were installed in Tokyo and Aichi Prefecture to provide remote control instructions to around twenty HSRs located at the Japan National Stadium. To simplify the system, all of the remote control terminals and robots were connected to a single control server. Then, to ensure reliability, a fault tolerant (FT) server was provided with redundant backup hardware. **Fig. 2** shows the system configuration.

*¹ R Frontier Div., Frontier Research Center

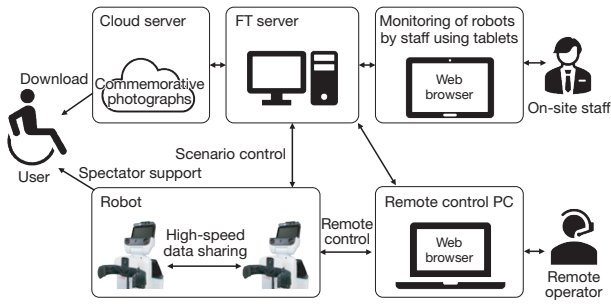


Fig. 2 Outline of System Configuration

When remote control is carried out, any remote control terminal can be paired on a one-to-one basis with any robot. In actual operation, multiple remote operators would operate multiple robots by switching control to and from each robot to support spectators in wheelchairs.

2.2 Communication system

To enable a wide range of movement, the robots are controlled by wireless communication. The robot communication system uses the 4.9 GHz frequency band, which allows highly reliable interference-free communication. Multiple wireless access points (APs) were installed at the Japan National Stadium and the robots were provided with compact and lightweight client wireless devices. The robots are capable of moving over a wide range inside the stadium while automatically switching connection between the APs. To ensure that remote control is uninterrupted when switching between the APs, the wireless system was designed to accomplish the switching procedure in less than 200 ms. The agile and high-speed Web Real-Time Communication (WebRTC) protocol was adopted to transmit the various types of data required. **Table 1** lists the details of the main types of communication carried out with the robots.

Table 1 Details of Remote Control Communication

Details		Cycle (Hz)	Communication rate (kbps)
Robot coordinate system		10	250
Images Audio	From HSR to control PC	30	Total: 2,000
	From control PC to HSR	15	
Control commands		10	10

3. Robot Hardware

Before the Games, HSRs had mainly been used in indoor household environments. The significant differences between this type of environment and the environment at the Japan National Stadium are as follows.

- Direct contact with strong sunlight

- The presence of people moving in all directions around the robot
- The need to audibly interact with people in noisy surroundings

Several items of hardware on the existing HSR⁽⁴⁾ needed to be modified to address these challenges (**Fig. 3** and **Table 2**).

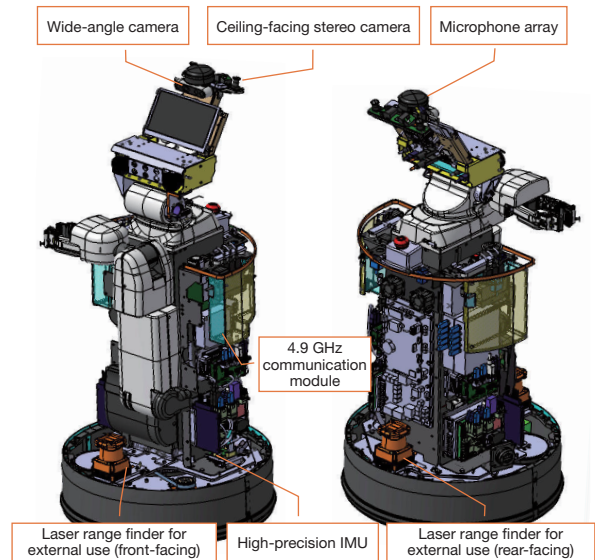


Fig. 3 Changes to Robot Hardware

Table 2 Details of Changes to Robot Hardware

Item	Details
Wide-angle camera	Camera with a 165° angle of view used for remote control
Ceiling-facing stereo camera	Stereo camera directed at the ceiling to enable localization when surrounded by people or objects (Section 4)
Microphone array	Microphone with noise cancelation function for remote control conversations
4.9 GHz communication module	See Section 2.2 for the details of the communication system.
Laser range finders for external use	Two-dimensional (2D) lidars provided at the front and rear for object detection and localization map generation (Section 4)
High-precision IMU	Inertial measurement unit used to correct the position estimation (localization function of the robot (Section 4)).

4. Development of Movement Technologies

4.1 Operation in areas filled with people moving in all directions

Ordinary autonomous movement algorithms that use 2D lidar cannot effectively utilize sensor information and maps in environments filled with people moving in all

directions. This issue has a major adverse impact on the accuracy of localization. This project developed a method that enables stable localization using a ceiling-facing camera that is less affected by moving objects.

4.2 Configuration of localization function

Fig. 4 shows the configuration of the developed localization function.

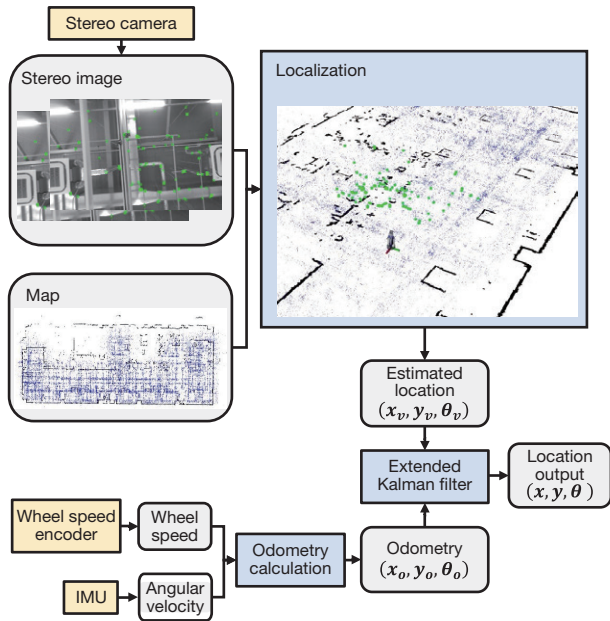


Fig. 4 Configuration of Localization Function

The robot carries out localization using characteristic points obtained from stereo camera images of the ceiling and correspondence between characteristic point groups and the map. The system combines the outputs of the HSR wheel speed encoder and IMU to calculate the robot odometry. It then applies the extended Kalman filter to these calculated odometry results to output a final location.

4.3 Localization using ceiling-facing stereo camera

This project applied the following refinements to a visual simultaneous localization and mapping (visual SLAM) technique⁽⁵⁾ that uses characteristic points. These refinements enabled map creation and localization using a stereo camera.

- (1) To remove the effects of people and other moving objects during map creation, localization results obtained using high precision 2D lidar in a static environment were inputted as reference values to optimize the map creation process.
- (2) To adjust to changes in lighting conditions over time, maps created at multiple timings were combined. This involved the selection and combination of maps for which the localization function satisfied criteria for

test data obtained at multiple timings.

- (3) To enhance the recovery rate when localization using the stereo camera fails, the matching process was set to use only areas extracted from the map within a set range centered on the location of the robot immediately before the failure.

Fig. 5 shows the map created in the Japan National Stadium after these refinements were carried out. The blue points on the map are the characteristic points obtained by the ceiling-facing stereo camera.

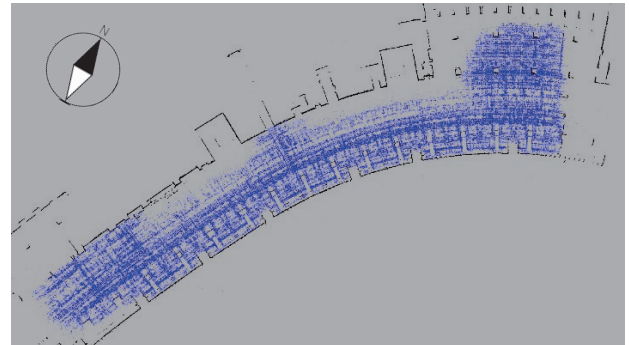


Fig. 5 Created Map of the Japan National Stadium

4.4 Evaluation of localization performance

The accuracy of the development localization function was measured at the Japan National Stadium. **Fig. 6** shows the relationship between the path of the robot and the localization error. **Fig. 7** is a pictogram that categorizes every localization result output in terms of the size of the error and plots the number of outputs in each category.

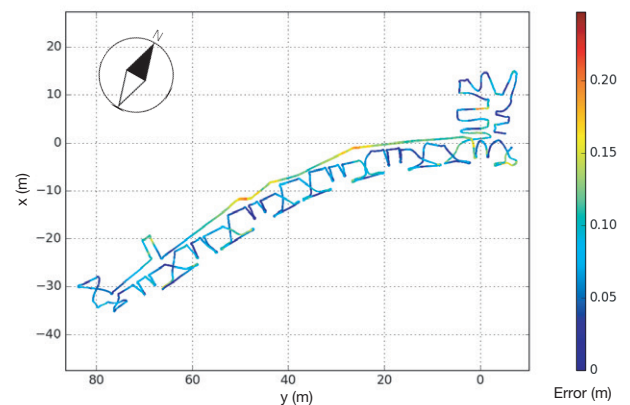


Fig. 6 Relationship between Robot Trajectory and Localization Error

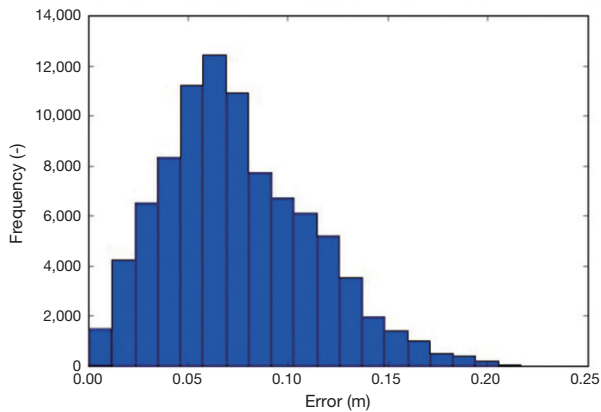


Fig. 7 Localization Error Pictogram

The root mean square error (RMSE) of the localization function was 0.084 m and the 3σ range of the error was 0.19 m. These results demonstrate that the function realized highly precise localization inside the Japan National Stadium.

5. Remote Control System

5.1 Outline of remote control system

As shown in **Fig. 8**, the remote operator uses a mouse connected to a remote control PC to operate the head, arm, and wheeled trolley portions of the robot.

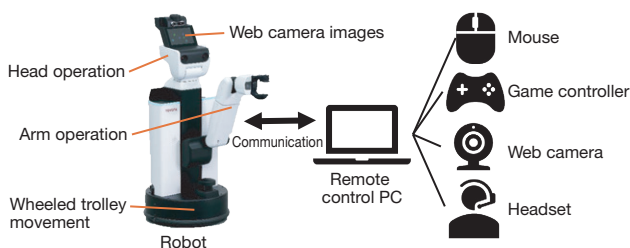


Fig. 8 Outline of Remote Control System

5.2 Remote control function

Fig. 9 shows the configuration of the remote control screen. The distinctive features of this screen include the autonomous movement function and three-dimensional (3D) view area. When the robot is moving along a path that has been determined to some degree in advance, the operator sets the destination and allows the robot to move autonomously. This function is used for movement within the concourse of the Japan National Stadium. In contrast, the game controller is used to move the robot freely around the seats of spectators in wheelchairs.

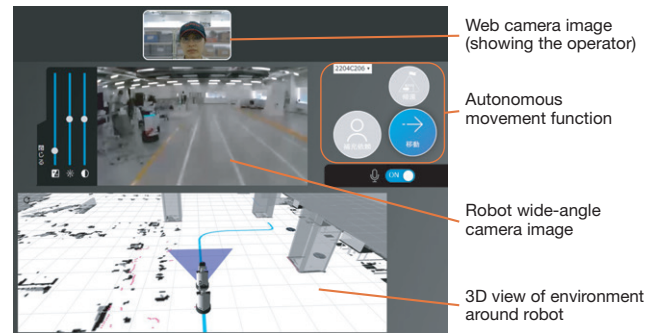


Fig. 9 Remote Control Screen

The 3D view combines static objects such as pillars and the like with information about moving objects and people recognized around the robot. During remote control, the operator identifies the presence of surrounding objects on the 3D view while monitoring the spectator in the wheelchair through the wide-angle camera installed on the robot. The viewpoint of the 3D view can be moved freely, zoomed in to identify the specific details of an object close to the robot, or zoomed out to confirm the approximate position of the object (**Fig. 10**).

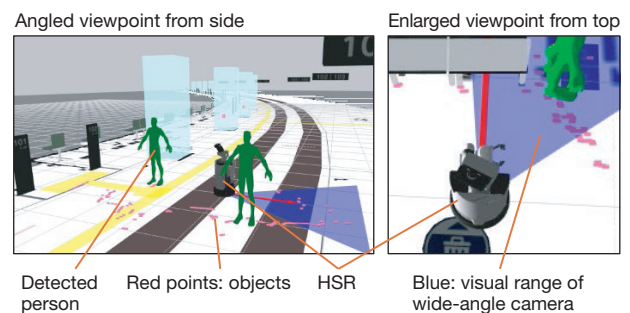


Fig. 10 Examples of 3D View

To prevent collisions with people caused by operator error, the robot is equipped with the following safety functions. These allow the robots to be operated remotely in safety and confidence.

- (1) The robot is equipped with a function that automatically adjusts the direction of the robot around the periphery of detected objects. This is mainly effective for avoiding static objects.
- (2) If the robot approaches an object that function (1) cannot avoid, the robot is equipped with a virtual bumper function that automatically stops the robot before physical contact occurs. This is mainly effective for avoiding moving objects.

6. Conclusion

This article has described the functions developed to provide support for spectators in wheelchairs at the Japan National Stadium using remote controlled HSRs. In the future, it is planned to carry out further research and

development into more advanced methods of commanding robots using a combination of autonomous and remote controls in various formats.

Acknowledgments

The authors would like to extend their sincere gratitude to everyone at the Frontier Research Center, R Frontier Division, Advanced Service Robot Group, and the Olympic and Paralympic Division for their invaluable assistance leading up to the Tokyo 2020 Games.

References

- (1) *For Innovation at the Olympic and Paralympic Games Tokyo 2020* (in Japanese). <https://olympics.com/tokyo-2020/ja/games/vision-innovation/>
- (2) T. Yamamoto, Terada, Ochiai, Saito, Asahara, Murase. “Development of Human Support Robot as the Research Platform of a Domestic Mobile Manipulator.” *ROBOMECH Journal* 6(1) (2019) pp. 1-15.
- (3) *Tokyo 2020 Robot Project Phase 1* (in Japanese). <https://olympics.com/tokyo-2020/ja/news/news-20190315-02-ja>
- (4) Toyota Global Newsroom. https://global.toyota/en/detail/8709541?_ga=2.149816246.1082389497.1637039641-1211030701.1558057516
- (5) R. Mur-Artal, Tardos. “ORB-SLAM2: An Open-Source SLAM System for Monocular, Stereo, and RGB-D Cameras.” *IEEE Transactions on Robotics* (2017) pp. 1-8.

Authors



T. TODA



K. TANAKA



Y. IWANAGA



K. TAKESHITA



Y. ONUMA



T. MORI

Development of the T-TR2 Telepresence Robot

Takahiro Nakayama*¹
Yusuke Kida*¹

Abstract

The original T-TR1 telepresence robot was developed to help elderly and physically disadvantaged people experience normally inaccessible locations through a design approach evaluated by its success in increasing connections between people. This article describes the results of the development of the next-generation T-TR2, which extended and updated this concept to create an even more realistic sensation of being in far-away places while making people in those places seem even closer.

Keywords: telepresence robot

1. Background and Purpose

Toyota's first telepresence robot, the T-TR1,⁽¹⁾ projects images of a person from a remote location that are realistic enough to make that person appear to be right in front of the user. The T-TR1 combines communication devices such as cameras, a microphone, display, and speaker with a mobile platform so that the caller can accompany the user's movements.

The T-TR1 was designed to enable people interested in or unable to attend the Olympic and Paralympic Games Tokyo 2020 to attend the Games virtually. With this objective, the T-TR1 was developed and operated based on the idea of providing opportunities for communication. More specifically, the T-TR1 was designed to project images of torchbearers unable to attend the Torch Relays and depict them carrying the Olympic flame. It was planned to use the T-TR1 at three legs of the Torch Relays: at the Tokyo 2020 Olympic Torch Relay in Aichi Prefecture in April and in Tokyo in July, and at the Tokyo 2020 Paralympic Torch Relay in Tokyo in August. **Fig. 1** shows an outline of the T-TR1. The T-TR1 is equipped with an arm capable of carrying the Olympic torch in the Torch Relays. The dimensions of the robot are 2,070 mm (height) × 942 mm (length) × 668 mm (width, including arm: 866 mm). The T-TR1 weighs 152 kg and uses an LED display to make sure that the images on the screen are visible during the day and in direct sunlight.

The screen size is equivalent to 60 inches and the number of pixels is 240 × 600. **Fig. 2** shows the system configuration. The upper part of the T-TR1 consists of the communication devices and the upper PC that connects the devices. The lower part consists of the lower PC that is used to control the wheels, sensors, a motor driver, an in-wheel motor, and a battery. The T-TR1 is powered by a 24 V battery (operating voltage: 20 to 28.8 V) that directly supplies power via a fuse box to a DC-DC converter that sets the specific voltage. The robot is

operated by a 920 MHz wireless controller. The system is designed so that operator controls the robot from close range as a safety supporter in the Torch Relay team.

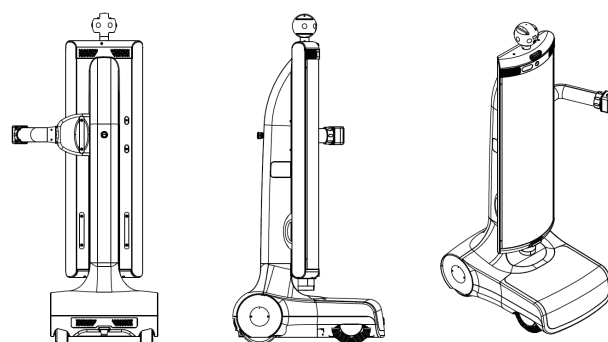


Fig. 1 External Appearance of T-TR1

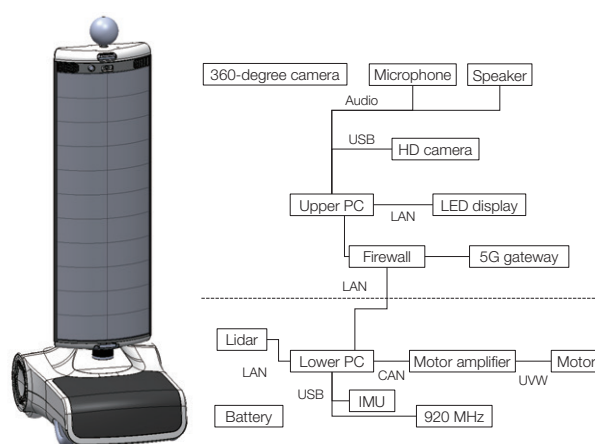


Fig. 2 System Configuration of T-TR1

*¹ New Business Planning Div., Business Development Group

2. Development of Updated Robot

2.1 Background

With the Tokyo 2020 Games being delayed a year, an updated version of the T-TR1 was developed by supplementing the basic concept of the T-TR1 (to increase connections between people and to help elderly and physically disadvantaged people experience normally inaccessible locations) with the following two important elements.

- The creation of a highly realistic sensation of being in a far-away location
- The creation of a convincing impression that a person in a far-away location is actually present (through projections on the robot screen)

First, to create a highly realistic impression of being in a far-away location, the development aimed to enhance the sensation of carrying the Olympic flame in a Torch Relay. More specifically, this meant supplementing the operation of the T-TR1, which was only capable of raising and lowering the Olympic torch, with the ability to move the robot in a straight line via the actual wheelchair of the torchbearer projected on the screen.

Next, to create a convincing impression that a person in a far-away location is actually present (through projections on the robot screen) to the people around the robot, the development studied the adoption of a multi-directional display. Since the T-TR1 is only equipped with a front-facing LED display this was supplemented in the T-TR2 by a rear-facing display. The screens were also upgraded to organic electroluminescent displays (OLEDs) with full high-definition (HD) resolution so that the facial expressions of the people being projected can be seen clearly. As a trade-off effect, however, since these OLEDs are not particularly bright, it was assumed that the robot would be used indoors or after sunset.

In addition, by combining images of the remote user with images obtained from the robot cameras, the development aimed to create the impression that the user was actually running in the Torch Relay.

Other updates included changing the replaceable battery of the T-TR1, which was an issue because the remaining battery charge could not be monitored, with the rechargeable battery used in the Human Support Robot (HSR). This simplified the running of the Torch Relays without having to change the power supply voltage or main component parts. The front and rear wheels were also equipped with suspensions to enhance the maneuverability of the robot.

2.2 Development to enhance sensation of being in far-away location

A system was constructed so that the robot can be operated using a normal wheelchair.

Fig. 3 shows the hardware configuration of this system. To identify the speed of the wheelchair, parallel values

outputted from encoders positioned on a dynamometer are converted to angular values by an interface (I/F) device, and inputted to the portal PC at the remote location via USB. The portal PC converts these angular values to command values and transmits the converted values to the robot via the Internet. The lower PC inside the robot then outputs operational commands to the motor driver by CAN communication.

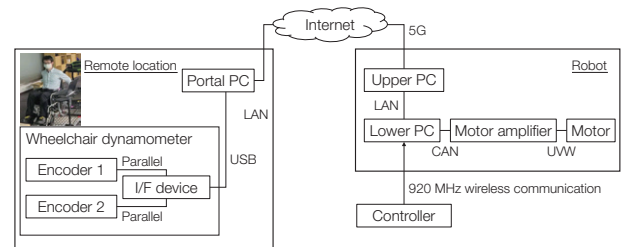


Fig. 3 Hardware Configuration of Wheelchair Operation

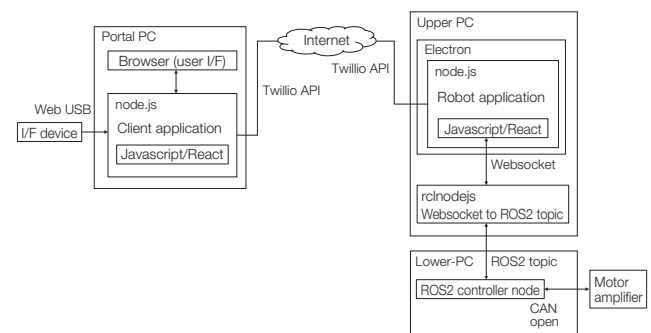


Fig. 4 Software Configuration of Wheelchair Operation

Next, **Fig. 4** shows the software configuration. The encoder values are obtained by the client application from the I/F device using the Web USB protocol. The client application directly generates straight-on movement and turning commands based on the values obtained from the I/F device. A Twilio application programming interface (API) is used to transmit these commands to the robot via the Internet. The robot is installed with an application that obtains these command values, which are converted to Robot Operating System 2 (ROS2) topics via the WebSocket protocol and transmitted to the lower PC. The lower PC then converts the obtained command values to the CAN open protocol and transmits the values to the motor amplifier.

Tests confirmed that this hardware/software configuration is capable of turning and moving the robot in a straight line via the Internet. However, when operation was confirmed using the actual robot, it was found that delicate robot control using only the remote portal PC was difficult due to Internet communication delays, the response of the motor amplifier, the condition of the road surface, and the like. As a result, remote control was restricted to movement in a straight line. If

the robot strays off course, a safety operator close to the robot would override the remote control with a signal from the 920 MHz wireless controller to correct the position of the robot.

2.3 Development to enhance impression that person in far-away location is present

A system was constructed that combines images obtained from the robot cameras with solo images of the remote user as a way of effectively projecting the remote user onto the robot and enhancing the impression that the remote user is actually present.

Fig. 5 shows the hardware configuration of this system. The robot is equipped with both a front- and a rear-facing screen and two accompanying front and rear cameras. The images from the front-facing camera are shown on the rear-facing display, and images from the rear-facing camera are shown on the front-facing display.

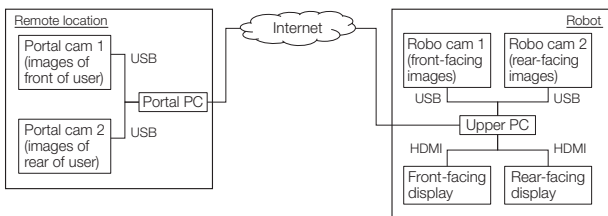


Fig. 5 Configuration of Hardware to Enhance Impression that Person in Far-Away Location Is Present

Fig. 6 shows the software configuration. The two front- and rear-facing cameras are integrated with the upper PC via the GStreamer framework. Simultaneously, the system obtains images of the front and rear of the user from remote portal cams 1 and 2 via the Internet.

The portal PC recognizes and extracts the user from the images obtained from portal cams 1 and 2. Ranges other than the user are transmitted via the Internet to the robot with the following color values: red (R) = 0, green (G) = 255, and blue (B) = 0. The user is extracted from the images by range and skin detection.

Processing by the robot makes the non-user elements of the image transparent by setting the G = 255 pixel alpha value of the user images obtained via the Internet to zero. By superimposing these zero values on the display, the system can insert the remote user into the background of the robot.

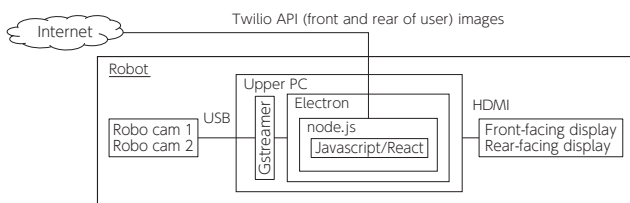


Fig. 6 Configuration of Software to Enhance Impression that Person in Far-Away Location Is Present

Fig. 7 shows the results when a person is superimposed onto the background using the T-TR1 simulator. In addition, **Fig. 8** shows the verification results using an actual display in the event that the web API is used instead of the GStreamer framework. In this verification configuration, ordinary web cameras were connected to the upper PC for the robot cameras and the front-facing display was used.



Fig. 7 Superimposed Image of User and Background



Fig. 8 Verification Using Actual Display

3. Updated Robot Development Results

3.1 T-TR2

Fig. 9 shows the T-TR2 robot that was developed for the Tokyo 2020 Olympic Torch Relay at Toyota's Head Office in April. **Table 1** lists the main specifications. Because of the larger curvature of the OLEDs, the T-TR2 is approximately 10 cm wider than the T-TR1. The T-TR2 weighs around 140 kg and is equipped with 55-inch full-HD front- and rear-facing OLEDs that have a curvature of 1,000 R. The speed of the T-TR2 is the same as that of the T-TR1. A top speed of 6 km/h was assumed based on the fast walking pace used in the Torch Relays.

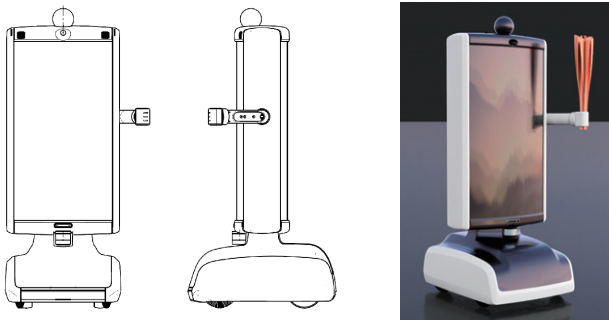


Fig. 9 External Appearance of T-TR2

Table 1 Main Specifications of T-TR2

	Height (mm)	Length (mm)	Width (mm)	Weight (kg)	Screens (inches)	Pixels
T-TR2	1,907	1,000	780	140	55	1,920 × 1,080
T-TR1	2,070	942	668	152	60	240 × 660

3.2 Issues and measures for the future

Several issues were identified in the test runs and rehearsals carried out before the actual Torch Relays.

(1) Directional stability at low speed

The directional stability of the robot deteriorated at low speed, which was probably due to an issue of motor calibration. This issue occurred when the left/right position of the robot was adjusted by short-range wireless control during operation of the robot via the user's wheelchair. The cause was identified as the reduction in speed that occurred when the wireless speed command was slower than the current speed of the robot.

As a consequence, it was decided to suspend the wheelchair-based straight line movement control during the actual Torch Relays.

In the future, the development team intends to study how to combine the command values from the remote and short-range controllers in accordance with motor calibration and its characteristics.

(2) Accuracy of user extraction from images

In the verifications, the accuracy of skin detection deteriorated due to the effects of the environment (lighting and background) at the remote test venue (a hall at the Mikawa Aotori Medical Consultation Center in Aichi Prefecture). It was found that hand waving particular affected accuracy and that the RGB quality of the user range images was not high enough. As a result, the processing was changed to include nearby children cheering on the user as a way of raising the resolution of the displays.

In the future, the development team intends to study a user extraction technique based on the background matting method⁽²⁾ to help enhance the accuracy of images combining the user and background.

4. Conclusion

The development of the updated T-TR2 focused on two important person-centric concepts of the T-TR1, namely the sensation of being in a far-away location, and the impression that a person in a far-away location is actually present.

At the Torch Relay held at the Toyota Head Office in April, remote users were successfully projected onto the robot, creating the impression that those people were actually present at the Relay. The development team plans to address the issues identified in the development project for the next Torch Relay.

The authors would like to express their sincere gratitude to everyone on the virtual mobility (VM) team, including Dr. Gill Pratt and Mr. Max Bajracharya, the Chief Executive Officer and Vice President (VP) of the Toyota Research Institute (TRI), for providing the connection concept and base system for the T-TR2 in this development, as well as everyone in the New Business Planning Division, the R Frontier Division, and the Olympic and Paralympic Division for their invaluable support leading up to the Torch Relays.

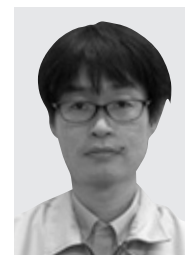
References

- (1) Toyota Research Institute News & Features. <https://www.tri.global/news/toyotaintroduces-tris-t-tr1-a-virtual-mobility-2019-7-22/>
- (2) S. Sengupta et al., "Background Matting: The World Is Your Green Screen," *Proceedings of IEEE Conference on Computer Vision and Pattern Recognition (CVPR)* (2020) pp. 2288-2297.

Authors



T. NAKAYAMA



Y. KIDA

Development of Field Support Robot (FSR)

Takeshi Kuwabara*¹
Satsuki Yamane*²
Takeshi Shigemoto*¹

Abstract

A field support robot (FSR) was developed to assist the throwing and rugby sevens events at the Olympic and Paralympic Games Tokyo 2020 while working in close proximity to people. In the throwing events, the FSR used artificial intelligence (AI) and robotics technologies to carry and autonomously transport the thrown objects recovered by the event officials, thereby helping to reduce recovery times and reduce the physical burden of the officials. In the rugby sevens event, the FSR autonomously delivered and dropped the ball at the center of the field before kick-off to help make the games run more smoothly. In addition to the autonomous driving mode realized using lidar, cameras, batteries, and other components, the FSR was also provided with a human-following mode, a mode to avoid collisions with objects, a manual driving mode, and an emergency stop mode.

Keywords: FSR, autonomous mode, following mode, collision avoidance, AI, lidar, camera, GNSS, robot, karakuri

1. Introduction

Under the concept of mobility for all, Toyota used various types of robots to provide support to visitors and organizers at the Olympic and Paralympic Games Tokyo 2020. One of these was the field support robot (FSR) developed to assist the throwing and rugby sevens events while working in close proximity to people (**Fig. 1**).



Fig. 1 FSR

2. Approach to FSR Development

The FSR used artificial intelligence (AI) and robotics technologies to carry and autonomously transport thrown objects recovered by officials in field events (the discus, javelin, and hammer throwing events in the Olympic Games, and the club throwing event in the Paralympic Games), thereby helping to reduce recovery times and reduce the physical burden of the officials.

In the rugby sevens event, the FSR autonomously delivered and dropped the ball at the center of the field immediately before kick-off to help make the games run more smoothly.

Previous Olympic and Paralympic Games used radio controlled cars to retrieve the thrown objects. However, at Olympic and Paralympic Games held in the middle of summer, it is extremely stressful and difficult to steer a radio controlled car to a point on the field several tens of meters away while avoiding athletes, officials, media personnel, electronic display boards, and the like. Repeatedly carrying the thrown objects, which weigh around 8 kilograms, to a radio controlled car waiting in the foul zone to the side of the field after the throw is also an exhausting task.

Therefore, for the Tokyo 2020 Games, Toyota took on various projects to help make the Games run more smoothly and to reduce the physical burden of the officials using automated technologies incorporating the robotics and AI technologies nurtured through its manufacturing expertise.

The fact that the FSR can follow behind the recovery officials to the location of the thrown object means that the thrown objects need to be transported for shorter distances. The autonomous driving capability of the FSR also means that radio control is no longer required.

3. Outline of FSR Operation

The autonomous driving system of the FSR consists of five modes: autonomous driving, collision avoidance, human-following, manual, and emergency stop modes.

1) After the athlete throws the object, a retrieval official moves from the standby position to recover the object. The FSR follows the official to the location of the thrown

*¹ CV Management Div., CV Company

*² Toyota Motor East Japan, Inc.

object.

2) At the location of the thrown object, the official picks up the object and places it into the FSR. The FSR determines that the object has been retrieved when a touchless switch activates. The FSR then switches into autonomous driving mode and goes to the object return location.

3) At the return location, another official recovers the thrown object from the FSR, which determines that recovery has been completed when the touchless switch activates again. The FSR then returns to the standby position in autonomous driving mode. This action is repeated during the event (Fig. 2).

4) The FSR is capable of autonomously driving while avoiding collisions with athletes, officials, media personnel, electronic display boards, and so on.

5) The FSR is also equipped with a wireless manual driving mode to transport the FSR and perform emergency stops, as well as an emergency stop mode.

Ball delivery during the rugby sevens event is carried out in autonomous driving mode.

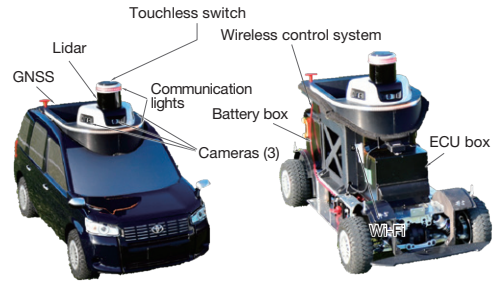


Fig. 3 Outline of FSR Configuration

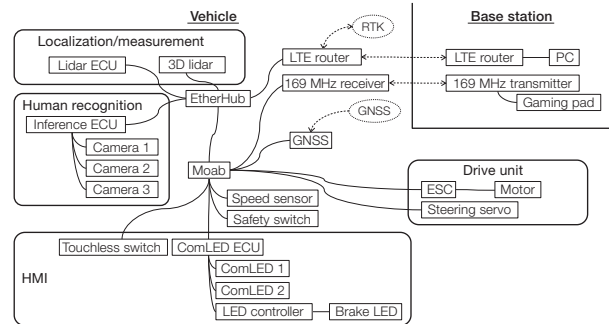


Fig. 4 FSR System Diagram

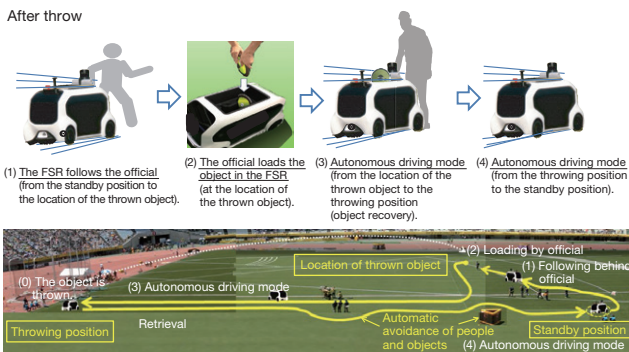


Fig. 2 Outline of FSR Operation



Fig. 5 Main ECU (Inside ECU Box)



Fig. 6 Internal View of Battery Box

4. Configuration of FSR

The FSR hardware consists of two NUC mini PCs manufactured by Intel Corporation, a vehicle control interface board, lidar, and three cameras (Figs. 3 and 4).

The two Intel NUCs function as the main autonomous system ECUs. One carries out lidar point group processing and vehicle control, while the other carries out the AI inference (Fig. 5).

The FSR is powered by six Japanese-made replaceable lithium-ion batteries (127 Wh) installed in series (Fig. 6). Nine DC-DC converters manufactured by Attraclab Co., Ltd. are used to step the voltage down from 24 V to 15 V, 12 V, and 5 V.

5. Autonomous Driving System of FSR and Associated Functions

This section describes the hardware and software that enables the autonomous driving system to realize the driving modes and functions of the FSR.

5.1 Autonomous driving

In autonomous driving mode, the FSR can travel at a top speed of 20 km/h from the location of the thrown object to the return position, and from the return position to the standby position.

At the return position, the official working with the FSR covers the touchless switch at the top of the FSR by hand to activate autonomous driving mode.

Although a mechanical switch was initially adopted, it was decided to adopt an infrared touchless switch as a measure to help prevent the spread of the novel coronavirus COVID-19.

In autonomous driving mode, information about the distance travelled obtained from the vehicle speed sensors installed at the rear wheels, information about the location of the FSR obtained by comparison between a pre-prepared map of the Competition Venue and the shape of the Competition Venue measured by lidar during FSR operation, and Real Time Kinematic-Global Navigation Satellite System (RTK-GNSS) information are combined to estimate the position of the FSR and guide it to the target destination.

The New National Stadium, which was the venue for the throwing events at the Tokyo 2020 Games, has a maximum length of approximately 130 meters between the walls of the event field. Therefore, a 200 meter-class lidar was adopted to ensure reliable measurement (Fig. 7).

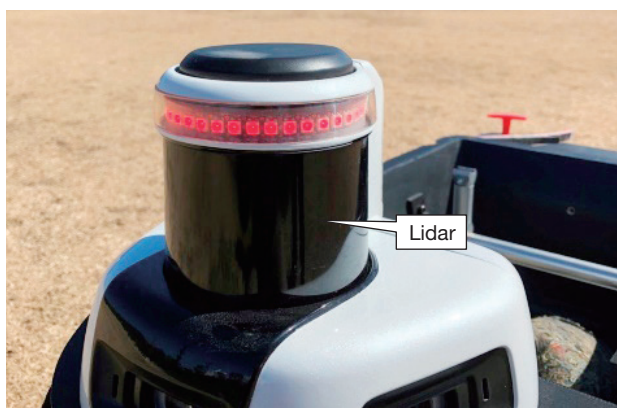


Fig. 7 Quanergy M8 Ultra Lidar

Hall integrated circuit (IC) type vehicle speed sensors are attached to the rear differential joint cups at the left and right of the FSR. These sensors are synchronized with the tire rotation and output four pulses per rotation.

To enhance accuracy and realize a fail-safe function, the FSR speed is calculated from the sensor information obtained from both left and right wheels (Fig. 8).

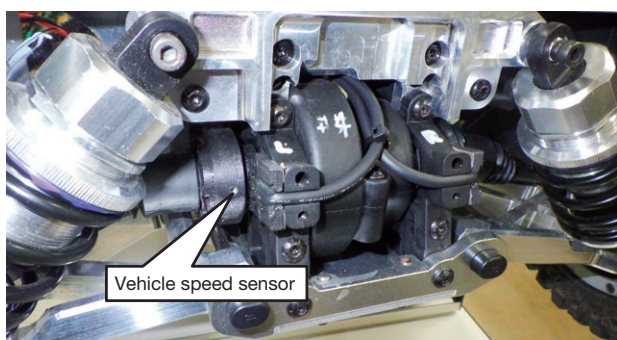


Fig. 8 Vehicle Speed Sensor

The FSR is capable of nine degree-of-freedom (DOF) acceleration. This function utilizes an acceleration sensor installed on the Moab vehicle control interface board kept in the rear ECU box (Fig. 9).

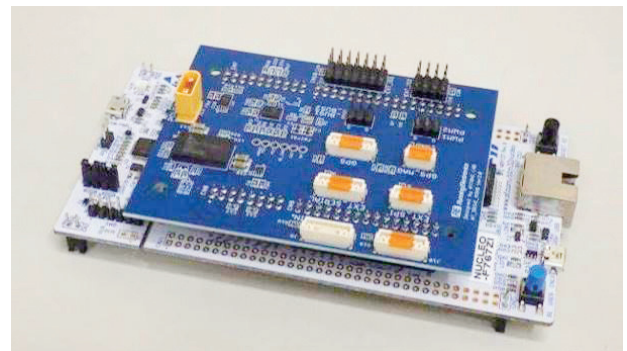


Fig. 9 Moab Board for FSR Manufactured by Attraclab Co., Ltd.

The Moab board is the most important control board in the FSR since it connects the drive control, steering, and autonomous driving systems. It was designed emphasizing reliability and features an extremely simple microcomputer and input/output (I/O) devices. When an object such as a javelin or hammer is placed in the FSR, the height of the center of gravity increases. To prevent the FSR rolling over when steered, the Moab board also incorporates an algorithm that restricts the maximum steering angle in accordance with the vehicle speed.

In autonomous driving mode, the lidar operates along a pre-set route (Fig. 10).

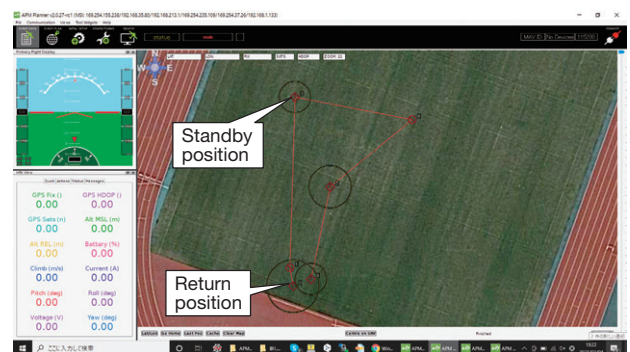


Fig. 10 Route Setting Screen

The driving route was studied using AI with learning carried out inside Toyota Motor East Japan, Inc.

Fixed camera images taken at events held at the National Sports Festival in Ibaraki were analyzed using AI, and a heat map of the positions of the officials and camera crews was created. Based on this heat map, the route of the FSR was designed to avoid interaction with people as much as possible (Fig. 11).



Fig. 11 Heat Map of Positions of Officials and Camera Crews Obtained by AI

5.2 Collision avoidance

In autonomous driving mode, the FSR activates a forward-monitoring collision-avoidance function.

This function detects objects using lidar. The lidar beams consist of a horizontal beam and two beams directed at three-degree downward angles (**Fig. 12**).

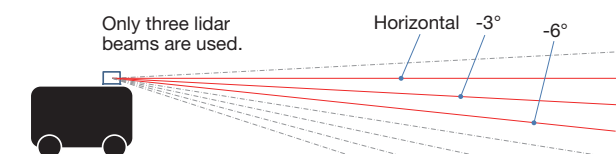


Fig. 12 Side View of Lidar Beam Lines

For enhanced reliability, the collision avoidance algorithm was developed to function based on simple rules.

The algorithm switches between three levels depending on the distance between the FSR and a detected object.

The area that extends one meter from the FSR is called the black zone, the area between one and three meters from the FSR is called the red zone, and the area between three and five meters from the FSR is called the yellow zone. Operation in these zones is defined in advance (**Fig. 13**).

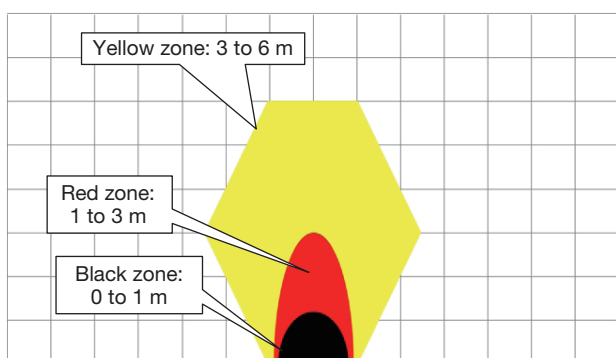


Fig. 13 Collision Avoidance Zones

If the object is in the black zone, the FSR will come to a stop by full braking and wait until the object moves away before starting to move again.

In the red zone, the FSR will slow to a forward speed of 2 km/h and avoid the object by turning up to the maximum steering angle.

In the yellow zone, the FSR will slow to 10 km/h and avoid the object by turning up to 50% of the maximum steering angle.

Model-based development (MBD) was used for part of the collision avoidance function development (**Fig. 14**).

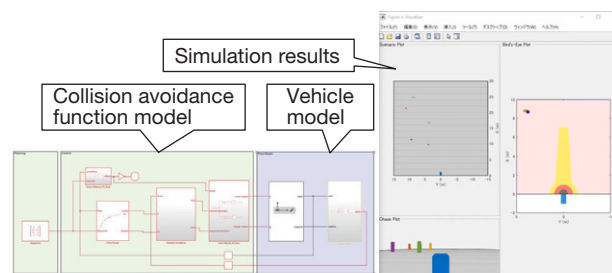


Fig. 14 Collision Avoidance Simulation

The characteristics of the FSR and the algorithm were modeled and simulations carried out to reproduce the shapes of the collision avoidance zones and the operation in each zone.

The simulation scenarios were generated using the AI-based location frequency analysis and line of movement analytical technologies developed by Toyota Motor East Japan, Inc. (**Fig. 15**).

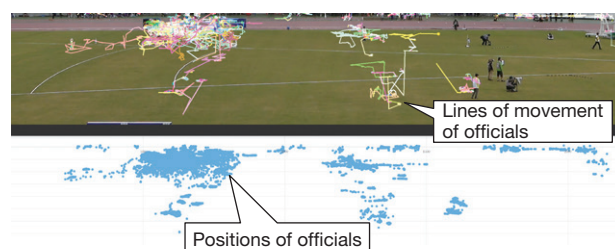


Fig. 15 Line of Movement Analysis

In addition to collision avoidance triggered by detection from the on-board sensors, the FSR is also provided with a geofencing function capable of registering objects to be avoided and areas in which driving is permitted. The geofencing function operates in conjunction with the FSR localization function and activates collision avoidance when the FSR approaches a set area even if the sensor signals do not detect an object. This function enables the FSR to fully avoid boards displaying the distance of thrown objects, electronic display boards, and camera crew seats.

5.3 Human-following

In human-following mode, the FSR uses AI to drive on the field behind an event official.

The FSR is equipped with the commercially available C930 web camera manufactured by Logicool Co., Ltd. In this mode, the event official is recognized using AI from RGB images obtained by this camera and a boundary box is created. The target angle to the event official is calculated using the center point of the boundary box. Next, the closest point to the FSR from a point group created by the horizontal lidar beam in the horizontal angle region defined by the boundary box is used as the distance to the event official. The processing described above is carried out for each frame and the FSR is

controlled to remain at a distance of three meters from the event official (**Fig. 16**).

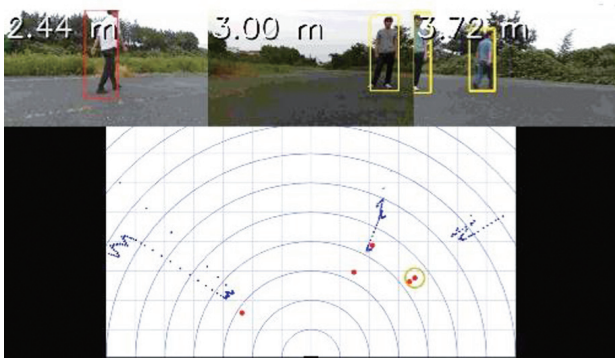


Fig. 16 Human Recognition Using On-Board Camera in Human-Following Mode

Combining a web camera with AI and lidar enables a following function with compact and agile processing.

5.4 Manual driving

The FSR is also installed with a wireless controller to transport the FSR and perform emergency stops (**Fig. 17**).

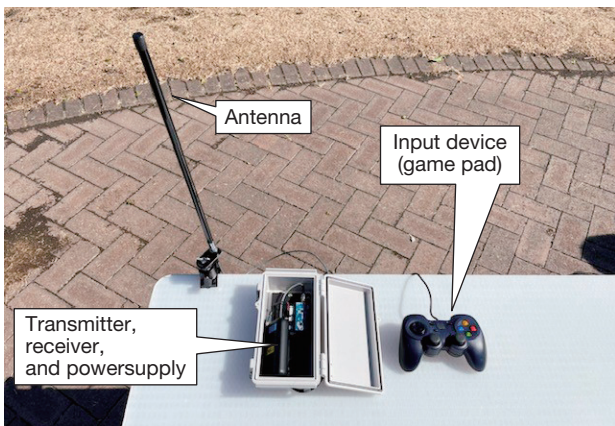


Fig. 17 169 MHz Controller

The FSR uses two control systems: a general-purpose 2.4 GHz radio controller and a controller that uses the dedicated 169 MHz frequency for drones.

During the period of the Tokyo 2020 Games, the FSR used the 169 MHz frequency since regulations prohibit the use of the 2.4 GHz frequency inside the New National Stadium.

5.5 Emergency stop

Although the FSR is equipped with an autonomous collision avoidance system, it can be stopped remotely if a collision looks imminent for some reason or a system error causes a loss of control.

An emergency stop command can be transmitted using

either the 2.4 GHz radio controller or the 169 MHz controller.

Emergency stop commands are inputted directly into the Moab board and transmit a full braking command directly to the drive device without passing through the autonomous system ECU or on-board local area network (LAN).

In addition, the FSR will also stop automatically if the 2.4 GHz or 169 MHz communication link is interrupted during autonomous driving.

5.6 Ball delivery function

For the rugby sevens event, a *karakuri* mechanism (*karakuri* refers to a traditional Japanese clockwork or mechanized device) developed by Toyota Motor East Japan, Inc. was installed in the bath tub storage area of the FSR.

The FSR drops the ball after stopping in the center of the field. This occurs when a signal is received from the autonomous system to activate a servo motor, thereby releasing the lock that fixes the *karakuri* mechanism in place (**Fig. 18**).

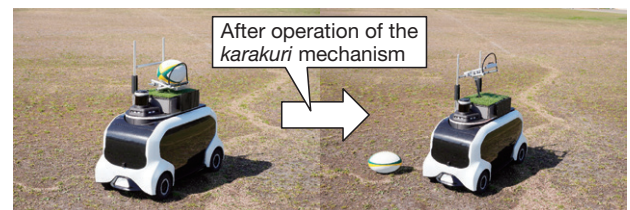


Fig. 18 Karakuri Mechanism

5.7 Communication function (lights)

One of the major characteristics of the FSR is its communication lights. The top of the FSR includes an LED ribbon capable of RGB animation. This ribbon shows the status of the autonomous driving system, detected objects, and the target direction during human-following mode.

When an AI-equipped intelligent robot is interacting with a human, it is important to communicate to that human what the robot is thinking and what decision it intends to implement next.

Looking people in the eye is an important part of human communication. Communication lights were developed for the FSR to simulate this capability.

The communication lights on the FSR consist of a small band of lights on the lidar and a larger ribbon of lights circling the top of the FSR.

The small band of lights turn on while waiting for an input to the touchless switch at the top of the FSR.

The color of the larger light ribbon communicates the mode of the autonomous driving system (**Fig. 19** and **Table 1**).



Fig. 19 Communication Lights

Driving mode	Color of communication lights
Autonomous driving mode	Purple and light blue (markers)
Human-following mode	Light blue and red (markers)
Stopped in fixed position	Green (flashing)
Manual operation	Orange and white (animation)
Emergency stop	White

Table 1 Relationship between Color of Communication Lights and Driving Mode

In autonomous driving mode, the direction of objects detected by the collision avoidance function is displayed by a light blue marker. This informs officials around the FSR that the FSR is about to carry out an avoidance maneuver.

In human-following mode, the direction of the human locked onto by the AI and lidar control is shown using a red marker. The presence of a marker shows the officials whether the FSR has recognized the human it should be following.

6. Calibration and Field Operational Tests (FOTs)

6.1 Calibration

Assuming that the FSR would be used on grass, the grassy area of a sports park in Susono, Shizuoka Prefecture, was borrowed to calibrate the FSR (Fig. 20).



Fig. 20 Calibrating the FSR

6.2 FOTs

During the development period, valuable cooperation was received from various people and organizations, including the Japan Association of Athletics Federations and the Japan Rugby Football Union. The operation of the FSR was tested and improved at events inside Japan, such as the National Sports Festival in Ibaraki.

6.2.1 Improvement of camera anti-fogging performance

When the FSR was tested in the rain, the camera lens fogged up, preventing the AI system from recognizing people. This issue was addressed by improving the ventilation path and led to the in-house development of an internal camera heater (Fig. 21).

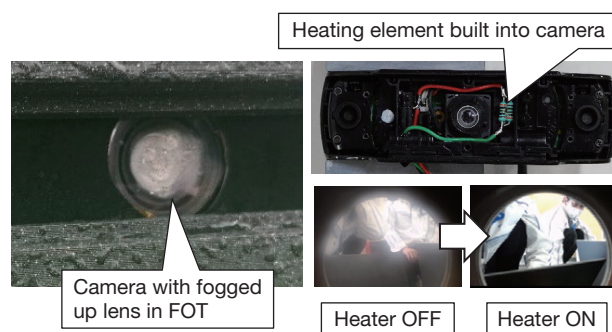


Fig. 21 Camera Heater

6.2.2 Reduction in driving noise

At the 2019 Japan Para Championships, athletes commented about the driving noise generated by the FSR.

Frequency analysis discovered that the main component of this noise was vibration caused by engagement of the primary reduction gear on the motor output shaft (Fig. 22). The following countermeasures were adopted.

Commercially available spur gears generate high levels of noise and vibration during gear engagement. Since the main cause of this gear vibration is transmission error fluctuation, a new helical gear with lower transmission

error fluctuation than a spur gear was designed and manufactured (**Fig. 23**).

To reduce the radiation of operation noise, a gear box was added around the gears to block generated noise (**Fig. 24**).

This gear box was fixed to the under body of the FSR through vibration-absorbing rubber, which helps to suppress the transmission of vibration to different parts of the FSR (**Fig. 25**).

Even quieter operation was achieved by fitting sound absorbing material to the back surface of the upper body to suppress noise radiation (**Fig. 26**).

These countermeasures reduced the driving noise of the FSR below the background noise of the event venue. No further comments were received from athletes in the FOTs about driving noise.

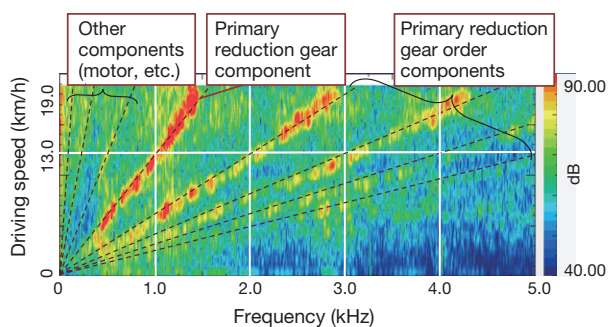


Fig. 22 Frequency Analysis of Driving Noise



Fig. 23 Helical Gear

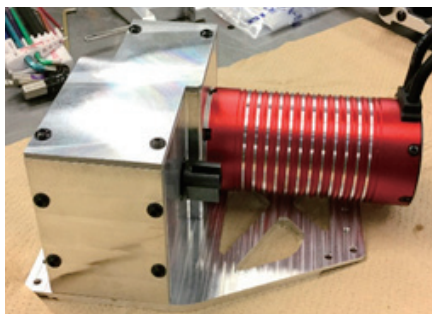


Fig. 24 Gear Box

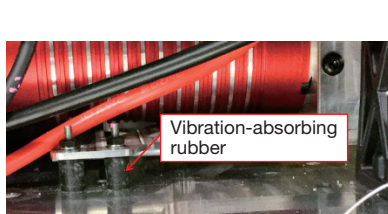


Fig. 25 Vibration-Absorbing Rubber



Fig. 26 Sound Absorbing Material

7. Conclusion

A compact autonomous driving FSR with friendly design and behavioral characteristics was developed. These characteristics are regarded as having potential applications in different fields, and the goal is to use the experience gained through developing the FSR to provide new types of services in the future.

The development of the FSR was carried out with the invaluable cooperation of a large number of people, including those involved in each of the events. The authors would like to extend their sincere gratitude to everyone that contributed to this development.

Authors



T. KUWABARA



S. YAMANE



T. SHIGEMOTO

Development of Tokyo 2020 Mascot Robots

Tomohisa Moridaira*¹
Hirohito Hattori*¹
Masahiro Doi*¹
Hiroyuki Iyama*¹
Hiroyuki Kondo*¹
Kazuya Yamamoto*¹

Abstract

As part of the Tokyo 2020 Robot Project, the Tokyo 2020 Organising Committee and Toyota developed robotic versions of Miraitowa and Someity, the official mascots of the Olympic and Paralympic Games Tokyo 2020. In addition to making extensive refinements to the original models that were announced in 2019, the specifications of the new models were upgraded to create realistic mascot characters. While following the endearing design cues selected and voted for by elementary school students, highly expressive mascot robots were developed with smooth full-body movements and various eye expressions. This article describes the development of these mascot robots.

Keywords: *Olympic and Paralympic Games Tokyo 2020, humanoid robot, soft skin, GaN, remote control, VR*

1. Introduction

Under the vision of staging the most innovative Games in history and bringing a positive legacy to future generations, the use of advanced technologies in a wide range of fields was planned for the Olympic and Paralympic Games Tokyo 2020 (abbreviated below as “the Games”). In the robotics field, the Tokyo Organising Committee of the Olympic and Paralympic Games worked with Toyota, Panasonic Corporation, and other partner companies to launch the Tokyo 2020 Robot Project. In this project, the use of robots was studied in various scenarios such as event and spectator support. As part of this approach, Tokyo 2020 Mascot Robots were developed and announced at an event in 2019, a year before the original date of the Games.⁽¹⁾ The aim of these mascot robots was to help children unable to come to the venues to enjoy the Games from afar. This event showcased the remote operation and force-feedback functions that enabled people to interact with each other through the motions of the robots, as well as the image and voice recognition-based autonomous human interaction functions of the robots.⁽²⁾

The subsequent year-long postponement of the Games prompted a re-examination of this approach. With the coronavirus pandemic forcing a wide range of restrictions on school activities and the like, discussions were held about using the mascot robots to help create positive memories of the Games in children. Therefore, it was decided to substantially alter the specifications of the mascot robots to create a much richer user experience through, for example, making the robots seem more real, enabling interaction with children and coordinated dancing, while retaining the computer graphic (CG) style proportions of Miraitowa and Someity (the official

mascots of the Games) that symbolize the mascots' backstory of being transported from the digital world, as highlighted when the mascots were announced.

The original 2019 models were developed based on the concept of remote control and were not equipped with autonomous movement functions. In contrast, the new 2021 models were developed as full-scale humanoid robots with a higher quality external appearance and high-performance dynamic functions, including the capability to walk and perform full-body dance moves.

The development focused on the following three points with the aim of realizing realistic mascot robots capable of acting as a natural part of the surroundings.

- (1) An external appearance that de-emphasized the robotic look of the original model
- (2) The realization of nimble and smooth movements
- (3) Natural human interaction

To realize these points while maintaining the design and proportions of the original robots, the development supplemented Toyota's existing humanoid robot technologies⁽³⁾⁽⁴⁾ with a wide range of new technologies. This article describes an outline of these technologies.

2. Mechanisms

2.1 Comparison of basic mechanisms of original and new models

Figs. 1 and 2 compare the external appearance and **Table 1** compares the basic specifications of the original 2019 models and the new 2021 models.

*¹ R Frontier Div., Frontier Research Center



Fig. 1 One of the Original Models



Fig. 2 The New Models

Table 1 Comparison of Basic Specifications of Original and New Models

	Original models	New models
Size	Height: 60 cm Weight: 6 kg	Height: 65 cm Weight: 10 kg
Joint DOFs	Arms: (4 active axes, 1 passive axis) × 2 Legs: (4 axes) × 2 Neck: 2 axes Total: 20 axes	Arms: (6 axes) × 2 Legs: (6 axes) × 2 Neck: 3 axes Pelvis: 1 axis Total: 28 axes
Shell Skin	Hard plastic	Soft shell Soft skin

The photographs show that the new models combine the endearing design cues of the original models with a more refined exterior incorporating a soft skin that covers the robot joints, as well as a much wider range of physical expressions.

Although the new models have more flexible joints with eight additional axes of movement, the new models are only approximately 5 cm taller than the original models.

Both the arms and legs of the new models have six degrees of freedom (DOFs), which allows the ends of the limbs to be moved into any position and enables fully humanoid actions. These specifications also enable free bipedal locomotion and dance steps. The DOFs of the pelvis and neck were also increased to further enhance the expressive capabilities of the robots.

2.2 Facial expressions

In addition to enabling greater physical expressions by increasing the joint DOFs, one of the major features of the mascot robots is the ability to express emotions via animated eye displays (Fig. 3).

Due to the large area occupied by the eyes and the highly curved head, a flat display would be incapable of following the three-dimensional curved surface of the head. The display surface would sink to the bottom of the eyes, causing an unrealistic impression. For this reason, the robots are equipped with flexible organic light-emitting diode (OLED) displays that bend along the two-dimensional curved surface of the head. These displays are protected by a transparent thin acrylic lens that has a

two-dimensional surface on the display side and a three-dimensional surface on the outside.

In addition to excellent color expression, the curved design of the OLED displays gives the robots a wide viewing angle and enables the expression of emotions.



Fig. 3 Wide Range of Emotional Expression Using Curved Displays

2.3 Adoption of soft skin and soft shell

A high-performance polyester fabric with excellent elasticity and recovery characteristics was used as soft skin to cover the whole body of the new model robots, hiding the joint seams and creating a realistic appearance (only the head exposes the carbon fiber reinforced plastic (CFRP) exoskeleton).

In addition, to maintain the outline of Miraitowa and Someity while enabling a wide range of joint movement, a soft shell structure was adopted around some of the joints (Fig. 4). This soft shell uses the rubber-like Agilus 30 material, which can be created using a 3D printer. The hardness of the soft shell was adjusted depending on the location and the hard and soft parts are manufactured as an integrated product. Softness was also increased by adopting a Y-shaped notch, which enables the shell to adjust to a wider range of movements at locations where three degrees of freedom concentrate, such as the hip joints.

This soft shell and soft skin combination improves the external appearance of the robots while enabling physical expressions with a wide variety of poses by maximizing the range of joint movement, despite the extremely short legs of the two humanoid mascot robots.

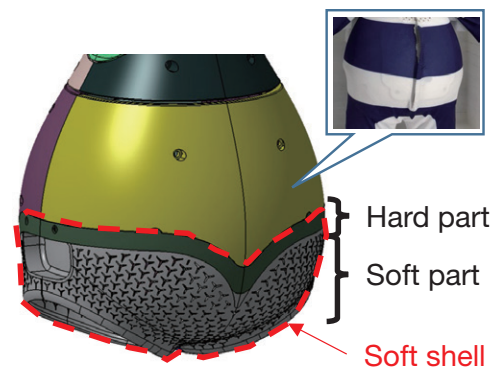


Fig. 4 Soft Shell Structure around Hip Joints

* The hard and soft parts are manufactured as an integrated product.

3. Electrical System

3.1 System configuration

Fig. 5 shows the configuration of the electrical system adopted for the new models. Although the new models have the same internal communication system as the original models (including the daisy chain wiring system using an Ethernet for Control Automation Technology (EtherCAT) bus), the dynamic performance of the robots was enhanced by adopting various new sensors and higher power devices.

Since size restrictions prevented the adoption of general-purpose six-axis force torque sensors, a force plate configuration with dispersed force sensors located at the corners of the bottom of the robots' feet was used to obtain the zero moment point (ZMP). The input voltage was also boosted from 24 to 42 V to enable high load movements such as walking and dancing. These changes were accompanied by the development of a battery pack with newly selected cells, the adoption of a higher power motor amplifier, and so on. The most significant changes incorporated by the new models are described in the following sections.

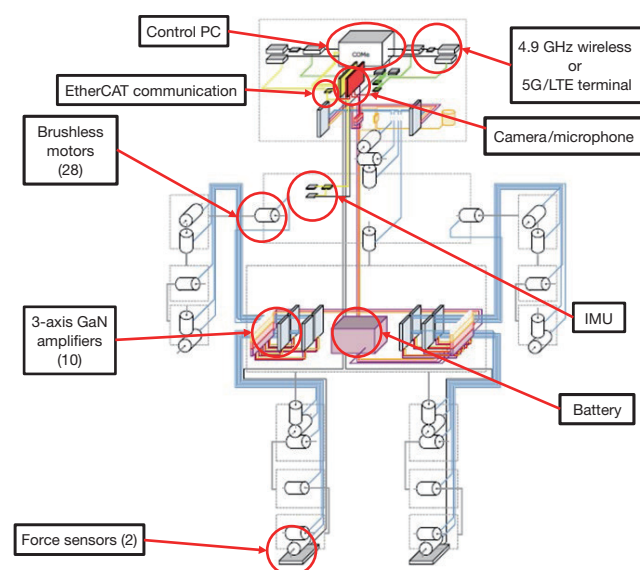


Fig. 5 Configuration of Electrical System

3.2 Actuators

To reduce the size and increase the torque of the actuators, frameless multi-pole outer rotor motors (44 poles, 48 slots) were adopted (**Fig. 6**). Based on the demand torque calculated via simulations and the installation size, three types of motors were then designed: 25 mm (diameter) × 10 mm (length), 29 × 9, and 35 × 10.

The original models used reduction gears that emphasized movement and force transmission via bilateral control. For this reason, reduction gears with

high back-drivability were adopted that permitted a slight amount of backlash. In contrast, since the new models emphasize dynamic performance, strain wave gearing devices were adopted.

A completely new joint configuration was realized by combining these multi-pole motors and wave gearing devices.



Fig. 6 Multi-Pole Outer Rotor Motor

3.3 Three-axis GaN amplifiers

An amplifier configuration capable of driving multiple motors is extremely effective for compact robots with limited installation space. The original models featured a newly developed three-axis amplifier. However, with the new models having a higher number of joint axes, smaller and more powerful amplifiers capable of fitting inside the body of the robots had to be designed. The greater density of amplifiers also created a serious concern about heat generation.

To address these issues, a new high-efficiency three-axis amplifier was developed using gallium nitride (GaN) as a power semiconductor material (**Fig. 7**). **Table 2** lists the main specifications of the motor amplifiers.

Fig. 8 shows thermographical images comparing the heat generated by silicon (Si) and GaN switching devices when a current with an effective value of 3 A is flowing in the device.

The temperature of the circuit board using GaN devices is clearly lower than that of the other board. As a result, the amplifier can tolerate higher currents while remaining within the rated temperature range of the devices. Therefore, the adoption of GaN enabled the installation of higher power actuators. This effect is actually due to the high efficiency of a circuit board equipped with GaN devices. **Fig. 9** shows the measured efficiency under actual assumed usage conditions when the developed amplifiers were driving the motors. The graph demonstrates that a high amplifier efficiency of at least 90% (maximum: 98%) was realized over a wide range.

This amplifier helped to resolve various issues by saving installation space, increasing power, and reducing the heat generated inside the robots.

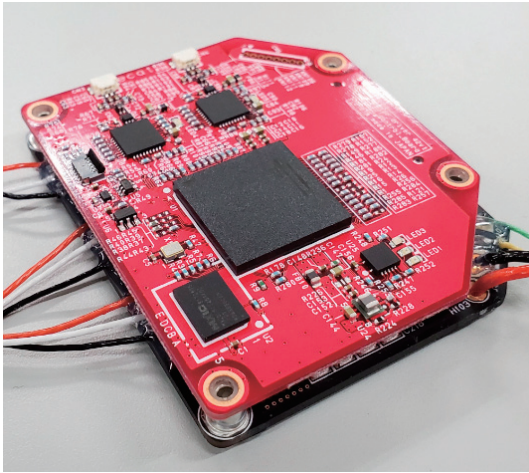


Fig. 7 3-Axis GaN Amplifier

Table 2 Main Specifications of Motor Amplifiers

Size	50 × 60 × 10 mm
Power supply voltage	Rating: 42 V
Motor current	Rating: 3 A × 3-axis output
ABS encoder	Single turn: 18-bit Multi-turn: 12-bit
Communication protocol	EtherCAT
Control system	Vector control
Control cycle	48 μs
Control modes	Current, speed, position, bilateral

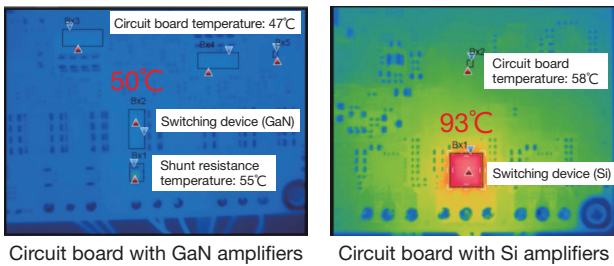


Fig. 8 Temperature Comparison with 3 A Effective Current Application

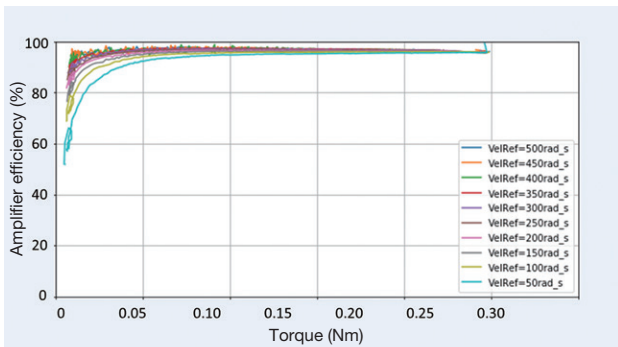


Fig. 9 Measurement Results of Amplifier Efficiency

3.4 Wireless communication

The new communication system adopted in the new models is compatible with the following two types of wireless communication protocols.

(1) 4.9 GHz band

This band is capable of highly reliable low-interference wireless communication using compact base stations. Use of this band requires an application.

(2) 5G (sub 6)/LTE

Commercial use of 5G communication systems has started. High-speed communication is available depending on the area. If radio wave reception is poor, the connection can be continued using the long term evolution (LTE) protocol.

During the actual Games, the optimum wireless protocol can be selected in accordance with the usage conditions, and the internal communication terminal swapped over. Film antennas that cover the frequency bands of both protocols are provided in both ears of the robots.

4. Control Software

4.1 Software configuration

Fig. 10 shows the software configuration. The central processing unit (CPU) installed in the robots runs control software on a Linux operating system (OS) incorporating the real-time (RT) patch. Commands to the motor amplifiers pass through the EtherCAT bus on a 1 ms cycle. Although the loaded modules differ slightly depending on the installed devices, the software itself was developed for compatibility with the T-HR3 life-size humanoid robot. The original assets of this software, specifically the walking function,⁽⁵⁾ whole body coordinated control function, and computation libraries can also be used by the mascot robots. In addition, although the control software was developed on Toyota's proprietary pfx software platform based on a state machine model, it is also provided with process-to-process communication functions that allow connections with common robot development platforms such as the Robot Operating System (ROS)⁽⁶⁾ and Choreonoid.⁽⁷⁾ The following sections describe the functions that were added during the development of the new models.

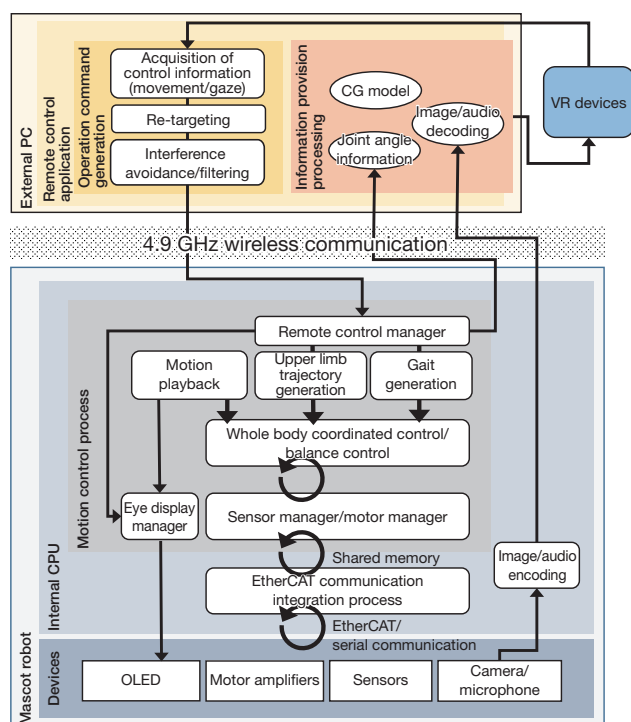


Fig. 10 Software Configuration

4.2 Intuitive control system

The development aimed to achieve smooth movements without any typical robot-like jerkiness. To realize this objective, a system that captures and reflects the actions of an operator in the movements of the robot in real-time was adopted (Fig. 11).

The remote control application shown in the top half of Fig. 10 manages the physical differences between the operator and robot (i.e., the differences in size and joint movement range) based on position and posture information obtained from virtual reality (VR) devices worn by the operator (eleven tracking devices including a headset, Fig. 12), and converts this information into position and posture commands for the upper body of the robot. Correction processing to prevent self-interference is then incorporated and target commands are transmitted to the robot.

The robot carries out autonomous feedback control to maintain its balance while tracking the joint position and posture commands in real time. The audiovisual information obtained by the camera and microphone installed on the robot is presented via the head-mounted display, enabling the operator to take direct intuitive control of the robot (Fig. 13). The status of the robot can also be confirmed from a third-person perspective using a computer graphic (CG) model superimposed on the head mounted display.

The pupil movement and eye opening/closing information of the operator can also be obtained from the eye tracker inside the head-mounted display, which can then be expressed in real-time by the robot eye animation. This enables natural interactions, such as eye movements

followed by face movements when the robot notices a person.

The Master Foot controller realized for the T-HR3 life-size humanoid robot⁽⁴⁾ is also used to enable intuitive walking instructions.

These remote control functions are used to turn the mascot robots into genuine performers.



Fig. 11 Remote Control in Action

Fig. 12 VR Measurement Positions



Fig. 13 Operator View

4.3 Motion generation method

The control method described in Section 4.2 is well suited for situations requiring real-time interaction. However, a method that plays back recorded motions is more appropriate for set-piece actions such as dance performances to music. Therefore, a method was developed that incorporates and uses human movements from the intuitive control system described in Section 4.2 to generate natural motions.

The motion generation procedure of each part of the robot is described below.

(1) Generation of head and arm motions

Time-series joint angle sequences converted from human movements for the mascot robot by the remote control application are used as the base data for these motions. This data is decimated and set into key frames at intervals of approximately 15 ms. Smooth interpolation

between the key frames enables smooth head and arm motions with less load applied to the joints, while retaining the characteristics of human movement.

(2) Generation of leg motions

When the operator raises a foot and places it on the ground, the position and posture of the foot and the time this motion occurs are obtained from the master device. Re-targeting is applied to that information to automatically generate a leg trajectory that factors in the physical characteristics of the robot, such as the length of its legs. In addition, to create kicks and other characteristic leg raising movements, key frames are inserted manually and the leg trajectory is derived by automatic interpolation. Improvements are ongoing to enable the expression of distinctive leg trajectories based on human movements.

(3) Generation of pelvis motions

These motions also record and use pelvis positions and postures obtained from the master device. However, the motions are generated differently during the single and double support phases. During the double support phase, human-derived pelvis positions and postures, which are obtained in the same way as for the upper limb joints, are corrected and used within the joint movement range of the robot. In the single support phase, the pelvis position and posture are generated from the balancing controller in conjunction with the leg motion. This process uses the pelvis to ensure that the robot is balanced during walking and taking steps. At other times, pelvic motions such as vertical or rotational movements can reproduce fine human actions.

(4) Eye movements and expressions

Pupil position information and eye opening/closing information are obtained from the eye tracker mounted on the headset and converted into the position of the black part of the robot's eyes and the blinking expressions. This enables the reproduction of realistic gaze movements and winking in accordance with the movement of the robot. Characteristic emotional expressions (such as tears, anger, heart displays, or the like) can be edited in manually at a later stage when desired.

The original robots were designed so that all motion commands needed to be generated manually using a motion editor. With the new robots, motion commands are generated automatically based on recorded human motion data. Then, after checking using a simulator or the actual robot, slight manual adjustments are made as necessary, resulting in lifelike and highly efficient motion creation. As an example, the joint dance performance of the song Paprika featuring the group Foorin and the mascot robots, which was broadcast by the Japan Broadcasting Corporation (NHK) in April 2021, was extremely well received.⁽⁸⁾

4.4 MR Ride

The walking speed of the developed mascot robots is approximately 1 km/h, which is too slow to accompany

people walking at a normal pace. Therefore, to enable faster movement, MR Ride was developed as a moving skateboard for the mascot robots (**Fig. 14**). This skateboard is driven using the two opposing wheels at the rear, with ball casters provided at the front and center as balancing wheels. The floor of the skateboard was lowered to enable the robots to step on and off the board without assistance. The velocity of MR Ride is controlled independently by the two rear wheels, which allows agile acceleration and deceleration in the forward and backward directions, and while turning. When standing on the skateboard, the robot must carry out precise center of gravity control in accordance with the acceleration or deceleration of MR Ride to prevent toppling over and maintain balance at all times. **Fig. 15** shows the balancing processing carried out when an arbitrary velocity command input is received for MR Ride from the control device.



Fig. 14 Robots Standing on MR Rides

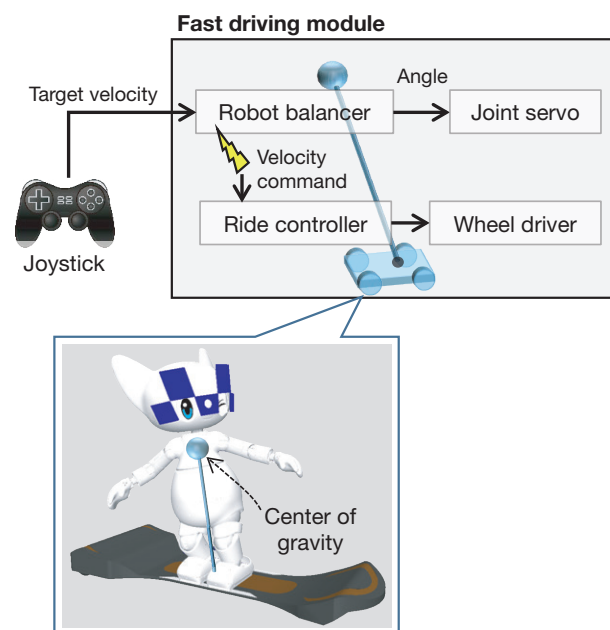


Fig. 15 Coordinated Control with MR Ride

First, the velocity command is inputted to the balance controller inside the robot. The balance controller carries out online optimization calculations using a center of gravity (COG) bogie model of the robot and MR Ride. This process determines the COG position of the robot and the skateboard velocity to maintain the robot balance while satisfying restrictions imposed by the skateboard specifications, friction limits, and so on.

The robot uses the relationship between both feet and the COG position to calculate and control the target angle of each joint. The controller installed in MR Ride controls the two opposing rear wheels to the target velocity received by wireless communication.

This process enables stable high-speed movement by coordinated control between the robot and MR Ride.

5. Conclusion

This article has described the main technologies that enabled the evolution of the Tokyo 2020 Mascot Robots into realistic compact humanoid robots.

At the time of writing (May 2021), the world was still in the grips of the coronavirus pandemic and the specific form that the Tokyo 2020 Games would take was unclear. Despite this situation, the mission of the mascot robots remains the same: to bring smiles to the faces of as many children as possible through the Games. For this reason, the development team remains totally committed to perfecting these robots and looks forward to further opportunities to showcase their capabilities.

Finally, this project to substantially upgrade the mascot robots in a short period of time during the coronavirus pandemic was supported wholeheartedly by the Tokyo Organising Committee of the Olympic and Paralympic Games, as well as a team of *monozukuri* professionals from inside Toyota. The authors would like to express their gratitude to everyone involved.

References

- (1) *Tokyo 2020 Robot Project Phase 2* (in Japanese). <https://olympics.com/tokyo-2020/ja/news/news-20190723-02-ja>
- (2) *Tokyo 2020 Mascot Robot (Original Model*, in Japanese). <https://gting.tokyo2020.org/image/upload/production/bqdkj5d1cwn5haqd2zmz.pdf>
- (3) S. Takagi. “Toyota Partner Robots” (in Japanese). *Journal of the Robotics Society of Japan* Vol. 24, No. 2 (2006) p. 208.
- (4) *Why is Toyota Developing Humanoid Robots?* (T-HR3 Press Release). https://global.toyota/en/newsroom/corporate/30609642.html?_ga=2.169374689.1937694916.1637641383-1211030701.1558057516
- (5) M. Doi. *Center of Gravity Trajectory Generation Device and its Generation Method and Program* (in Japanese). Japanese Patent No. 5803751.
- (6) ROS.org. <http://wiki.ros.org/>

(7) The Choreonoid Homepage. <https://choreonoid.org/ja/>

(8) *Paprika with Miraitowa and Someity* (in Japanese). https://www.nhk.or.jp/minna/songs/MIN202104_03/

Authors



T. MORIDAIRA



H. HATTORI



M. DOI



H. IYAMA



H. KONDO



K. YAMAMOTO

Development of the CUE5 AI Basketball Robot

Takayoshi Tsujimoto*¹
Masazumi Yagi*¹
Ryo Takizawa*¹
Masahiro Doi*¹
Tetsushi Harada*¹
Yuya Yasui*¹
Hikaru Sano*¹

Abstract

Toyota developed the fifth generation of its CUE basketball robot with the objective of showcasing its performance at the Olympic Games. The previous generation robot, CUE4, was capable of taking continuous shots at the basket, holding the ball, and autonomous movement. CUE5 also features the ability to dribble the ball while moving and take extremely long shots from behind the midcourt line. This article describes the details of the development to realize these functions.

Keywords: model predictive control, CFRP frame, high-power lithium-ion battery, high-power motor, ball trajectory prediction

1. Details and Background of Development

This project started with a proposal made at a 2017 meeting of the Toyota Engineering Society (TES), an informal group affiliated with Toyota, to take on the challenge of developing a humanoid robot. This proposal resulted in the development of CUE1, a robot capable of shooting basketball free throws, which seemed to be the most enjoyable and simple way of achieving this target. CUE1 was registered as a player on the Alvarik Tokyo professional men's basketball team, which plays in Japan's B.League. Since then, development work was continued with the aim of exhibiting a basketball robot at the Olympic and Paralympic Games Tokyo 2020.

CUE2, which was unveiled in November 2018, was a humanoid robot capable of shooting from the three-point line.

In April 2019, the capabilities of CUE2 were further developed by CUE3, which was able to shoot from the center circle. In the following month, CUE3 set a Guinness World Record for the most consecutive basketball free throws by a humanoid robot (2,020 successful attempts).

CUE4, which was unveiled in November 2019, was capable of autonomous movement, grasping a ball, and taking a series of consecutive shots. CUE4 took part in the three-point shootout at the B.League All-Star Game in January 2020.

Building on this progress, CUE5 was developed for the Olympic Games Tokyo 2020 with the aim of combining human-like dexterity with capabilities impossible for a human player to accomplish, specifically, the ability to dribble the ball like a human player and to take extremely long shots from behind the midcourt line (**Fig. 1**).



Fig. 1 History of the CUE Series Development

2. CUE5 System Configuration



Fig. 2 External Appearance of CUE5

Table 1 lists the specifications of the CUE5 system configuration.

CUE5 is a humanoid robot capable of executing basketball moves such as shooting and dribbling (**Fig. 2**).

The ability to dribble the ball while moving requires

*¹ R Frontier Div., Frontier Research Center

the ability to flexibly track the body and hand positions of the robot in accordance with the movement of the ball. This was accomplished by developing robotic arms with seven rotatable axes, legs with five rotatable axes, and a torso with one rotatable axis. Mecanum wheels were incorporated into the feet of the robot to allow smooth movement in all directions.

To enable CUE5 to shoot from behind the midcourt line, a new high-power motor (Section 3.1) was developed that operates around the joint pitch axes that require high power outputs. A double motor system was adopted at the axes that require particularly high levels of power, such as the pitch axes of the knees and ankles.

To help prevent radio wave interference at the Saitama Super Arena, which was the venue for Olympic basketball games, wireless communication with the robot adopted the 169 MHz frequency for control switches such as the power supply, emergency stops, and the like, and the 4.9 GHz frequency for operator controls.

Table 1 Specifications of CUE5

Height	213 cm
Weight	110 kg
Power supply	High-power lithium-ion battery
Number of rotatable axes	Right arm: 7 axes Left arm: 7 axes Neck: 2 axes Torso: 1 axis Right leg: 5 axes Left leg: 5 axes Wheels: 4 axes Total: 31 axes
Actuators	Newly developed high-power motor: 20 axes DC brushless motor: 13 axes Reduction gear-integrated compact motor: 2 axes
Motor drivers	70 A, 5.6 kW: 7 drivers 50 A, 4.0 kW: 26 drivers
Communication	Wireless communication using the following two frequencies - 169 MHz: for control switches - 4.9 GHz: for operator controls
CPU	Intel Core i7
Sensors	- For hoop detection One ToF camera - For ball trajectory detection One ToF camera - For ball stand detection Two RGB-D cameras - For surrounding object detection Four laser range finders - For ball detection Two ToF cameras

3. Development of Basic Technologies

The following sections describe the basic technologies developed for the CUE5 robot.

3.1 Development of high-power motor

Long-range shots require the instantaneous application of high speeds and torque to the ball. Issues include shots falling short of the hoop due to insufficient power and the complete loss of the shooting function due to excess heat generation. As described below, a high-power motor was developed to resolve these issues.

- (1) The permanent magnets of the rotor were laid out in a Halbach array configuration (a combination of bar- and fan-shaped magnets) to augment the magnetic field (**Fig. 3**).
- (2) Permendur (an alloy with 1.5 times the permeability of electrical steel sheets) was adopted for the core material in combination with the latest automotive neodymium magnets (coercive force approximately doubled by grain boundary diffusion).
- (3) Loss was reduced by the adoption of high-density winding (occupancy: 50%) using copper wiring with a diameter of 1.3 mm (**Fig. 4**).

As a result, the maximum power of the developed motor is 2.5 times higher than a conventional motor (**Fig. 5**) and the temperature rise of the winding can be held to approximately 40°C with a continuous fixed phase current of 50 A applied for 5 seconds. A single shooting action of CUE5 requires approximately 300 msec, which is sufficient for long-distance shooting. This motor was adopted at pitch axes requiring high power to shoot a ball a long distance (such as the knees, shoulders, elbows, and wrists), as well as at the wheel axes that require continuous torque while moving. Motors with two core stacked thicknesses (25 and 50 mm) were developed. The 25 mm type was installed in the wrists, which have limited space, and the 50 mm type was installed at the other axes.

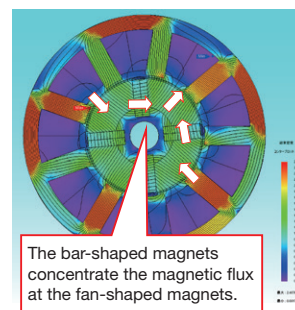


Fig. 3 Motor Magnetic Analysis Results

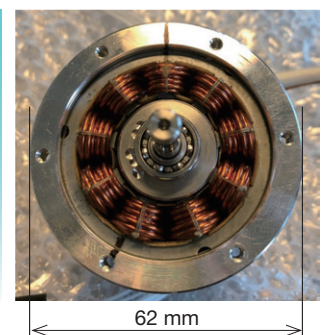


Fig. 4 Motor Winding

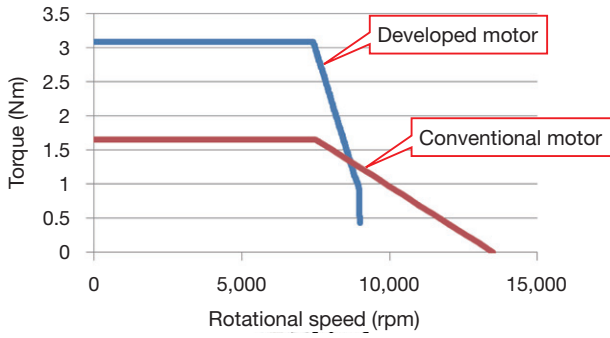


Fig. 5 Rotational Speed and Torque Characteristics of Developed Motor

3.2 Development of high-power battery

A high-power compact battery was developed to power the shooting, moving, and dribbling functions of CUE5. The following requirements were set for the battery specifications to enable the battery to be installed inside the body of the robot while realizing sufficient capacity for use at the planned events.

- (1) Voltage: min. 60 V (including voltage drop at maximum power)
- (2) Capacity: sufficient for at least one three-point shootout
- (3) Size: 213 mm (width) × 160 mm (thickness) × 230 mm (height)

Multiple lithium-ion cells were arranged in series to satisfy these requirements and realize high power.

The developed battery is capable of maintaining a minimum voltage of 60 V up to the final twenty-fifth shot of a three-point shootout requiring the highest power consumption (twenty five shots and four changes in court position, **Fig. 6**). In addition, the battery capacity is sufficient to allow CUE5 to complete at least two consecutive three-point shootouts (**Fig. 7**).

The battery weighs 7.1 kg and is installed in the upper torso. It can be attached and detached easily from the back of the robot (**Fig. 8**).

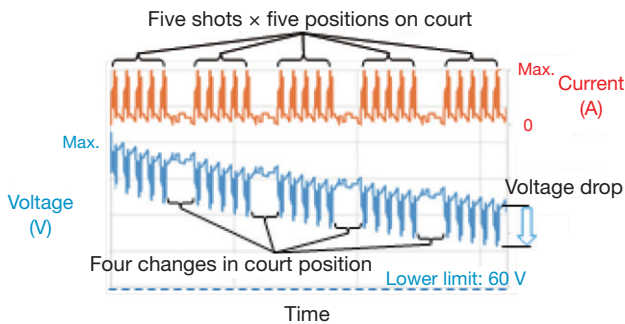


Fig. 6 Voltage and Current Characteristics of Three-Point Shootout

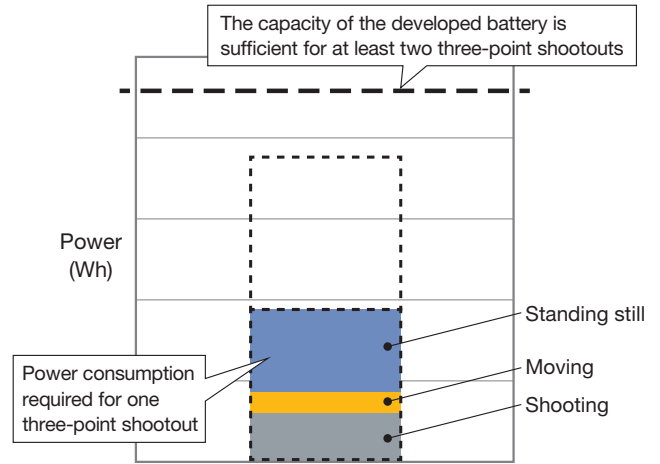


Fig. 7 Power Consumption and Battery Capacity of Three-Point Shootout

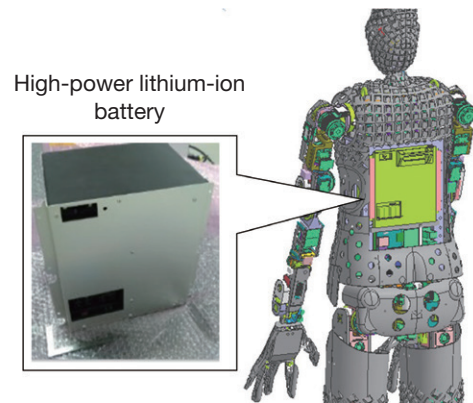


Fig. 8 Battery Installation Position

3.3 Weight reduction technologies

To enable instantaneous actions such as shooting and dribbling, the development worked to both increase the power of the actuators and reduce the weight of the robot body.

CUE1 to 3 adopted an aluminum frame (specific gravity: 2.7). However, CUE5 adopted carbon fiber reinforced plastic (CFRP, specific gravity: 1.5) for the upper arms, thighs, and calves to reduce weight and improve its shooting range. Since joints between CFRP sheets are not strong enough, the required rigidity was ensured using an L-shaped molded structure (**Fig. 9**).

The development also worked to reduce the weight of the reduction gears, which account for approximately 20% of the overall weight of the robot.

The following measures reduced the weight of the reduction gears by 40%.

- (1) Integration of the reduction gear housing with the robot frame
- (2) Adoption of lightweight thin cross roller bearings
- (3) Elimination of unnecessary gaskets depending on the usage environment.

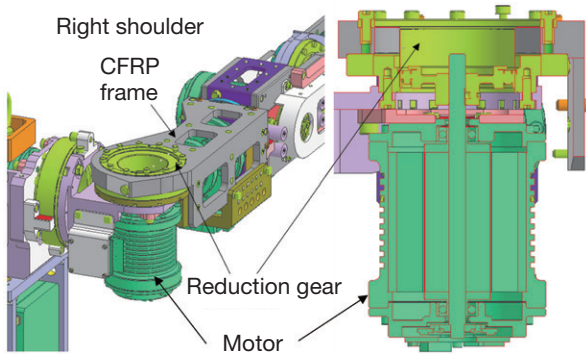


Fig. 9 Structure of CFRP Frame (Upper Arm) and Lightweight Reduction Gear

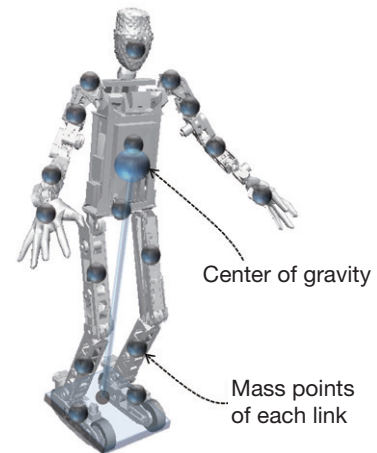


Fig. 10 Model of Relationship between Center of Gravity and Foot Trolley

3.4 Whole body balance control

Both CUE4 and CUE5 are equipped with Mecanum wheels at the bottom of the feet to enable movement in all directions. The whole body balance control adopted by CUE4 allows high-speed movement between the ball stands used in a three-point shootout. CUE5 features additional roll axes at the waist and ankles, which give both legs five degrees of freedom and enables the robot to dribble the ball in accordance with the movement of the ball.

Since a robot configured like CUE5 has a high center of gravity located over a small wheeled foot trolley, fast movement requires precise balance control that tracks the movement of the foot trolley when accelerating, decelerating, and turning. At the same time, the control must also satisfy physical restrictions such as the output of the wheel motors, and the limits of friction between the wheels and the floor.

Therefore, a robot model was created to simulate the relationship between the center of gravity and the foot trolley (**Fig. 10**), and online optimization logic using model predictive control was adopted. This control is capable of generating a trajectory for the foot trolley and center of gravity that satisfies as far as possible the target trajectory of the foot trolley within the range of these restrictions in real time (**Fig. 11**). The joint angle of the whole body and the speed of each wheel is then calculated from the calculated relationship between the center of gravity and foot trolley, thereby controlling the balance of the robot with respect to centrifugal force, acceleration, and deceleration when turning and moving.

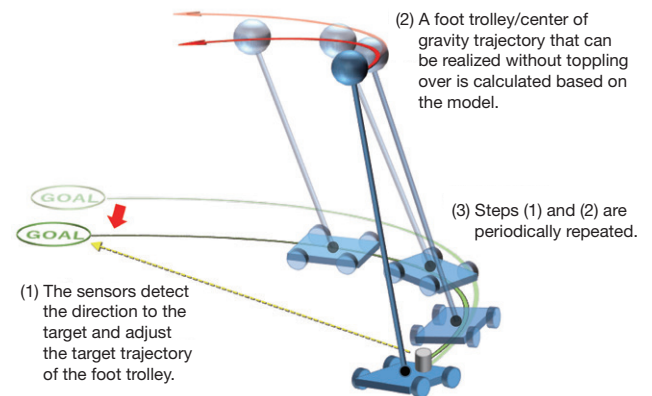


Fig. 11 Concept for Calculating Target Trajectory

3.5 Shooting trajectory analysis system

A system that can identify the ball trajectory accurately, rapidly, and concisely is necessary to verify shooting performance indices such as the distance of the ball through the air and the accuracy of ball positioning. However, the existing motion capture system has a long analysis time of approximately 15 minutes per shot. To verify the repeat accuracy of shooting, an evaluation of several hundred shots is required, and there is also no realistic measurement method available.

Therefore, it was decided to construct a system that uses a time of flight (ToF) camera to detect and analyze the trajectory of the ball then and there after shooting. An upward-facing ToF camera was set just under the hoop to detect the ball after shooting. Using the position of the hoop and depth information (**Fig. 12**), the shooting trajectory was then calculated by analyzing the trajectory of the ball centered on the hoop (**Fig. 13**). Since the trajectory of the ball can be identified in real time, efficient evaluations can be carried out to improve the shooting variation and adjust the target shooting position.

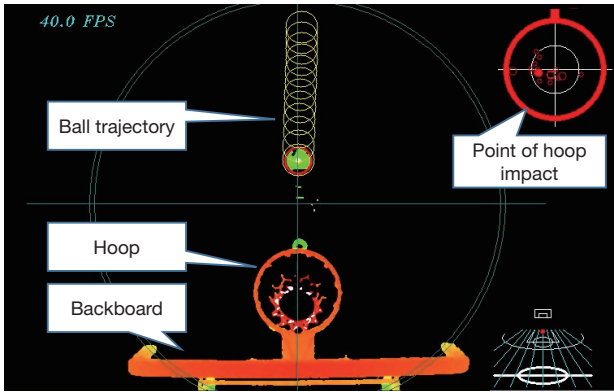


Fig. 12 ToF Camera Image of Shooting Analysis System

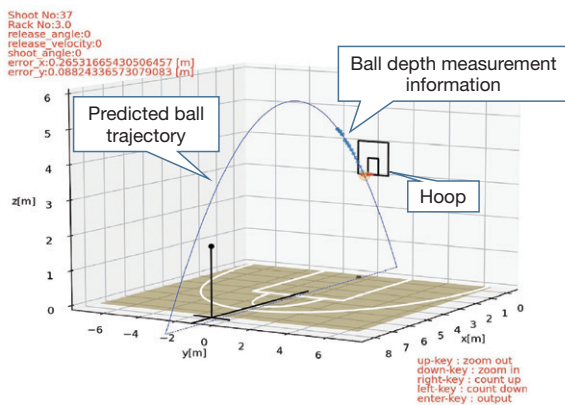


Fig. 13 Trajectory Analysis Results Using Shooting Analysis System

4. Development of Functions

4.1 Extremely long distance shooting function

To sink extremely long shots from behind the midcourt line, the distance of the ball through the air must be calculated efficiently by balancing the output from each axis within the permitted performance range. However, since it is difficult to accurately model the state of contact between the hand and ball, it is impossible to properly estimate the ball throwing method and necessary torque. Therefore, the shooting motion had to be decided by actually shooting the ball.

Therefore, the following approach was adopted to identify the command values for each axis based on an actual extremely long distance shooting evaluation. To reduce the number of search parameters, the leg movement of the robot was fixed to the pattern that empirically realized the most balanced output. The shooting action that satisfies the following conditions was then identified with the shoulder, elbow, and wrist pitch axes fixed at the maximum rotational speed.

- (1) The action that minimizes the average maximum current generated by the three axes
- (2) The action that minimizes the maximum current variance generated by the three axes
- (3) The action that maximizes the distance of the ball through the air

(3) The action that maximizes the distance of the ball through the air

The starting and finishing angles of the three axes and the start timing of the shooting action were set as the parameters of the shooting command values. The multiple objective optimization described above was then accomplished through Bayesian optimization. An actual shooting evaluation was carried out to obtain the shooting command parameters and the results with respect to those parameters (Fig. 14). The parameters for the next shot were then identified by sampling the obtained functions while updating the prediction model on a shot-by-shot basis.

As a result, after roughly fifty shots, the parameters for shooting from a distance of seventeen meters within the permitted output range of each axis were successfully identified. Fig. 15 shows the robot actually taking a shot.

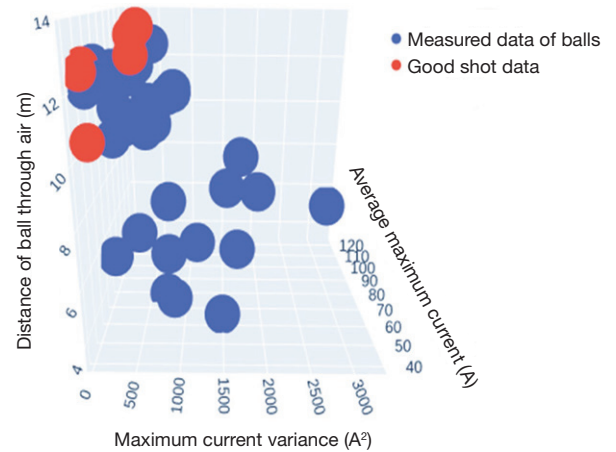


Fig. 14 Actual Distance of Ball through Air, Average Maximum Current, and Maximum Current Variance

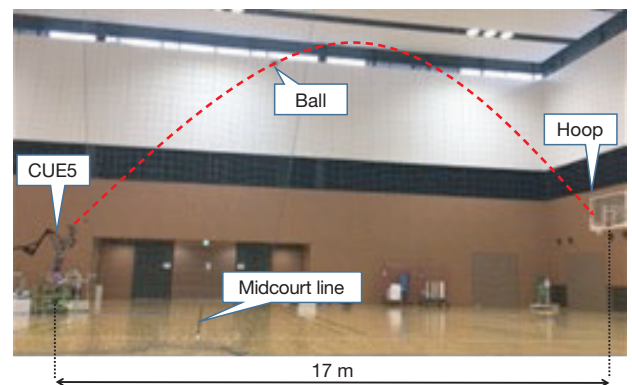


Fig. 15 Shooting from Extremely Long Distance

4.2 Dribbling function

Using a ToF camera attached to the end of the robot feet to estimate the position and velocity of the ball while dribbling and predict the trajectory of the ball, the dribbling action was realized by controlling the position,

posture, and velocity of the hand in real time in accordance with these prediction results. To maintain stable dribbling, the ball must be struck so that it bounces back from the floor within the subsequent range of the hand. In this process, the next horizontal position of the ball is controlled by determining the position, posture, and direction of the downward motion of the hand to ensure that the ball impacts the target position based on the predicted trajectory of the ball. In addition, the next height of the ball is controlled by determining the downward velocity of the hand using the predicted trajectory of the ball based on a pre-calculated map of the relationship between the maximum achievable height of the ball, the height at which the ball is struck, and the downward velocity of the hand (Fig. 16). Fig. 17 shows the measured hand position and ball height results while dribbling. It shows that stable dribbling was realized at the target height of around 1.2 meters (Fig. 18).

When moving, translational velocity must be applied to the ball with respect to the direction of movement. Therefore, the control was set to realize continued dribbling while moving at a speed of 1.5 m/s by appropriately adjusting the hand posture to strike the ball in the direction of travel.

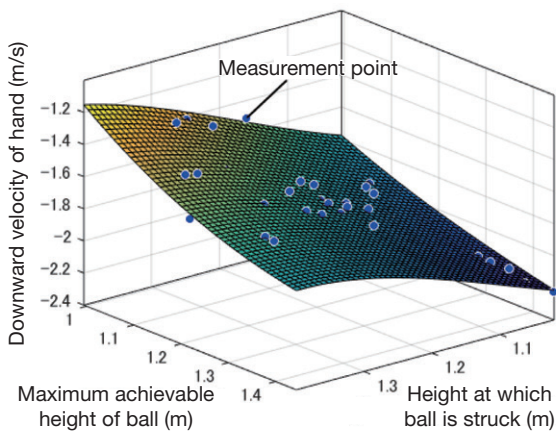


Fig. 16 Calculated Map of Downward Velocity of Hand

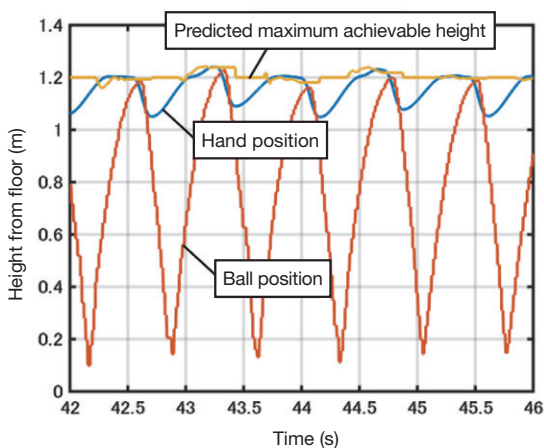


Fig. 17 Ball Motion and Hand Position while Dribbling

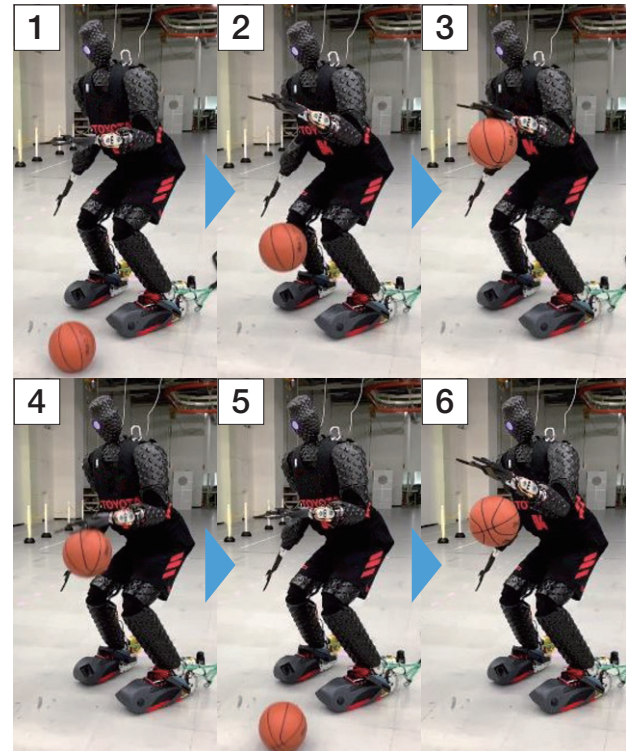


Fig. 18 Dribbling Action

5. Conclusion

This article described the CUE5 humanoid robot that was developed for the Olympic Games Tokyo 2020 with the aim of combining human-like dexterity with capabilities impossible for a human player to accomplish.

CUE5 was realized through new motor and battery development to enable shooting, dribbling, and other actions requiring high power outputs, the application of weight reduction measures, as well as the development of basic hardware and software technologies including whole body balance control to enable stable movement and a ball trajectory measurement system to verify the shooting function of the robot.

Due to these basic technologies, CUE5 is able to take extremely long shots from behind the midcourt line 17 meters away from the hoop, something that is not possible for a human player. At the same time, CUE5 is also able to dribble at a speed of 1.5 m/s with human-like dexterity.

Despite these accomplishments, CUE5 has not yet achieved human-like levels of smoothness, flexibility, and robustness. The development team intends to continue development of humanoid robots by adding more capabilities that only robots can achieve while ultimately realizing human-like fluid movements.

Authors



T. TSUJIMOTO



M. YAGI



R. TAKIZAWA



M. DOI



T. HARADA



Y. YASUI



H. SANO

Development of Peer-to-Peer Energy Trading System Including Plug-In Hybrid Electric Vehicles

Kazuki Obata*¹
 Yuki Kudo*²
 Satoshi Kikuchi*¹
 Hiromitsu Kigure*¹
 Kazutaka Kimura*¹

Abstract

The aims of this research are to develop a peer-to-peer (P2P) energy trading system that allows the participation of electrified vehicles and to make more efficient use of renewable energy. A system that can store surplus power generated from renewable energy in electrified vehicle and home batteries, and autonomously adjust supply and demand is seen as an effective way of helping to meet the growing need for environmentally conscious energy usage. The economic potential and renewable energy utilization rate of the developed system were verified through demonstration tests that included the participation of electrified vehicles, homes, and businesses.

Keywords: smart grid, peer-to-peer energy trading, VPP, electrified vehicles, V2G, renewable energy

1. Introduction

The aims of this research are to develop a peer-to-peer (P2P) energy trading system that allows the participation of electrified vehicles and to make more efficient use of renewable energy.

Wind, solar power, and other renewable energy sources are becoming more prevalent around the world as demand for environmentally friendly energy use increases. Accompanying this trend, because the output of renewable energy sources is unstable and fluctuates depending on the weather conditions, storage batteries are being increasingly regarded as a potential means of stabilizing this output in line with supply and demand. For example, much research and testing has been carried out into the concept of aggregation-type virtual power plants (VPPs), in which scattered storage batteries are formed into a cluster and charge-discharge commands are issued from the energy supply side.⁽¹⁾⁻⁽³⁾

As demand for environmentally friendly vehicles is also growing, the market is shifting toward electrification. Because the batteries in these vehicles can be used to store energy and because vehicles tend to be parked for long periods of time, the application of electrified vehicles to VPPs is also being studied.⁽⁴⁾⁽⁵⁾

This research focused on P2P energy trading as a way of using electrified vehicle batteries to help adjust energy output in line with supply and demand (**Fig. 1**). Unlike an aggregation-type VPP, this approach adjusts energy supply and demand from the demand side. Under this approach, the participants function autonomously to stabilize the system. For electrified vehicles, the hardware configuration is similar for either type of VPP since charge-discharge commands are received remotely in both cases. In contrast, dedicated P2P software must be

developed for the participatory-type system to enable participation in the market and the like. This research constructed, tested, and evaluated the effectiveness of an algorithm enabling the participation of electrified vehicles in a P2P energy trading market. This article mainly focuses on the economic aspects of the system and its use of renewable energy. It should be noted that the field operational test (FOT) was conducted under the approval of the Research Ethics Committee of Toyota Motor Corporation (permission number: 2019MK0001), and carried out with the cooperation of the Tanaka Laboratory at Tokyo University and Trende Inc.

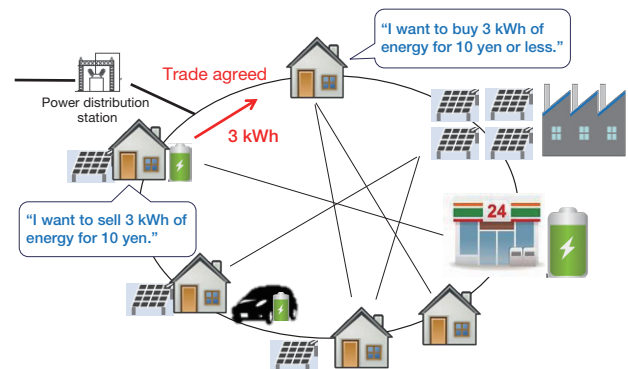


Fig. 1 Conceptual Diagram of P2P Energy Trading

2. FOT at Toyota Technical Center Higashi-Fuji

2.1 Outline

This P2P energy trading system was demonstrated in the eastern area of Shizuoka Prefecture in a FOT that started in June 2019. One office and twenty people working at the Toyota Technical Center Higashi-Fuji with their own homes were invited to participate in energy trading. **Table 1** summarizes the equipment possessed by

*¹ R Frontier Div., Frontier Research Center

*² Sustainability Management Dept.

each participant. In the table, “C” (consumer) refers to participants without solar power generation equipment and “P” (prosumer) refers to participants with solar power generation equipment. Sub-categories of both consumers and prosumers were also defined based on the different equipment possessed by the participants in each category. The office was selected based on actual data about demand and solar power generation equipment at the Toyota Technical Center Higashi-Fuji. Data about individual demand was collected via smart meters and home energy management system (HEMS) devices. Communication devices were installed on the plug-in hybrid electric vehicles (PHEVs) and automotive charge-discharge units provided to nine of the individual participants. This allowed the project to remotely collect data about remaining PHEV battery charge and the charge-discharge unit connection status. The PHEVs connected to the charge-discharge units are charged or discharged automatically based on the energy trading results.

Figs. 2 and 3 show the configuration of the FOT. In the FOT, an autonomous bidding agent linked with each participant was used to place bids and there was no actual involvement by individual participants. Each autonomous bidding agent formed a bidding strategy appropriate for each individual based on past information. The test used four types of autonomous bidding agents: home agents, vehicle agents, office agents, and grid agents, representing the homes, PHEVs, offices, and grid, respectively. Although the PHEV agents placed bids independently from the home agents, the homes and PHEVs were associated with each other and were provided with a means of coordination. The grid agent would sell power from the grid when the energy possessed by a participant was determined to be insufficient and buy power when the participant was determined to have surplus energy. For this purpose, the grid agent would place bids for selling and buying a practically infinite amount of energy at a fixed price. In addition, separately from the bidding process, energy supply and demand information from each participant was transmitted to the market and used to confirm consistency with the market trading results. This system also used blockchain technology to construct the following three functions.

- Recording of the power pool
- Market transaction processing (contract processing)
- Power generation station authentication and tracking

Table 1 Participants and Equipment

	C1	C2	P1	P2	P3	P4	Office
Number of participants	6	6	2	3	1	1	1
Solar panels			○	○	○	○	○
Storage battery				○		○	
PHEV		○			○	○	
Charge-discharge unit		○			○	○	○



Fig. 2 FOT

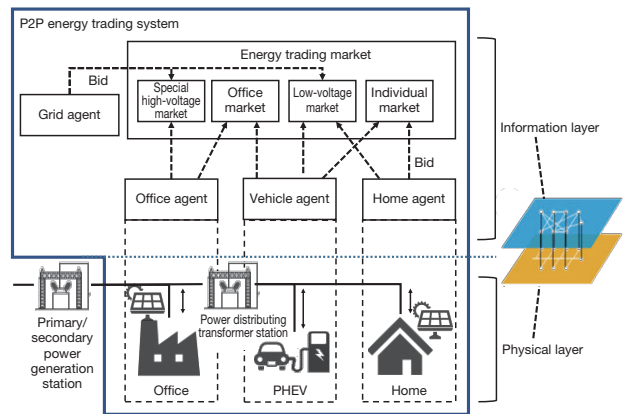


Fig. 3 Overall Configuration of FOT

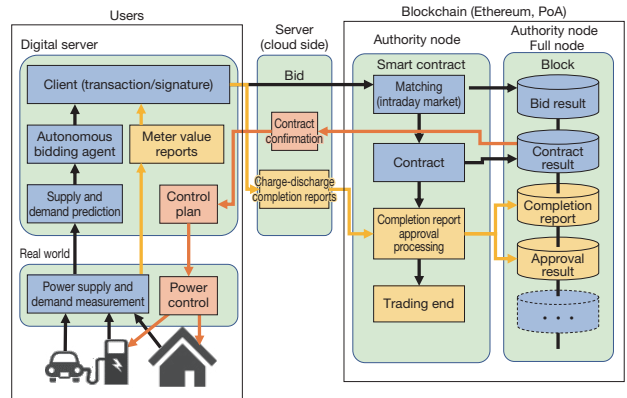


Fig. 4 Overall Image of Information Flow

Fig. 4 shows the flow of information from the user to the blockchain processing. The bids, which are created by the agents based on measured data, are incorporated into the blockchain smart contract. The bid result, contract result, power pool completion report, and contract result are recorded on the blockchain.

2.2 Market

The tested P2P energy trading system used the intraday market, which operates based on two rules: one

prioritizing price and the other prioritizing time. Bids can be submitted for a single trading period of thirty minutes or for 48 half-hourly trading periods twenty-four hours ahead. Each trading period is further divided into five-minute periods, which provides six bidding opportunities within one trading period. Bidding information includes the time, whether the bid is to buy or sell, the price, and amount of energy to be traded, and tags. The tags are used to indicate whether the electricity involved is special high-voltage or low-voltage electricity, whether it was derived from renewable energy, and whether it involves an interchange between the same facility. This final item refers to power pools that do not pass through the grid, for example between PHEVs that are connected to homes, or between an office and a commuter vehicle.

When power is purchased, a wheeling fee (surcharge) is added to the market price. This fee was set to 4 yen/kWh for the special high-voltage market, 8 yen/kWh for the low-voltage market, and 0 yen/kWh for trades within the same facility since these do not use the grid. This fee is borne by the buyer after the contract is finalized and is not reflected in the market price. In addition, the following prices were set for bids on the power retail market: 18 yen/kWh (selling) and 5 yen/kWh (buying) for the low-voltage market and 11 yen/kWh (selling) and 4 yen/kWh (buying) for the special high-voltage market.

3. Vehicle Agent

3.1 Optimization calculations

Fig. 5 shows the processing flow for the vehicle agent. To enable the active purchase cheap surplus renewable energy, an energy cost minimization algorithm was set at the center of the process. This cost minimization algorithm is as follows.

$$\operatorname{argmin} \sum_{i=MN}^{MN+47} \{E_{\text{buy}}(i)(Y_{\text{pre}}(i) + Y_{\text{rand}} + Y_{\text{fee}} - Y_{\text{back}}) - E_{\text{sell}}(i)(Y_{\text{pre}}(i) - Y_{\text{rand}})\} \quad (1)$$

where,

E_{buy} : purchase bid amount
 E_{sell} : selling bid amount
 Y_{pre} : market price
 Y_{fee} : wheeling fee
 Y_{back} : payback
 Y_{rand} : random number

The random number is applied to create variation in the vehicle agent price and to prevent bids from becoming concentrated in the same market. A uniform wheeling fee of 8 yen/kWh was set and payback applied to markets without a wheeling fee. For example, for trades within the same facility, the payback would be 8 yen/kWh.

Table 2 Vehicle Agent Constraints

Constraints	Details
Energy must be ensured for driving.	The agent must ensure that there is enough battery charge to drive the vehicle when the vehicle is started. If there is insufficient energy immediately before the vehicle is driven, the agent places a bid at the retail price
Charging or discharging may not occur during driving.	Since charging and discharging via the charge-discharge unit is not possible during driving, bidding is not possible while the vehicle is being driven.
Charge-discharge capacity of charge-discharge unit	Since the output of the charge-discharge unit is 5.9 kW, the maximum charge-discharge capacity for a single trading period (30 minutes) is 2.95 kWh.
Relationship between remaining battery charge over each time period	Under this constraint, the remaining battery charge of the vehicle decreases by the amount driven or discharged, or increases by the amount charged.
Initial and final remaining battery charge of optimization period	The initial remaining battery charge is the current actual state of charge. The final remaining battery charge was set to 4.4 kWh.

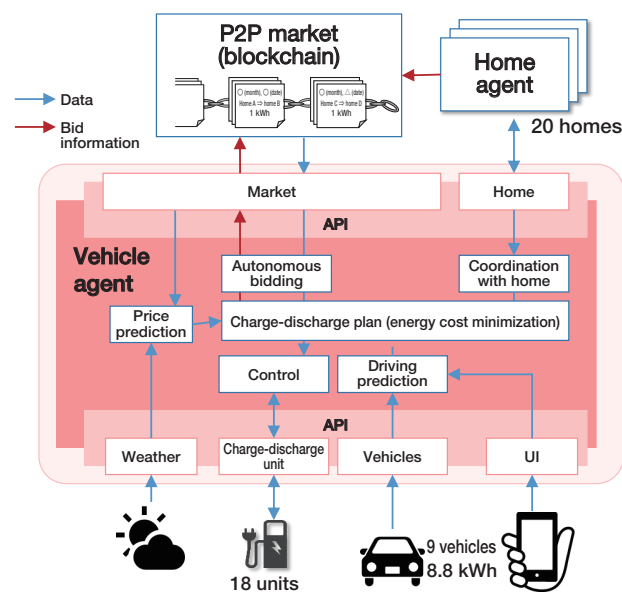


Fig. 5 Vehicle Agent

3.2 Vehicle movement prediction

To minimize the cost of energy, it is important to predict vehicle behavior. The future movement of the vehicles was predicted based on past movement data accumulated by the vehicle movement prediction process. Electrified vehicles can only charge or discharge while connected to the charge-discharge unit. Therefore, bidding to the energy trading market must be carried out during the periods that the vehicle is connected to the

charge-discharge unit (Table 2). Global positioning system (GPS) and state of charge (SOC) data is sent from the vehicle to the server every thirty seconds during driving as well as during charging or discharging. This data is used to construct a model for predicting the vehicle state (at home, at the office, moving).

The problem to be solved is a three-class problem, in which the vehicle state must be classified as “at home,” “at the office,” or “moving” every thirty minutes. However, in the case of a vehicle used for commuting, the driving time is much shorter than the time spent parked at home or at the office. With unbalanced data such as this, it is important to set an evaluation index and carry out learning. As described above, predicting when the vehicle will be connected to the charge-discharge unit is important for predicting vehicle movement. The vehicle state is first categorized into two classes: moving and not moving (i.e., at home + at the office). The key element in the prediction process is the level of recall that can be accomplished when this initial classification is made. Based on this classification, Fig. 6 shows the vehicle movement prediction flow.

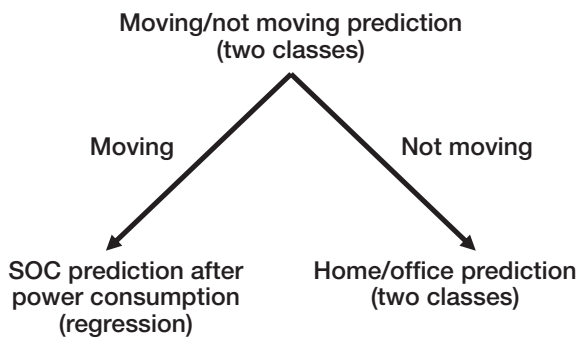


Fig. 6 Vehicle Behavior Prediction

First, the issue of classifying the vehicle as moving or not moving was resolved. Since the volume of “moving” data is very small, an under-sampling process was applied to the “not moving” data. When the vehicle is judged to be moving, the SOC to be used for that time is predicted from past data. When the vehicle is judged to be not moving, the process proceeds to determine whether the vehicle is in one of two classes: “at home” or “at the office.” This approach reduces the three-class problem to a two-class problem, allowing prediction from unbalanced data.

Many machine learning methods have been developed to solve classification problems. However, it is extremely difficult to determine in advance which method best matches the individual human patterns, amount of data, and so on. Therefore, this test used multiple methods within the vehicle movement prediction process to construct and evaluate models, with the most suitable method being selected (automated machine learning). Five learning methods were adopted: the logistic regression, k-nearest neighbors algorithm, random forest, gradient boosting, and multilayer perceptron methods.

4. Method of Evaluating Economic Efficiency

In P2P energy trading, the balance is calculated for each 30-minute trading period. The vehicle balance is the sum of the following two items:

- The contract result in the P2P energy trading market
- The non-contract balance

A non-contract balance occurs when a participant presses the charge-discharge button, when charge-discharge stop communication to the charge-discharge unit is delayed, or when a charge-discharge contract could not be implemented.

To evaluate the balance of participation in P2P energy trading, the electricity fee without P2P energy trading was calculated as a comparison. With reference to Meter Rate Lighting B (a Japanese power supply contract) set by the Tokyo Electric Power Company (TEPCO), the purchase price for this electricity was set to 26 yen/kWh and the buyback price was set to a minimum of 7 yen/kWh (the price set by the former general electricity utility companies in 2020). Therefore, the equation for the balance P is as follows.

$$P = -26E_p + 7E_s \quad (2)$$

where,

E_p : amount of power purchased

E_s : amount of power sold

The difference between the balance calculated by the P2P energy trading result and the balance calculated using Equation (2) is the amount of saving achieved in electricity fees.

5. Results and Discussion

5.1 Overall FOT

The following section describes the results for the FOT between August 1 and August 31, 2020. In August 2020, Toyota was closed for the summer holidays between August 10 and 14, and on Saturdays and Sundays. In addition, according to the Japan Meteorological Agency, the hours of sunlight for the eastern area of Shizuoka Prefecture in August was 257.3 hours in Mishima city and 223.2 hours in Gotemba city. These are conditions likely to generate surplus renewable energy.

Fig. 7 shows the market price trends. This figure indicates the energy trading market as a box plot that shows the cumulated trades every thirty minutes from 00:00 to 23:30. Surplus energy was traded at a lower price than the grid price.

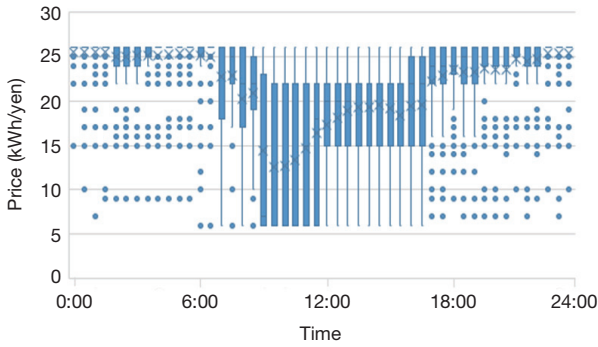


Fig. 7 P2P Trading Price

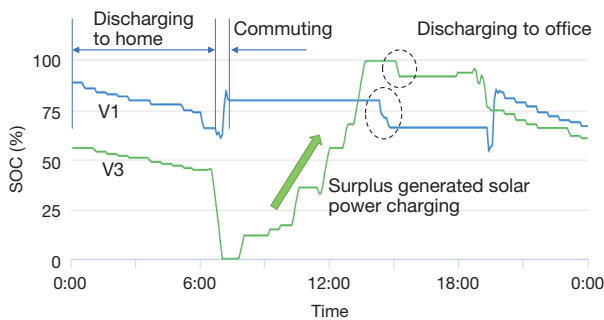


Fig. 8 PHEV SOC Trends

Fig. 8 shows the typical SOC trends for two PHEVs. This data is taken from August 18, 2020. V1 and V3 in the figure indicate the PHEV ID. The SOC is the trend created by charging and discharging under the instructions of the vehicle agent, non-energy trading charging and discharging, and power consumption and regeneration that occurs while driving. The SOC for both vehicles V1 and V3 gradually decreases during the night until morning. This indicates that the vehicle is discharging to the home. The increase in the SOC of vehicle V1 during commuting at around 07:00 is derived from regenerative energy as the PHEV travels downhill. In addition, although the SOC of vehicle V3 is 0% from 07:00 to 07:46, this is normal for a PHEV, which can drive using the gasoline engine when the battery charge is depleted. The SOC of vehicle V3 increases to 100% between 08:00 and 13:00. This indicates that the PHEV purchased and charged itself using surplus solar power. These trends demonstrate how the PHEVs absorbed the surplus solar power generated at the office during the day by discharging energy to the home at night. The results in Fig. 7 also show that the power cost minimization algorithm functioned as intended by purchasing power at timings when the price is low. The SOC of both vehicles V1 and V3 decreased at 15:00. At this timing, the office purchased power at 28 yen/kWh from the PHEVs, thereby helping the office to cut demand for power during peak periods.

Table 3 Balance Results

Vehicle ID	A. Conventional amount paid	B. Amount paid under P2P system	Difference (B - A)
V1 ^{*1}	-468	251 ^{*2}	737
V2	-3,456	-2,844	612
V3	-3,823	-2,388	1,435
V4	-3,774	-2,380	1,394
V5	-2,420	-2,121	299
V6	-4,843	-4,750	93
V7	-3,373	-1,232	2,140
V8	-6,039	-5,316	724
V9	-2,529	-2,148	381
Average	-3,416	-2,548	868

*1 Entered as a reference value due to driving mode setting error.

*2 Positive value since the participant made a profit.

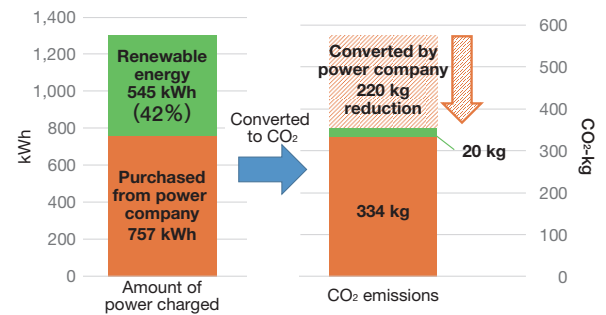


Fig. 9 Type of Purchased Power and Equivalent CO₂ Amounts (for Nine Vehicles)

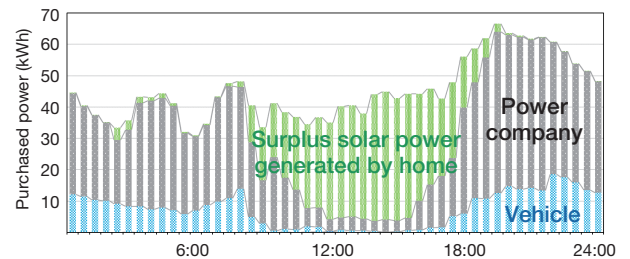


Fig. 10 Sources of Power Purchased by Consumers (for Nine Homes)

5.2 Economic efficiency

This section describes the results for the calculated balance. Without participation in P2P energy trading, the average electricity fee for each PHEV in August 2020 was 3,416 yen. In contrast, with participation in the P2P energy trading system, the average electricity fee was 2,548 yen. Table 3 summarizes the calculated balance of each PHEV. Participation in the P2P energy trading system resulted in average electricity fee savings of 868 yen.

5.3 Utilization of renewable energy

This section discusses the renewable energy utilization rate. **Fig. 9** shows the type of power purchased by the PHEVs between August 1 and 31, 2020 and the CO₂ emissions generated by the power used for charging. The left side of **Fig. 9** indicates that approximately 40% of the power used to charge the PHEVs was covered by renewable energy in the P2P energy trading market. The right side of **Fig. 9** shows the purchased power converted to CO₂ emissions. The values disclosed by TEPCO and the lifecycle assessment values for solar panels disclosed by the Central Research Institute of the Electric Power Industry were used for this conversion.⁽⁶⁾⁽⁷⁾ Of the power used for driving, the use of renewable energy by nine PHEVs reduced CO₂ emissions by approximately 220 kg.

The breakdown of the power purchased by the home agent was also confirmed. **Fig. 10** shows a breakdown of the sources of power purchased by the consumers each hour. Since these homes (consumers) have no power generation equipment, there should be no means for the consumers to purchase power other than from the power company. However, **Fig. 10** demonstrates that, during the daytime (09:00 to 17:00), 80% of power was purchased from the surplus solar power generated by other homes. In addition, in other time periods, 22% of power was purchased from PHEVs. Since solar power cannot be generated at night, the homes are forced to purchase power from the power company. However, the graph shows that a part of the power demand at night was covered by purchasing power accumulated by the PHEVs during the day. This demonstrates that the system functions to absorb the surplus renewable energy generated by other homes during the day and to meet demand for power at night.

6. Conclusion

PHEVs equipped with a function that autonomously absorbs surplus renewable energy were used in a P2P energy trading FOT and the resulting electricity fee balance was evaluated. Compared with the electricity fee calculated under equivalent conventional conditions, an average saving of 868 yen was achieved in the single month of August. In addition, 42% of the power used to drive the electrified vehicles used in the test was derived from renewable energy. Furthermore, 80% of the daytime power demand and 22% of the nighttime power demand of homes not equipped with power generation equipment was derived from renewable energy. These results indicate that the tested P2P energy trading system was both economically efficient and successfully utilized renewable energy.

In the future, it is planned to continue verifying and enhancing the performance of each part of the system,

with the aim of expanding its scale of application.

Finally, the authors would like to extend their sincere gratitude to Associate Professor Kenji Tanaka of the University of Tokyo, Trende Inc., and everyone inside Toyota that cooperated in this FOT.

Original Paper

K. Obata et al. "Development of Participatory-Type Peer-to-Peer Power Trading System Including Plug-In Hybrid Electric Vehicles" (in Japanese). *Presentation Materials for the Gijutsusha no Ichinichi Research Status Report Meeting of the Toyota Engineering Society*.

References

- (1) H. Saboori et al. "Virtual Power Plant (VPP), Definition, Concept, Components and Types." *2011 Asia-Pacific Power and Energy Engineering Conference* (2011) pp. 1-4, doi: 10.1109/APPEEC.2011.5749026.
- (2) L. van Summeren et al. "Community Energy Meets Smart Grids: Reviewing Goals, Structure, and Roles in Virtual Power Plants in Ireland, Belgium, and the Netherlands." *Energy Research & Social Science* Volume 63 (2020) 101415.
- (3) A. Elgamal et al. "Optimization of a Multiple-Scale Renewable Energy-Based Virtual Power Plant in the UK." *Applied Energy* Volume 256 (2019) 113973.
- (4) B. Jansen, Binding, et al. "Architecture and Communication of an Electric Vehicle Virtual Power Plant." *2010 First IEEE International Conference on Smart Grid Communications* (2010) pp. 149-154.
- (5) M. Vasirani et al. "An Agent-Based Approach to Virtual Power Plants of Wind Power Generators and Electric Vehicles." *IEEE Transactions on Smart Grid* Vol. 4 No. 3 (2013) pp. 1314-1322, doi: 10.1109/TSG.2013.2259270.
- (6) TEPCO. https://www.tepco.co.jp/ep/notice/news/2020/1549626_8908.html
- (7) Central Research Institute of the Electric Power Industry. <https://criepi.denken.or.jp/jp/kenkikaku/report/leaflet/Y06.pdf>

Authors



K. OBATA



Y. KUDO



S. KIKUCHI



H. KIGURE



K. KIMURA

The TRI Approach to Advanced Automated Driving in Complex Urban Environments

Ryan Eustice*¹
 Wolfram Burgard*¹
 John J. Leonard*¹
 Ryan W. Wolcott*¹
 Robert Zidek*¹
 Gill Pratt *¹

Abstract

Building cars that can perform transportation tasks in an automated fashion and without drivers is an extremely challenging task that is currently being addressed by major car manufacturers and highly effective start-ups. But what does it require to build a self-driving car that can operate autonomously in a complex urban environment? This article describes several of the efforts that the Toyota Research Institute (TRI), in collaboration with collaborating companies from within Toyota Motor Corporation and its partner companies, have undertaken to advance the state-of-the-art in automated driving. In particular, it describes the technology that was built for the so-called Tokyo Olympics Capability Showcase (OCS) designed to demonstrate Toyota's technological leadership in the area of automated driving and driver assistance technology. The described system embodies innovative approaches in hardware and software platform design, mapping, localization, perception, machine learning, motion planning, vehicle maneuvering, and control, to demonstrate a robust Chauffeur capability. The system has been extensively tested on the TRI P4 Lexus LS automated driving platform, as well as on the Toyota LQ vehicle, in the Odaiba district of Tokyo. This article provides a brief overview of the system objectives and design, and provides several performance highlights from extensive real-world operations.

Keywords: *automated driving, perception, machine learning, prediction, planning, control, user experience*

1. Introduction

One of the major objectives of the Toyota Research Institute (TRI) is to create advanced automated driving capabilities to help enhance safety and mobility. To this end, TRI is developing two systems, namely the Chauffeur system to navigate in an automated fashion through complex environments and the Guardian system, which is an advanced driver assistance system to help reduce crashes. Both systems share common technology such as the ability to perceive and understand the environment, predict what is going to happen, and plan actions that control the vehicle most safely.

This article describes TRI's technology development for a robust self-driving car system that builds the basis for both the Chauffeur and Guardian systems. In particular, it describes the system TRI developed for the Olympics Capability Showcase (OCS), during which Lexus LS and Toyota LQ vehicles were to perform automated driving on public roads in a complex environment in Tokyo. While the COVID-19 pandemic has caused a cancellation of these demonstrations during the Olympics, the system is nevertheless being completed to showcase the developed technology.



Fig. 1 The TRI P4 Lexus LS Automated Driving Test Vehicle Deployed in Odaiba, Tokyo

TRI has developed advanced capabilities in hardware, software, and algorithms for automated driving. This includes a highly integrated platform with state-of-the-art sensors and computing capabilities, and a state-of-the-art software stack. The hardware (shown in **Fig. 1**) is a TRI P4 that consists of a Lexus LS augmented by a rich suite of sensors in its enclosure, powerful on-board computation, and data logging. The software stack has been built from the ground up with extensibility in mind and adopts a one-system/two-modes paradigm whereby many of the core capabilities of the Level 4 Chauffeur application can also be deployed for personal vehicles in a Guardian active safety application. It furthermore facilitates a dialable system that can enable selected Guardian functionality. The resulting automated driving (AD) software stack is highly flexible and allows some of the strong assumptions typically made in Level 4 systems to be relaxed, such

*¹ Toyota Research Institute

as dense 360-degree lidar and high definition (HD) maps.

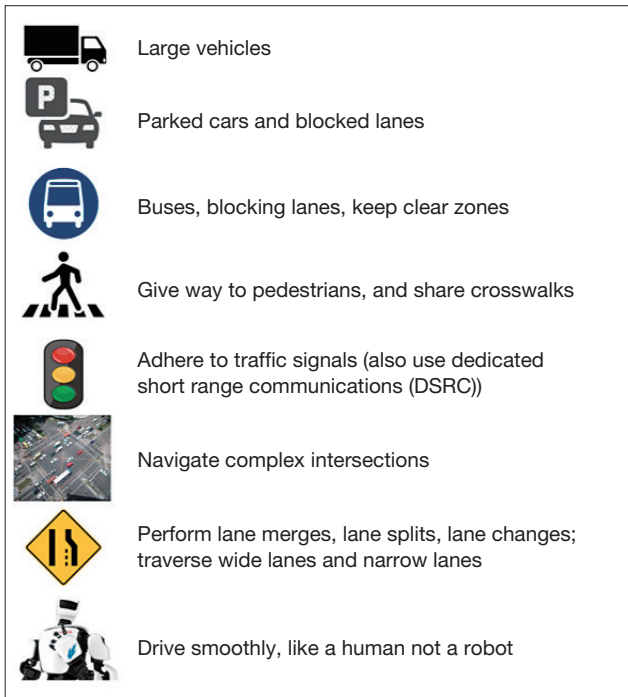


Fig. 2 System Requirements.

The system has been extensively tested in a major part of Odaiba, which is a complex Tokyo driving environment that presents numerous technical challenges, as shown in **Fig. 2**, including the following.

- Driving among numerous trucks and other large vehicles
- Maneuvering appropriately around parked vehicles that are blocking lanes
- Safely navigating among pedestrians
- Sharing crosswalks when appropriate
- Obeying traffic signals
- Navigating complex intersections
- Executing lane merges and lane splits
- Traversing narrow lanes
- Maintaining passenger comfort
- Adhering to all traffic laws

The following sections present different solutions to several of these challenges and describe how these solutions contribute to the robustness of TRI's technology.

2. System Overview

2.1 Vehicle hardware and sensor suite

Fig. 1 shows the TRI P4 automated driving test vehicle, which is based on the fifth-generation Lexus LS flagship sedan. **Fig. 3** shows its sensor-rich platform design, which includes eight cameras, four Luminar lidars, four Velodyne VLP-16 lidars, and ten radars. On-

board computing includes a high-performance CPU and GPU processing system.



Fig. 3 The Sensor Configuration of the P4 Including an Array of Advanced Camera, Lidar, Radar and Navigation Sensors, Combined with Powerful Onboard Computation

2.2 Localization and mapping

The vehicle's localization system adopts an innovative OneMap world-scalable mapping framework, illustrated in **Fig. 4**. This enables the blending of *a priori* maps and live perceptual data for accurate lane-level localization.

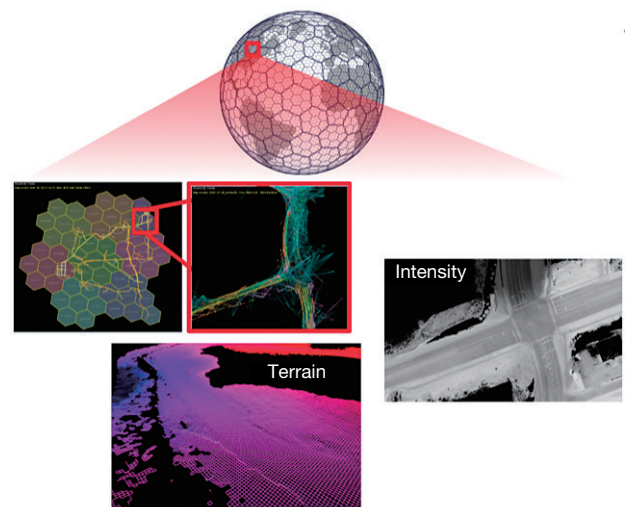


Fig. 4 The TRI OneMap World-Scalable Mapping Framework

Technical Papers/Technical Articles

Fig. 5 shows a semantic segmentation example for lane-detection, showing both a camera-view and a bird's-eye view of the scene, in which each pixel in an image is assigned to a semantic class, with objects and lanes identified, to aid in real-time localization and further perceptual processing.



Fig. 5 Semantic segmentation and birds-eye map view

2.3 Perception and machine learning

TRI has also developed several advanced machine-learning-based solutions for challenging perception and decision-making problems. The corresponding models extend the state-of-the-art and have been published in leading academic research venues.⁽¹⁾⁽²⁾ Where possible, TRI pursues self-supervised machine learning and leverages large data sets obtained in frequent real-world testing.

An important goal for TRI's machine learning research is to develop computer vision modules that provide cost-effective solutions to challenging perception problems and, at the same time, relax the dependency on cost-expensive lidar sensors. For example, TRI has developed SuperDepth, a state-of-the-art approach based on deep networks, which infers depth obtained from monocular images.⁽³⁾ **Fig. 6** shows the typical performance of the system. This network efficiently calculates the depth for every pixel in the input image and helps TRI vehicles to perform better in situations in which lidars encounter difficulties or are not available. In extensive scientific experiments, this technology showed superior performance compared to the best models developed thus far. A further advantage of this approach is that it does not require manual labeling and thus can effectively learn from data obtained using safety systems deployed in the Toyota fleet.



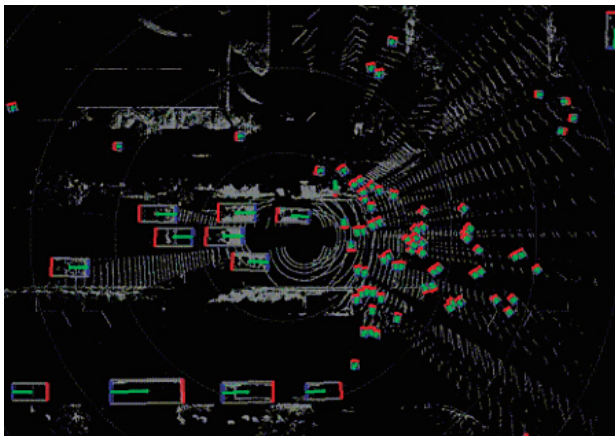
Fig. 6 Inferring Depth from Monocular Vision to Help Reduce Requirements for Expensive Lidar Scanners, Top: Traffic Scene in Odaiba, Bottom: Depth Inferred by the Network (Yellow Means Close and Violet Means Far Away)⁽³⁾



(a) 2-D object detection



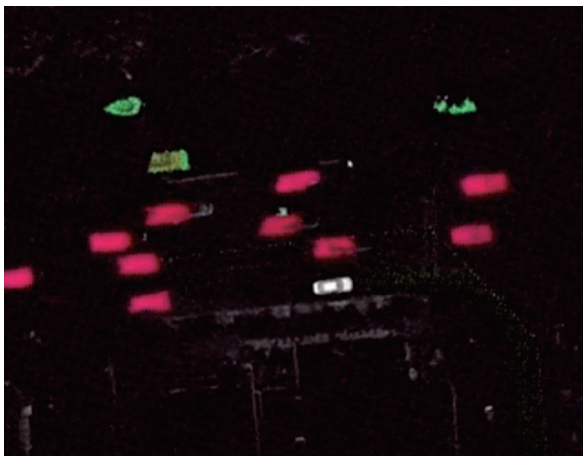
(d) Traffic light estimation



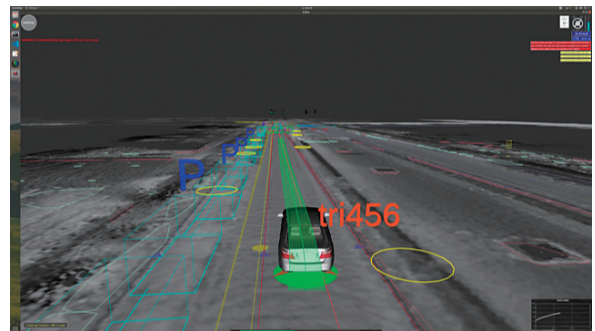
(b) Bird's-eye view 3D detection



(e) Semantic segmentation



(c) Bird's-eye view Scene flow



(f) Parked car classifier

Fig. 7 Overview of Machine Learning Models Employed for Perception, Tracking, and Prediction

Machine learning enables detection, tracking and prediction algorithms that process vision and lidar data to determine “what is where?” in the driving scene and to predict what will happen next. **Fig. 7** provides an overview of key elements of the detection and tracking pipeline, including clustering, learned object detection from lidar and vision, and velocity estimation. This yields an overall local model of the scene with semantic labels, velocity estimates, and intent prediction for all objects in the vicinity of the vehicle.

Machine learning is also used in the planning and prediction components, e.g., for parked vehicle classification or corridor intent and path prediction, illustrated in **Figs. 8** and **9**, respectively.

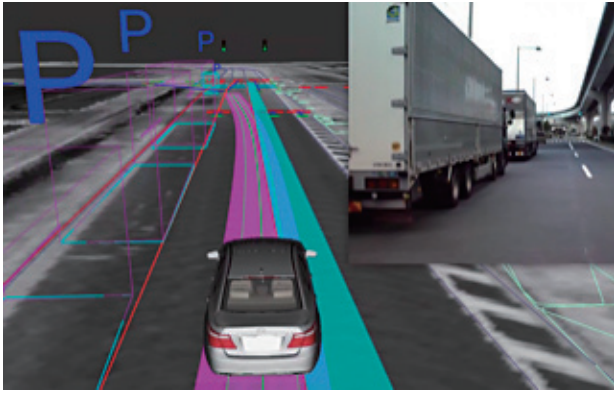


Fig. 8 Parked Vehicle Classification Example Showing the AV Needing to Borrow Part of the Adjacent Lane (Cyan Color) to Pass the Parked Trucks on the Left

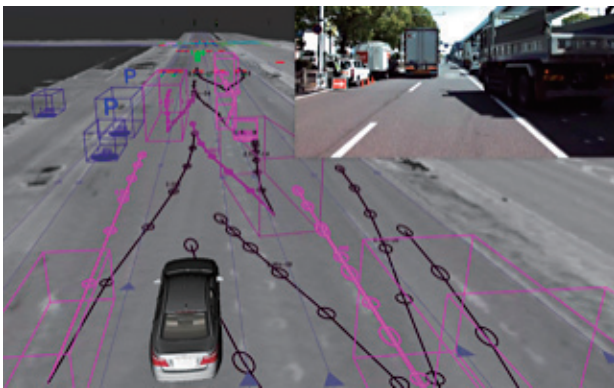


Fig. 9 Corridor Intent and Path Prediction with Different Likelihoods

2.4 Planning and control

The perception and machine learning algorithms described above provide inputs to the planning and control module shown in **Fig. 10**. The main task of this module is to compute the control inputs (steering, braking, and acceleration) so that the automated vehicle (AV) reaches the desired destination safely and comfortably. The planning and control module is subdivided into four different sub-modules: the route planner, the behavior proposer, the main planner, and the controller.

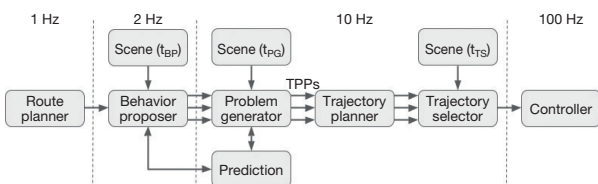


Fig. 10 Planning and Control Architecture

The first sub-module is the so-called route planner that calculates the optimal route on a road-level network to reach the desired goal destination from the current

position of the vehicle. In addition to static inputs (e.g., road speed limits), this module supports handling of dynamic traffic information (e.g., current road congestion).

The second sub-module is the behavior proposer whose task is to determine tactical aspects of driving while following the route. Based on the available scene provided by the perception stack, the behavior proposer compares the advantages of driving along the available lanes and drivable surface to capture the long-term reward associated with tactical decisions. A search-based approach is adopted in which motion primitives (e.g., to stay in lane or to change lanes) for the AV and other actors (vehicles, pedestrians, and the like) are employed to construct a graph on the map. Similar solutions are clustered into so-called behavior descriptions, which are representations of different maneuvers of the vehicle (e.g., change lanes to the left).

The third sub-module is the main planner, which consists of the problem generator, the trajectory planner, and the trajectory selector. The problem generator receives the most promising behavior descriptions from the behavior proposer and generates, for each behavior description, several trajectory planning problems. A trajectory planning problem captures specific constraints for generating a trajectory. A generic trajectory planning problem formulation was carefully designed, which can represent the full spectrum of AV maneuvers and driving scenarios. This interface makes the trajectory planner agnostic to the semantics of the planning problem. The advantage is a highly scalable system where new AV capabilities can readily be developed without needing to change the trajectory planner.

The prediction component is also part of the main planner. Prediction is a critical capability that links perception with planning by providing estimates of the intent and future motion of the surrounding actors. It can provide multiple hypotheses per actor. A mix of heuristic-based as well as machine-learning-based prediction models is employed with a plan to further increase machine learning models in the future. Pedestrian tracking and prediction uses a learned estimated risk map (**Fig. 11**) that facilitates decision-making at crosswalks as well as general risk-aware driving behavior. Using the prediction information, the problem generator selects the relevant objects for each trajectory planning problem and makes decisions about how relevant objects should be interpreted (e.g., stay-behind or stay-ahead). The final stage of the problem generator selects the most relevant trajectory planning problems, up to a specified number, to be solved in parallel by the trajectory planner.



(a) Tracking pedestrians and estimating risk at a crosswalk



(b) Pedestrian risk map inference

Fig. 11 Pedestrian Tracking and Risk Estimation

The trajectory planner applies an iterative trajectory optimization algorithm that is based on differential dynamic programming and generates a trajectory for each trajectory planning problem. Trajectory generation is followed by a two-step certification process to verify that each trajectory is both feasible and safe. The trajectory selector performs the final part of the decision-making process. It selects the trajectory to be executed by the lower-level controller using the latest scene information. A quasi-lexicographical ordering framework is employed to compare and rank the trajectories based on different criteria including feasibility and safety, risk, routing, progress, action consistency, and comfort.

The commanded trajectory is passed to the low-level vehicle controller, which provides robust trajectory tracking performance with low cross-track and along-track errors.

2.5 Software platform and cloud infrastructure

The algorithms described above have been implemented in a cloud-based software platform with extensive continuous integration and simulation testing to ensure robust system performance as new capabilities are added. Each modification to the software is put through an extensive battery of tests in simulation and via data log replay, followed by closed-course testing and subsequently public road testing using highly trained

vehicle technicians. The entire development process is guided by a strong culture of safety system engineering.

3. System Performance

The system components described above have been fully integrated and deployed in the Odaiba district of Tokyo, for the demonstration of sustained automated driving. The system has also been operated extensively in Ann Arbor, Michigan, and Los Altos, California. **Fig. 12** shows examples of the in-car experience and **Fig. 13** shows the UX display and front camera view during various moments during an automated journey in Odaiba. Each journey typically involves complex interactions, in which machine learning (ML) and perception algorithms combine with planning and decision-making to achieve sophisticated real-world driving behavior.



Fig. 12 User Experience during Automated Operation

For example, one key AV capability for driving in Odaiba is handling parked vehicles. There are numerous challenging scenarios in which parked vehicles can block the path of an AV in Odaiba (a parked bus blocking the entire lane, a sequence of parked trucks in a wide lane, taxis pulling over to park, and so on). To robustly handle all possible scenarios, a learning-based parked vehicle classifier was developed. The classifier has been trained using thousands of examples from the AV fleet. **Fig. 14** shows an example of a lane change to the right in order to overtake a parked bus. **Fig. 15** shows a row of parked trucks at an intersection exit where the AV decides to borrow part of the adjacent lane to progress forward.

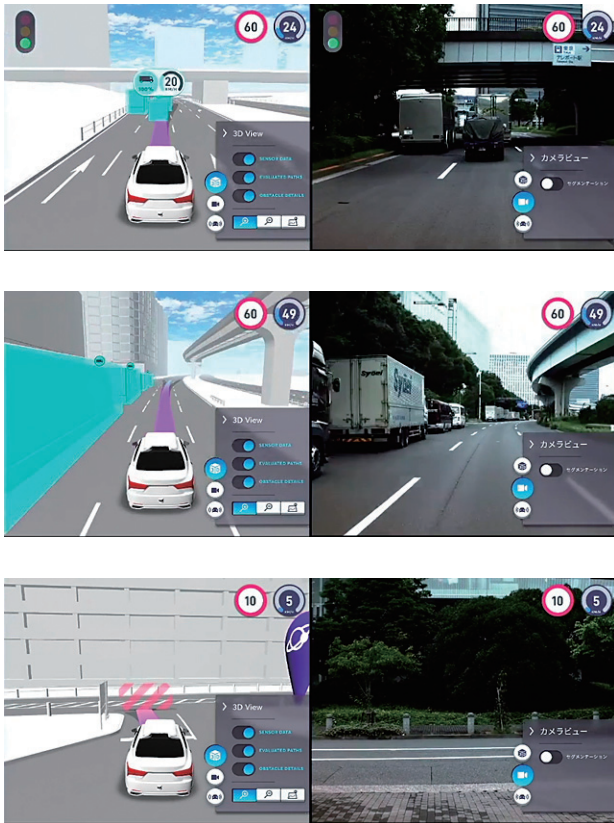


Fig. 13 UX Display and Forward Camera View Showing Operation of the System at Selected Locations in the Odaiba Testing Environment

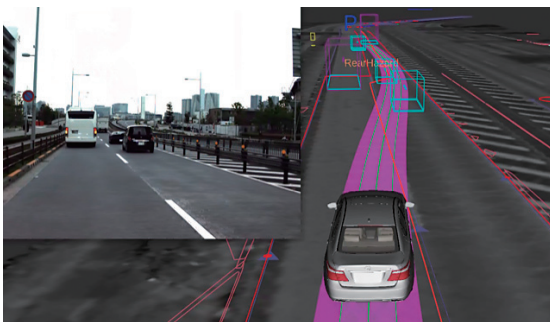


Fig. 14 Changing Lanes to Pass Parked Vehicles

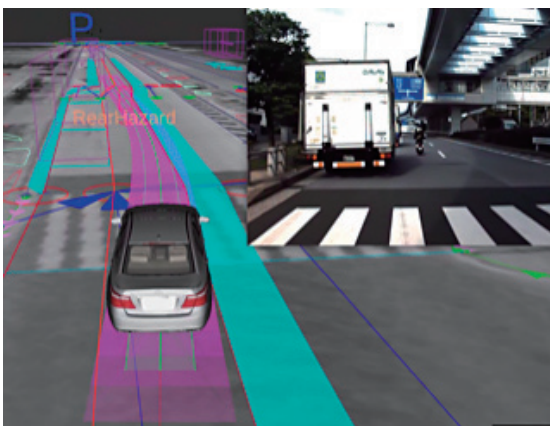


Fig. 15 Borrowing Adjacent Lane to Pass Parked Vehicles

4. Conclusion

TRI has combined innovations in hardware, software, machine learning, perception, planning and control to realize a fully integrated automated driving system that has been fully deployed in the Odaiba district of Tokyo. These technologies will help advance Toyota's vision to create a safer future of mobility for all.

Continued experimentation is underway to expand the operational design domain of the system to encompass challenging weather conditions and to perform operations in ever-larger environments. TRI is also working with its partners at TMC and Woven Planet to transition modules of the system to future Toyota products.

Acknowledgments

The authors wish to express their gratitude to the entire TRI automated driving team and its partners in various parts of Toyota Motor Corporation and its affiliates, for all of their tremendous contributions in developing and testing the automated driving system.

References

- (1) R. Hou, Li, Bhargava, Raventos, Guizilini, Fang, Lynch, Gaidon. "Real-Time Panoptic Segmentation from Dense Detections." *Proceedings of the IEEE/CVF Conference on Computer Vision and Pattern Recognition* (2020) pp. 8523 and 8532.
- (2) V. Guizilini, Ambrus, Pillai, Raventos, Gaidon. "3D Packing for Self-Supervised Monocular Depth Estimation." *2020 IEEE/CVF Conference on Computer Vision and Pattern Recognition (CVPR)* (2020) pp. 2482-2491.
- (3) S. Pillai, Ambrus, Gaidon. "Superdepth: Self-Supervised, Super-Resolved Monocular Depth Estimation." *2019 International Conference on Robotics and Automation (ICRA)* (2019) pp. 9250-9256.

Authors



Ryan Eustice



Wolfram Burgard



John Leonard



Ryan Wolcott



Robert Zidek



Gill Pratt

The JSAE Technological Development Award (70th JSAE Awards)
 2019 JSME Medal for New Technology
 Minister of Economy, Trade and Industry Award of the 55th JSPMI Prizes

Airless Coating Technology with Super-High Application Efficiency

Kazuki Tanaka*¹
 Yuki Murai*¹

Shinya Otake*¹
 Atsuo Nabeshima*¹

Shinji Tani*¹
 Wataru Murata*¹

1. Introduction

Vehicle paint systems consist of multiple layers and require a wide range of functionality, including anti-corrosion, weather resistance, and high-quality appearance. Of these layers, the primer, base, and clear topcoats of a paint system must have high surface quality (e.g., gloss) as well as high stylistic performance (e.g., color). To realize the required style with high productivity, vehicle paints are atomized before being sprayed onto the vehicle. Since this atomization process mainly uses air, yield (i.e., paint transfer efficiency) is adversely affected by scattering during spraying and rebounding of airborne paint from the object being painted. Since the quality of the paint system is also affected by scattered paint that contaminates the equipment, raising the transfer efficiency is a constant issue.

This issue was addressed by developing a technology capable of coating vehicles and other large objects using almost no air in the atomization process. The developed technology virtually eliminates paint scattering (**Fig. 1**) and raises the transfer efficiency by at least 30% compared to the conventional technology.

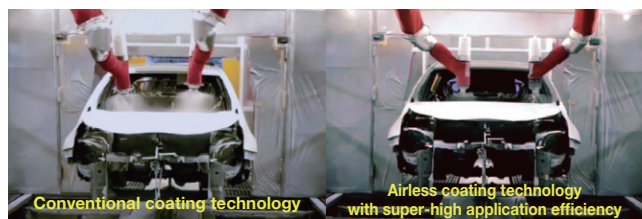


Fig. 1 Painting of Actual Vehicle on Mass Production Line

2. Details of Technology

This is an almost airless technology that atomizes the paint using electrostatic force alone before spraying the paint onto the vehicle.

The principle of electrostatic atomization is as follows. A charge is applied to the paint as it emerges from the nozzle, which extends the paint in a columnar fashion due to the electrostatic attractive force of the object being painted, which is in a grounded state. If a further charge

is applied, the electrostatic force exceeds the surface tension and viscosity of the paint, splitting and atomizing the paint columns. Since the paint is charged, it sprays onto and coats the object being painted following the electric field.

However, since this electrostatic atomization process is not particularly effective if the diameter of the extended columns is too large, the maximum volume of paint discharge from the nozzle is limited to 0.3 cc/minute. Therefore, because this volume is substantially lower than the 200 cc/minute discharge required for vehicle paints, this technology had not been adopted for the vehicle coating process.

This issue was addressed by carrying out the electrostatic atomization process through multiple serration-like grooves provided around the circumference of a rotating nozzle head on the painting equipment. By rotating the nozzle, electrostatically atomized paint is discharged simultaneously from the grooves and sprayed toward the object being painted, thereby ensuring the required discharge volume for the vehicle coating process (**Fig. 2**).

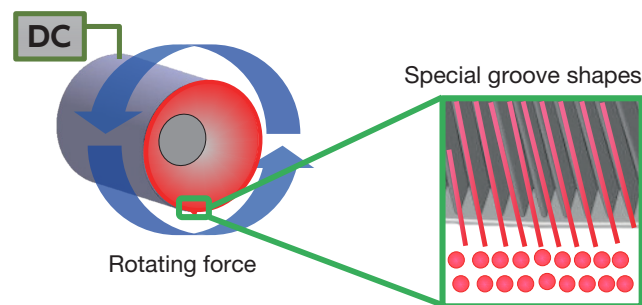


Fig. 2 Method of Ensuring High Paint Discharge Volume

In addition, a control to apply the charge to the paint was also developed, helping to realize stable coating quality even for vehicle and other objects with complex coating surfaces.

3. Conclusion

Since this technology helps to ensure that virtually all of the paint is sprayed onto the coating surface, it reduces the amount of paint used and allows the use of simpler equipment to recover uncoated paint.

Introduction of this technology also eliminates the need for large painting booths, which have conventionally been

*¹ Vehicle Production Engineering Development Div., Production Group

necessary to avoid paint contamination. This helps to reduce the size of the coating equipment (**Fig. 3**) and should enable substantial reductions in CO₂ emissions.

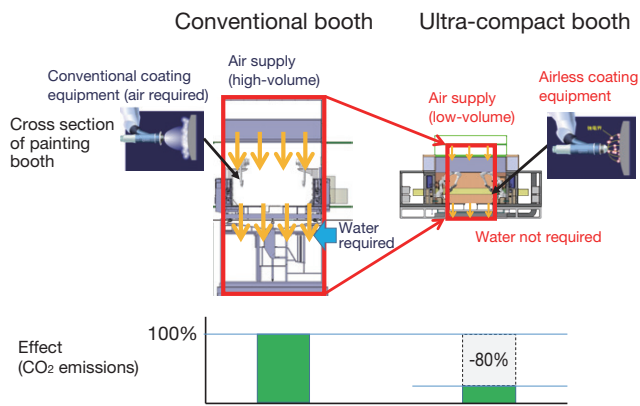


Fig. 3 Knock-On Effect of this Technology

Reference

- (1) K. Tanaka et al. "Super High Transfer Efficiency Application for Body Coating." *Project Report for the Japan Society of Mechanical Engineers* (2019) p .162.

The JSAE Technological Development Award (70th JSAE Awards)
Control Technology for Shock Absorber Damping Force at Very Low Speeds

Kazuyuki Mizuno*¹

Takeshi Yasui*²

Motoki Takagi*²

1. Introduction

As research into enhancing vehicle ride comfort progresses, major improvements have been achieved by adopting electronic control technologies to suppress large vehicle body motions. In contrast, this technology improves ride comfort on smooth national highways that generate small vertical body motions, which are difficult to address with conventional control technologies.

2. Configuration of Very Low Speed Shock Absorber Damping Force Control Valve

A different structure compared to conventional valves was considered to generate damping force at very low speeds. The following three design requirements were defined for this very low speed control valve. (1) The valve must have the capability to generate damping force at very low speeds and valve tuning must be possible. (2) The characteristics of the valve must ensure damping force saturation at speeds beyond the very low speed range. (3) The valve must act in both the extension and compression phases. The new valve was developed to realize the target characteristics by combining the damping force properties of a low speed valve and a conventional control valve (Fig. 1). Therefore, a linear structure was adopted in which a low speed valve is added inline with a conventional control valve (Fig. 2). The low speed valve consists of disc and leaf valves, with the leaf valve provided within the diameter of the disc valve. Unlike normal disc valves, a structure without a valve seat was adopted (non-seated valve). The adoption of a non-seated valve structure eliminated the major issues of abnormal noise caused by the oil hammer phenomenon and tapping noises when the valve contacts the seat. To generate damping force at very low speeds, the disc and non-seated valves were designed to achieve minimal clearance after assembly. Since the non-seated valve acts as the lid for the hydraulic fluid flow path, damping force is generated even at the extremely low hydraulic fluid flow rate that occurs at low speeds. In addition, the structure suppresses increases in the damping force beyond the low-speed range by instantaneously pushing on the non-seated valve. Since the non-seated valve is structured without a valve seat, it

opens in both the upward and downward directions, thereby functioning in both the extension and compression phases.

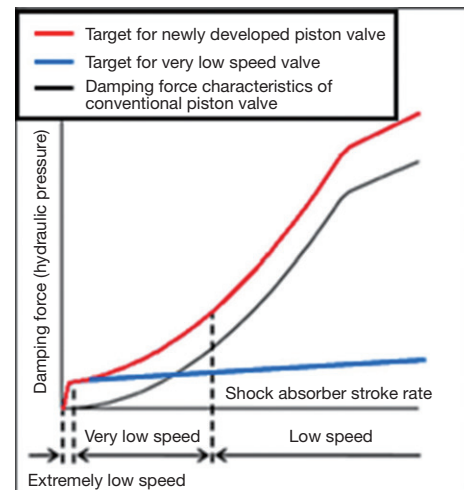


Fig. 1 Outline of Target Characteristics of Low Speed Valve

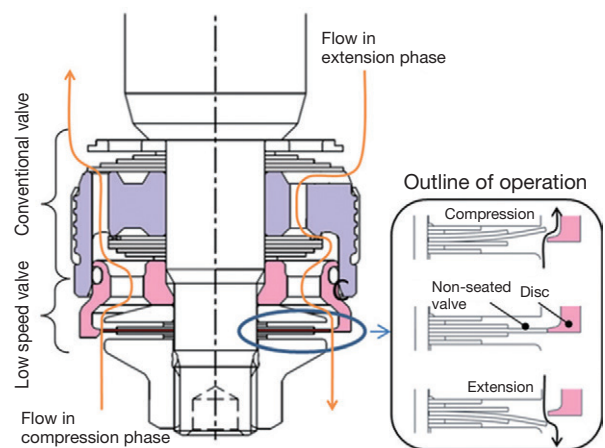


Fig. 2 Structure and Operational Principle of Newly Developed Valve

3. Importance and Effect of Damping at Low Speeds

The relationship between stroke rate and the proportion of driving times was analyzed to identify the ranges in which the shock absorbers are in action. As shown in Fig. 3, the shock absorbers operate for longer periods at lower stroke rates on smooth roads. At the same time, low stroke rate regions account for a higher proportion of

*¹ Chassis Development Div., Vehicle Development Center
 *² KYB Corporation

driving times. For these reasons, the damping effect at very low speeds should not be limited simply to when the vehicle is being driven on smooth roads.

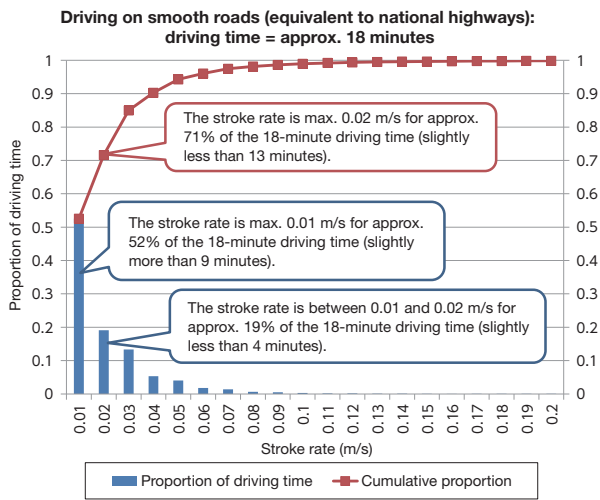


Fig. 3 Proportion of Driving Times per Stroke Rate on Roads Equivalent to National Highways

Even if the effect of damping at very low speeds is clear in subjective evaluations, it has been difficult to express this effect clearly in quantitative terms using conventional vehicle ride comfort evaluation methods such as the power spectral density (PSD) of sprung mass G due to the small differences involved. Therefore, to simplify vehicle motion and clearly define these differences, a four-wheel shaker was used to apply in-phase rectangular waveform vibration to each of the four wheels. **Fig. 4** shows an outline of the four-wheel shaker test. After carrying out subjective evaluations to identify the effect of the developed valves that apply damping at very low speeds, the vibration generated by driving over a bump was compared between control valves with standard specifications and the developed valves with a small (2 mm) rectangular waveform vibration input (**Fig. 5**). The tests identified a clear difference in the final convergence of sprung mass vibration, as shown in the circled areas of the graphs (these areas are likely due to vibration: damping factor $\zeta > 1$).

In addition, to confirm whether such small differences in displacement (1 mm or less) are actually perceptible, fourteen test subjects were asked to sit inside a vehicle on a four-wheel shaker. Verification tests were carried out in three modes of sprung mass motion (bounce, roll, and pitch), which should be perceptible to humans (**Fig. 6**). The horizontal axis shows the amplitude of the sprung mass and the vertical axis shows the frequency of vibration application. This figure plots the vibration felt by the test subjects in each mode. The test subjects began to perceive motion at around a sprung mass velocity of $v_p = 0.001$ m/s, and all test subjects perceived extremely small and low speed vehicle motion at an amplitude of 0.2 mm and a sprung mass velocity of $v_p = 0.002$ m/s.

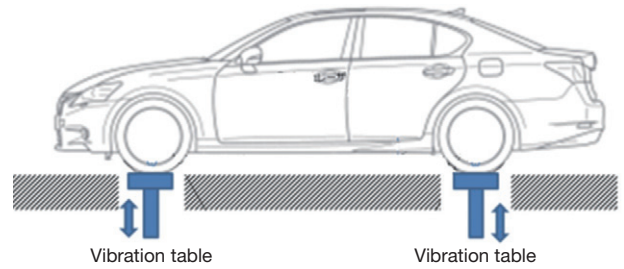


Fig. 4 Four-Wheel Vibration Generator (Shaker)

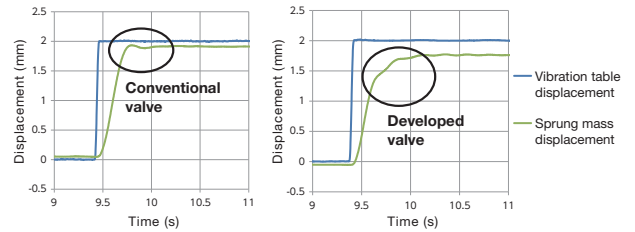


Fig. 5 Comparison of Vibration Application with Small Bump Input

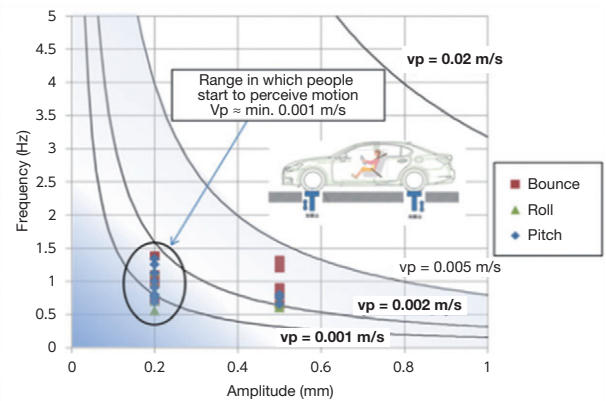


Fig. 6 Sprung Mass Motion and Human Sensitivity

4. Conclusion

It was confirmed that this technology enhanced ride comfort on smooth roads by controlling the convergence of sprung mass vibration with a very low amplitude. In the future, it is planned to combine this technology with suspension electronic control technology to help further enhance vehicle ride comfort on both smooth and rough roads.

Note: this article is based on the following published technical paper.

K. Mizuno et al. "Control Technology for Damping Force in the Range of Very Low Speed of Shock Absorber." *JSAE Journal* Vol. 74 No. 10 (2020) pp. 6-7.

A Study of Cornering Drag Caused by Camber Angle and its Effects on Vehicle Dynamics

Masaki Yamamoto*¹

Kozo Oyama*¹

1. Introduction

Reducing energy consumption while maintaining dynamic performance is a key issue requiring further development in the era of environmentally friendly vehicles. One important topic of development is how to most efficiently generate the tire forces required for cornering. The paper summarized in this article identified the mechanism by which the camber angle generates cornering drag, as well as the magnitude of that drag. In addition, considering these characteristics, the paper also examined methods of distributing lateral forces to reduce cornering drag and setting a wheel alignment that balances the necessary generation of lateral force with drag reduction.

2. Examination of Tire Forces based on Simplified Model

A linear brush model was used to examine the tire forces when the tires are moving in a straight direction with camber angle γ . Under these conditions, the contact patch deforms as shown in **Fig. 1** (where, a : contact length, b : contact width, and R : rolling radius). The lateral deformation of the contact patch δ_y forms an arc with the turning radius during free rolling of $\rho_f \approx R/|\gamma|$. This deformation generated lateral force (camber thrust) F_y .

$$F_y = -Q_y \gamma \quad (1)$$

$$Q_y = \frac{e_\alpha}{R} K_y \quad (2)$$

$$e_\alpha = \frac{a}{6} \quad (3)$$

where, Q_y is the camber stiffness, K_y is the cornering power (CP), and e_α is the pneumatic trail. In addition, since a tire with a camber angle has a different diameter in the width direction, longitudinal deformation of the contact patch δ_x is generated, which creates moment M_z .

$$M_z = -Q_m \gamma \quad (4)$$

$$Q_m = \frac{K_x b^2}{12R} \quad (5)$$

where, Q_m is the camber moment coefficient and K_x is the driving stiffness. Since lateral force and moment are generated simultaneously, the following equations can be formed by converting these equations as formal camber trail e_γ .

$$e_\gamma = \frac{Q_m}{Q_y} = \frac{b^2 K_x}{2a K_y} \quad (6)$$

$$M_z = -e_\gamma Q_y \gamma \quad (7)$$

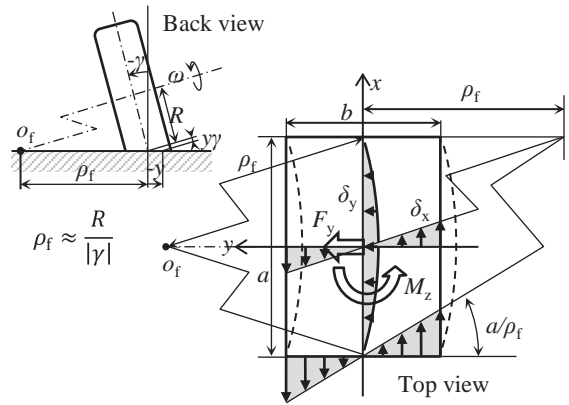


Fig. 1 Deformation of Contact Patch due to Camber Angle

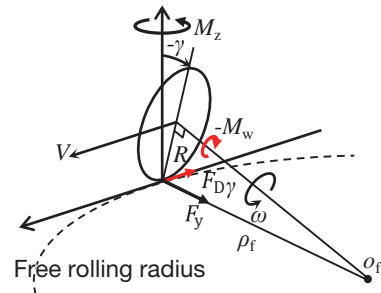


Fig. 2 Tire Forces due to Camber Angle

3. Cornering Drag Caused by Camber Angle

As shown in **Fig. 2**, the wheel surface components $M_w = M_z \sin \gamma$ of the camber moment M_z forms wheel torque that suppresses wheel rotation. Therefore, the force calculated by dividing this torque by the rolling radius is thought to form the drag caused by the camber angle.

*¹ Chassis Development Div., Vehicle Development Center

$$F_{D\gamma} = -\frac{M_w}{R} = -\frac{M_z \sin\gamma}{R} \quad (8)$$

$$\text{When } \gamma \ll 1, F_{D\gamma} \approx \frac{e_\gamma Q_y}{R} \gamma^2 = \frac{e_\gamma}{R} \frac{1}{Q_y} F_y^2 \quad (9)$$

The following dimensionless equations can be formed by dividing by load F_z .

$$\frac{F_{D\gamma}}{F_z} = \frac{e_\gamma}{R} \frac{1}{B_y} \left(\frac{F_y}{F_z}\right)^2 \quad (10)$$

$$B_y = \frac{Q_y}{F_z} \quad (11)$$

In contrast, the drag caused by slip angle α is as follows.

$$F_{D\alpha} = -F_y \sin\alpha \quad (12)$$

$$\text{When } \alpha \ll 1, F_{D\alpha} \approx K_y \alpha^2 = \frac{1}{K_y} F_y^2 \quad (13)$$

$$\frac{F_{D\alpha}}{F_z} = \frac{1}{C_y} \left(\frac{F_y}{F_z}\right)^2 \quad (14)$$

$$C_y = \frac{K_y}{F_z} \quad (15)$$

4. Verification by Measurement of Tire Forces

The tire forces generated in response to the camber angle and slip angle were measured using a flat belt tire tester. **Fig. 3** shows the analysis results for the magnitude of drag with respect to the generated lateral force. The forces calculated using Equations (8) and (12) are also superimposed onto these figures. It was confirmed that the drag generated by the camber angle and slip angle matches the force calculated geometrically from the moment and lateral force, that the drag due to the camber angle is larger than that due to the slip angle, and that this trend becomes more prominent as the load decreases.

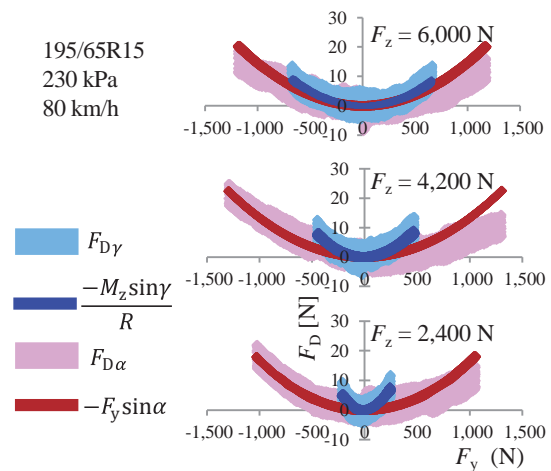


Fig. 3 Results of Tire Force Measurement

5. Method of Allocating Lateral Force to Reduce Cornering Drag

This study examined how to use camber thrust to reduce the cornering drag. The following equation expresses the drag generated during cornering while a slip angle and camber angle are applied simultaneously.

$$F_D = -(F_{y\alpha} + F_{y\gamma})\alpha - \frac{(-e_\alpha F_{y\alpha} + e_\gamma F_{y\gamma})}{R} \gamma = \left[1 - k + pk^2 - k(1-k)\frac{p}{q} \right] F_{D\alpha} \quad (16)$$

$k = \frac{F_{y\gamma}}{F_y}$: Lateral force allocation ratio of camber thrust

$p = \frac{F_{D\gamma}}{F_{D\alpha}} = \frac{e_\gamma K_y}{R Q_y}$: Cornering drag ratio

$q = \frac{e_\gamma}{e_\alpha} = 3 \frac{b^2 K_x}{a^2 K_y}$: Trail ratio

The parabola in **Fig. 4** shows the relationship between the lateral force allocation ratio of camber thrust k and the cornering drag. Compared to when a vehicle corners using lateral force generated by the slip angle alone ($k = 0$), the drag can be lowered by allocating some of that lateral force from the camber thrust. In this case, an extremely small $k = k_{Dmin}$ value is applied. However, if the allocation ratio of camber thrust is increased further, the drag increases. When only camber thrust is allocated ($k = 1$), the drag increases to p times (normally $p > 1$) of the value when cornering is carried out using the slip angle alone.

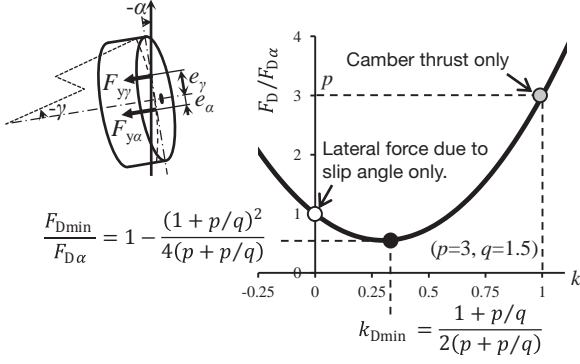


Fig. 4 Lateral Force Allocation Ratio and Drag during Cornering

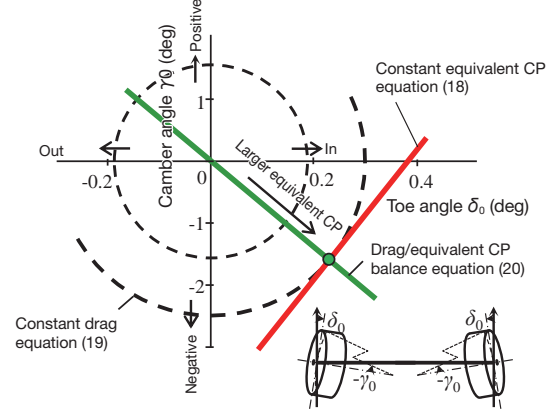


Fig. 5 Relationship between Running Resistance and Equivalent CP due to Wheel Alignment

6. Efficient Wheel Alignment Setting Method

This study also considered the method using the wheel alignment to balance the generation of the necessary equivalent lateral force with drag reduction. The tire CP has non-linear characteristics with respect to the load. The extent of these non-linear characteristics can be expressed by the load sensitivity λ_c of the normalized CP divided by the load.

$$\lambda_c = -\frac{\Delta C_y / C_y}{\Delta F_z / F_z} \quad (17)$$

The conditions for generating a constant equivalent CP⁽¹⁾ using the initial toe angle δ_0 and the initial camber angle γ_0 are as follows.

$$B_y \gamma_0 - C_y (1 - \lambda_c) \delta_0 = \text{constant} \quad (18)$$

In contrast, the running resistance generated by setting δ_0 and γ_0 is as follows.

$$\frac{F_D}{F_z} = C_y \delta_0^2 + \frac{e_y}{R} B_y \gamma_0^2 \quad (19)$$

The conditions for minimizing the running resistance with respect to the equivalent CP are as follows.

$$\gamma_0 = -\frac{R}{e_y} \frac{1}{(1 - \lambda_c)} \delta_0 \quad (20)$$

Fig. 5 shows the relationship between equations (18) to (20) with δ_0 and γ_0 plotted on two axes. The green line expresses Equation (20). A wheel alignment that balances the necessary equivalent CP with the running resistance can be set along this line.

7. Conclusions

This study identified that the drag generated by the camber angle is caused by moment. It also defined a method of using the camber thrust to reduce cornering drag and an efficient method of setting the wheel alignment.

Reference

- (1) M. Yamamoto. "Effect of Wheel Alignment on Handling and Stability." *JSAE Journal* Vol. 54 No. 11 (2000) pp. 10-15.

Development of New Four-Wheel Drive Control System for Front-Wheel Drive Based Vehicles

Ryohei Yuasa*1

Ryota Horie*2

Shunro Fukada*3

1. Introduction

The number of highly fuel-efficient vehicles, especially front-wheel drive (FWD) vehicles, is rising as vehicle fuel economy requirements grow increasingly stringent. Similarly increasingly stringent requirements also apply to four-wheel drive (4WD) models based on FWD vehicles. In addition, although customers are also demanding even better driving performance, this tends to have a generally conflicting relationship with fuel efficiency (Fig. 1). Therefore, a new 4WD system was developed with the aim of achieving a high level of both driving performance and fuel efficiency.

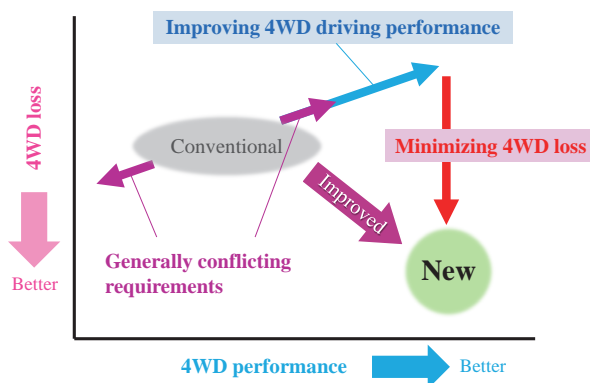


Fig. 1 New 4WD System Development Concept

2. System Outline

As shown in Fig. 2, the new 4WD system consists of a disconnection system that contributes to fuel efficiency, and twin coupling systems that contribute to driving performance.

2.1 Disconnection system

The disconnection system is provided with a ratchet-shift type dog clutch in the transfer and rear units. When the dog clutch is disengaged, the system is disconnected (i.e., two-wheel drive (2WD) mode is engaged). Since rotation of the propeller shaft is completely stopped, this

mode can potentially realize the same fuel efficiency as an FWD vehicle. This system functions to realize both driving performance and fuel efficiency in a 4WD vehicle by automatically switching between the disconnected (2WD) and connected (4WD) states in accordance with the road surface and driver intention. Fig. 3 illustrates the operation of the system. The system controls were developed from the following standpoints.

- Fuel efficiency: during steady-state or low-load driving on high-traction roads, the system should contribute to fuel efficiency by remaining in the disconnected state (2WD) as far as possible.
- Driving performance: when the driver requires high driving performance on a high-traction road, the system should connect (4WD) and delivery the required driving performance by a control that distributes driving force to the left and right wheels.
- Stability: on snowy and other low-traction roads, the system should remain connected (4WD) at all times to ensure the high driving performance of a 4WD vehicle.

In addition, since the switching judgment is carried out automatically, the control was constructed with maximum consideration to noise and shock during switching.

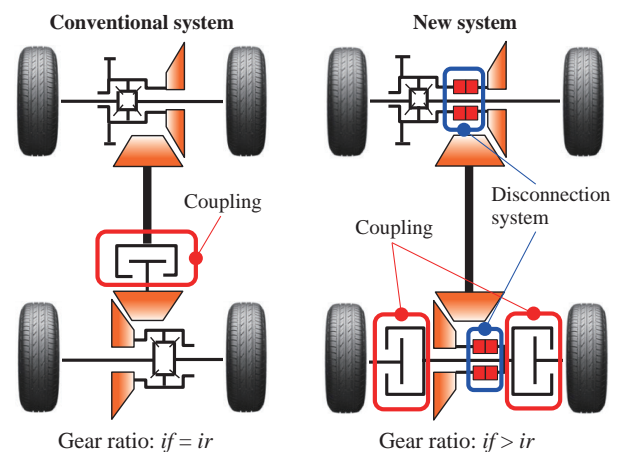


Fig. 2 Configuration of New 4WD System

*1 Lexus Powertrain Performance Development Div., Lexus International Co.

*2 Environment Affairs and Engineering Management Div.

*3 Electric Powertrain Control Function Development Div., Powertrain Company

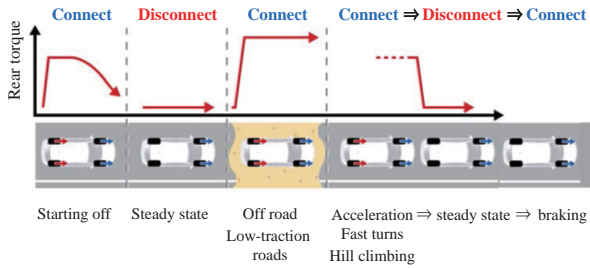


Fig. 3 Disconnection Control Concept

2.2 Twin coupling system

To combine cornering performance that matches driver intention with excellent off-road driving performance, a twin coupling system was adopted that eliminates the rear unit differential case and enables continuous distribution of driving force to the left and right rear wheels by locating couplings on the left and right sides.

As well as conventional 4WD performance on snow and the like, a control that distributes driving force to the left and right wheels was developed to enhance on-road performance, while also enabling significantly improved off-road performance on dirt roads, mud, and in driving scenarios where the tires lift off the ground by utilizing the capability of the system to transmit torque robustly to the road surface.

Fig. 4 shows the control architecture. The distribution of driving force to the front and rear wheels and to the left and right wheels is calculated independently. The same performance as conventional 4WD systems was ensured by adopting the same front and rear driving force distribution concept. In addition, the system also applies direct yaw moment control (DYC) by driving force distribution to the left and right wheels. Ultimately, the system is configured to prioritize driving force in consideration of the friction circles of the left and right wheels. For example, the system prioritizes yaw moment when the rear-wheel driving force for generating yaw moment is larger than the rear-wheel torque generated by the required front and rear driving force distribution. Fig. 5 shows an example of improved on-road vehicle performance.

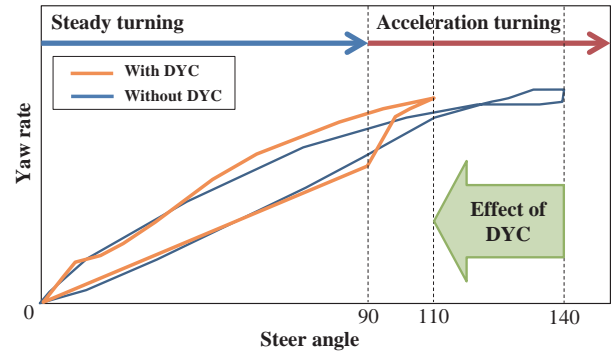


Fig. 5 Results of Driving Force Distribution Control to Left and Right Wheels

3. Conclusion

A new 4WD system was developed with a disconnection system and twin coupling system with the aim of achieving a high level of both driving performance and fuel efficiency. The system is equipped with a disconnection control that connects and disconnects the dog clutch based on various items of information, and a control that distributes driving force to the left and right wheels to enhance driving performance both on- and off-road.

Original Paper

R. Yuasa et al. "Development of the Control System of the New 4WD System for the FF Based Vehicle." *Proceedings of the JSAE Annual Congress (Spring)* (2019).

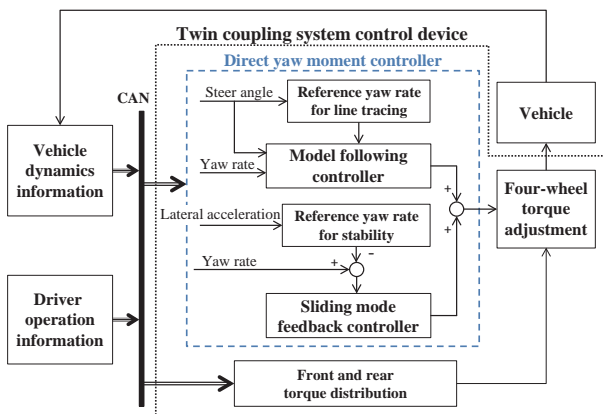


Fig. 4 Structure of Driving Force Distribution Control to Left and Right Wheels

Development of Low Fuel Consumption 0W-8 Engine Oil

Yuta Uematsu*¹
Shintaro Kusahara*³

Kazuo Yamamori*¹
Yu Misaki*³

Itsuki Miyata*²

1. Introduction

Increasing the thermal efficiency of engines will play an important role in combating global warming. Improving the properties of engine oil is one means of substantially reducing engine friction and churning losses, and is an effective way of improving the fuel economy of hybrid electric vehicles (HEVs) and other electrified vehicles. However, although reducing the viscosity of engine oil can help to lower churning loss, the resulting thinner oil films may adversely affect reliability by increasing wear. The newly developed 0W-8 engine oil improves fuel economy by 0.7% compared to conventional 0W-16 oil, while also ensuring reliability, and is the first in the world to achieve the JASO GLV-1 industry standard.

2. Details of Technology

Simply reducing viscosity to 0W-8 increased the contact between sliding surfaces compared to 0W-16 oil, resulting in no fuel economy improvements in actual engine tests. This issue was addressed by developing the following additive technologies (1) and (2), resulting in a 0W-8 engine oil capable of realizing both fuel economy and reliability.

- (1) An oil film former capable of reducing contact between sliding surfaces at lower viscosity
- (2) A detergent that accelerates the formation of a low-friction reactive coating on sliding surfaces

2.1 Development of oil film former

To reduce contact between sliding surfaces, it is important to form a thick oil film with respect to the load. For this reason, an oil film former was developed that increases the thickness of oil films between parts without affecting the viscosity characteristics of the oil (Fig. 1). It was confirmed that this oil film former increases oil film thicknesses by adsorption into the surfaces of the parts (Fig. 2).

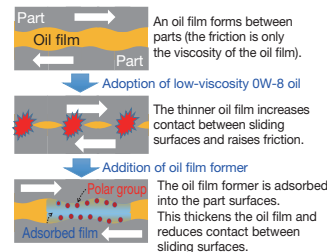


Fig. 1 Oil Film Formation Mechanism

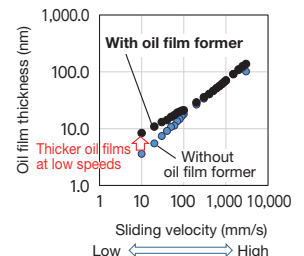


Fig. 2 Measured Results of Oil Film Thickness

2.2 Development of detergent

The formation of molybdenum disulfide (MoS₂) as a reaction byproduct of molybdenum dithiocarbamate (MoDTC) plays an important role in reducing sliding surface friction. Consequently, taking advantage of the known interaction between boron-containing components and MoDTC, a new boron-containing detergent was developed. This detergent generates large amounts of MoS₂ on sliding surfaces, while achieving lower friction than conventional carbonate-containing detergents (Figs. 3 and 4).

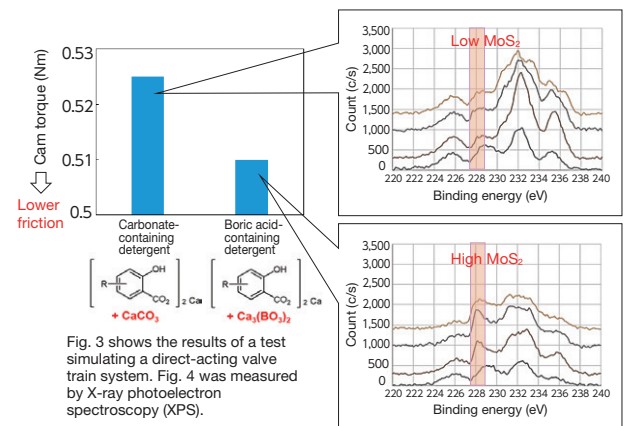


Fig. 3 Results of Part Sliding Test

Fig. 4 Sliding Surface Analysis Results

3. Conclusion

The 0W-8 engine oil developed using the technologies described above improves fuel economy while also ensuring reliability. As a result, this oil helps to achieve substantial reductions in CO₂ emissions. The authors would like to express their sincere gratitude to everyone involved in this development.

*¹ Electrification & Environment Material Engineering Div., Advanced R&D and Engineering Company
*² Powertrain Function Development Div, Powertrain Company
*³ ENEOS Corporation

References

- (1) Y. Uematsu et al. "Development of Low Fuel Consumption Engine Oil 0W-8." *Proceedings of the JSAE Annual Congress (Autumn)* No. 20196233 (2019).
- (2) K. Yamamori et al. "Development of Ultra Low Viscosity 0W-8 Engine Oil." *SAE WCX* No. 2020-01-1425 (2020).

Lightweight and Highly Rigid Body-in-White Design Method Considering Inertial and Vibration Characteristics

Koichi Daigaku*¹

Tetsuro Fukuhara*²

1. Introduction

The importance of a lightweight and highly rigid vehicle structure (referred to in this article as the “body in white” (BIW)) probably goes without saying.

The BIW can also be regarded as the heaviest single component in a vehicle, accounting for approximately one-quarter of the whole vehicle weight. It is also the only component present in all parts of the vehicle. Consequently, the weight distribution of the BIW is an extremely important factor affecting the inertial characteristics of the whole vehicle.

Considering these points, although it is impossible to uniquely define what makes a good BIW, in the same way as the best cuisine or music also cannot be defined, there are many vehicles around the world with excellent dynamic performance, some of which also have a high-performance BIW.

Therefore, since the best BIW cannot be specifically defined and quantified, the feasibility of a method capable of designing a BIW that approximates the best was examined. This article describes an investigation into vehicle A, using inertial characteristics and natural frequencies as substitute characteristics for several rigidity parameters. Subsequently, a new computer aided engineering (CAE)-based design method was applied to completely different vehicle B. Vehicle C was then designed to resemble vehicle A by realizing the characteristics described above without changing the weight. The sequence of this design study is described below.

2. Comparison of Natural Frequencies and Packaging

First, natural frequency analysis was applied to vehicles A and B (Fig. 1).

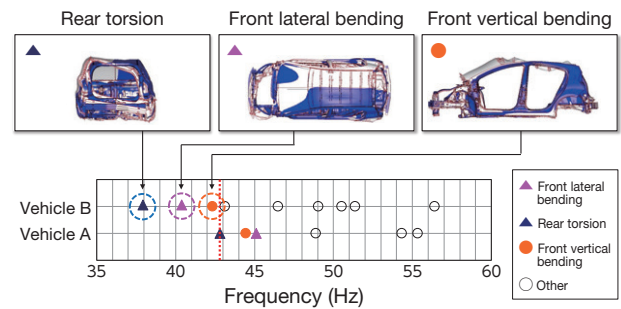


Fig. 1 Comparison of Natural Vibration Modes and Natural Frequency Arrangements

If these natural vibration modes are regarded as the degree of rigidity of each BIW, vehicle B has three less rigid characteristics than the least rigid characteristic of vehicle A (rear torsion frequency of 42.8 Hz). In sequence from the lowest, these natural vibration modes are a rear torsion frequency of 37.9 Hz, a front lateral bending frequency of 40.4 Hz, and a front vertical bending frequency of 42.4 Hz.

In addition, this study also considered the requirements for BIW rigidity in dynamic performance. When driving through a corner, it has been reported that the key aspect of BIW rigidity in planar motion is the front body lateral bending rigidity at the entrance to the corner, and the rear body torsional rigidity at the exit.

Of the three natural frequencies of vehicle B described above, two of the natural vibration modes correspond to these rigidity characteristics. Therefore, improving at least these two natural vibration modes should have some kind of positive effect on dynamic performance.

Consequently, this study aimed to raise these three vehicle B natural frequencies in vehicle C to above the level of the lowest natural frequency of vehicle A without changing the weight.

Next, the packaging was compared. After compensating for the differences in vehicle size, the center of gravity positions of vehicles A and B were superimposed onto a side view of vehicle B. The difference between vehicles A and B was found to be 26.4 mm in the longitudinal direction and 14.2 mm in the vertical direction (Fig. 2).

*¹ Vehicle Development Center

*² Advanced Project Promotion Div., Advanced R&D and Engineering Company

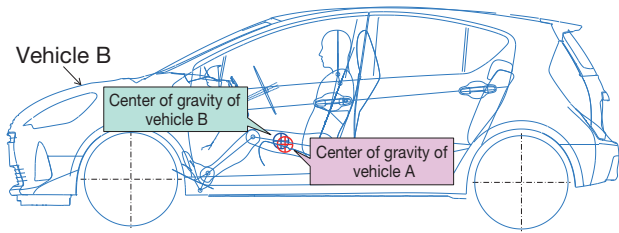


Fig. 2 Comparison of Center of Gravity Position

When the same front-seat occupant (driver) of vehicle A was superimposed on the figure, the driver was located 66.1 mm behind and 8.9 mm below the position of the driver of vehicle B (Fig. 3).

Since the positional relationship of the driver to the principal axis of inertia of the vehicle has a major impact on dynamic performance as perceived by the driver, the driver position of vehicle B was adjusted to that of vehicle A.

By doing so, the center of gravity changed by 9.7 mm to the rear and 1.3 mm downward. After compensating for this change, the final difference between the center of gravity positions of vehicles A and B was as follows: the center of gravity position of vehicle A was 16.7 mm behind and 12.9 mm below that of vehicle B.

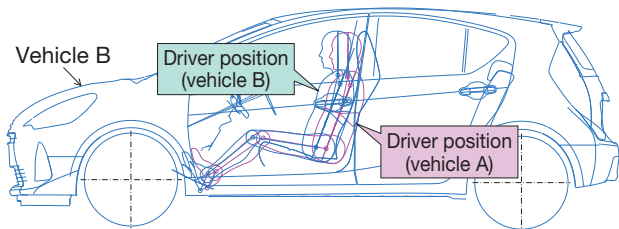


Fig. 3 Comparison of Driver Position

This study then aimed to realize these longitudinal and vertical differences in the center of gravity position in vehicle C by controlling the weight distribution of the BIW to resemble vehicle A (Section 4).

3. Natural Frequency Design

The following countermeasures (1) to (5) were applied: (1) change thicknesses, (2) change materials, (3) add parts, (4) remove parts, and (5) increase the rigidity of joints.

The study aimed to increase the three natural frequencies described above by adopting these countermeasures. The sections below describe the details of this approach.

3.1 Front lateral bending

Since this natural frequency is highly sensitive to weight reduction at the front end of the vehicle, the study started by reducing the weight of the colored part

in Fig. 4 below. Aluminum with a closed sectional structure was adopted in place of the open steel sectional structure used in vehicle B. This reduced the weight by 2.3 kg while also increasing rigidity. As shown in the lower half of the figure, this countermeasure substantially improved only the front lateral bending characteristic.

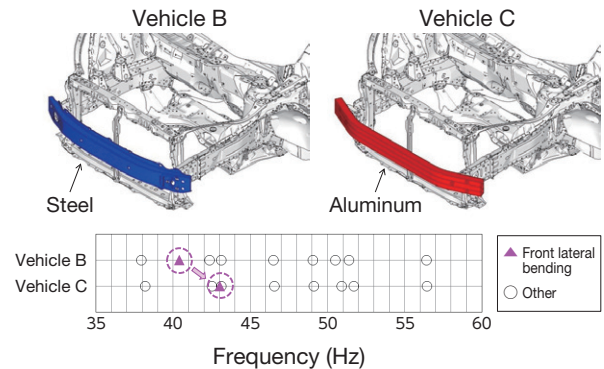


Fig. 4 Structural Comparison of BIW Front End

Next, the structure of the area shown in Fig. 5 was studied. Since this area is also highly sensitive to weight reduction, the lower half of the front portion was removed and plastic adopted for the remaining parts. These countermeasures reduced the weight of this area by 4.6 kg.

Two proposed structures, structure (a) and structure (b) (details omitted), were considered. When the natural frequency arrangement of each structure was compared, it was found that structure (b) realized a greater increase in the front lateral bending natural frequency.

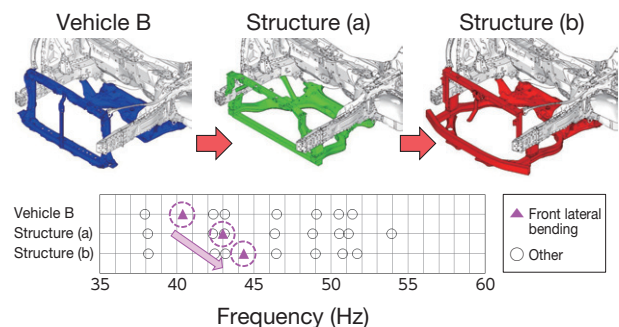


Fig. 5 Comparison of BIW Front Structure

3.2 Rear torsion

Increasing component thickness was determined to be the most effective way of improving this characteristic. By doing so, the weight of the BIW was deliberately increased by 6.8 kg.

In this process, the thickness was increased from the bottom in consideration of changes in the inertial characteristics and to ensure a minimum upward shift in the center of gravity. The corresponding changes in the natural frequency were confirmed (Fig. 6). It was found that structure (c) realized the same rear torsion as vehicle A.

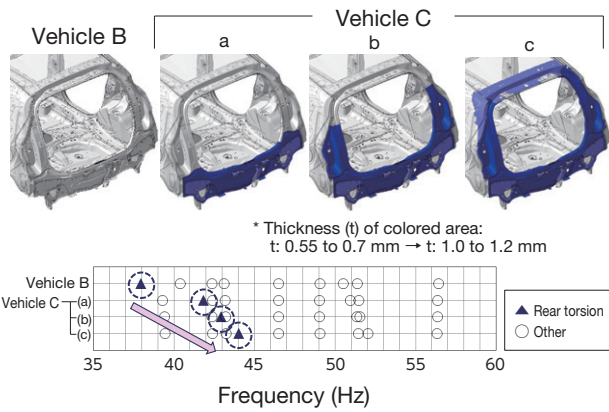


Fig. 6 Comparison of BIW Rear Structure

3.3 Front vertical bending

It was found that this natural vibration mode has a high sensitivity to the hardness of the adhesive used between the BIW and front windshield glass (Fig. 7). The hardness was increased while confirming the effects on other performance aspects.

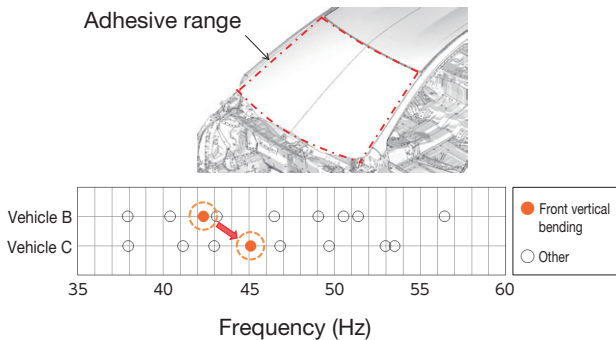


Fig. 7 Structure of Front Windshield Glass

3.4 Results of natural frequency design

As a result of these countermeasures, all three of the vehicle B natural frequencies were raised above the lowest natural frequency of vehicle A without increasing weight (Fig. 8).

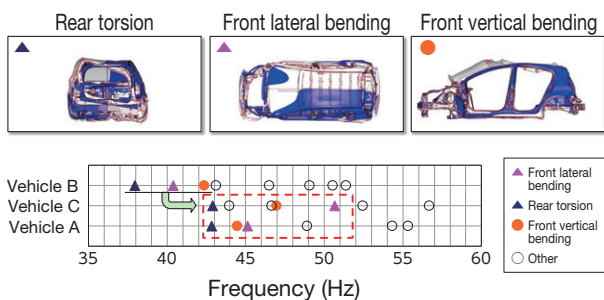


Fig. 8 Comparison of Natural Vibration Modes and Natural Frequency Arrangements Including Vehicle C

4. Inertial Characteristics Design

First, the material of the roof panel located high above the center of gravity was changed to plastic, which reduced the weight by 6 kg. At the same time, the thickness of center portion of the BIW, which is mostly located below the center of gravity, was increased (Fig. 9). This increased the weight by 4.1 kg while shifting the center of gravity downward.

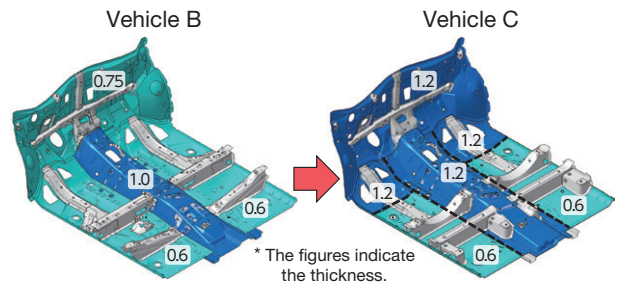


Fig. 9 Comparison of BIW Center Structure

Next, the material of the hood panel at the front of the vehicle was changed to plastic, which reduced the weight by 5 kg. In addition, to increase the rear torsional natural frequency, the weight of the rear of the vehicle was increased by 6.8 kg. This also had the effect of shifting the center of gravity to the rear.

These countermeasures shifted the center of gravity 11.1 mm to the rear and 4.7 mm in the downward direction (Fig. 10), achieving the targeted changes in direction with minimal changes in weight.

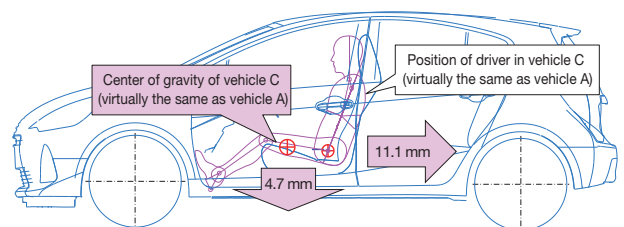


Fig. 10 Changes in Center of Gravity and Driver Position

5. Measurements and Driving Evaluation

5.1 Vibration characteristics

Fig. 11 shows the measured results for the vibration application point response.

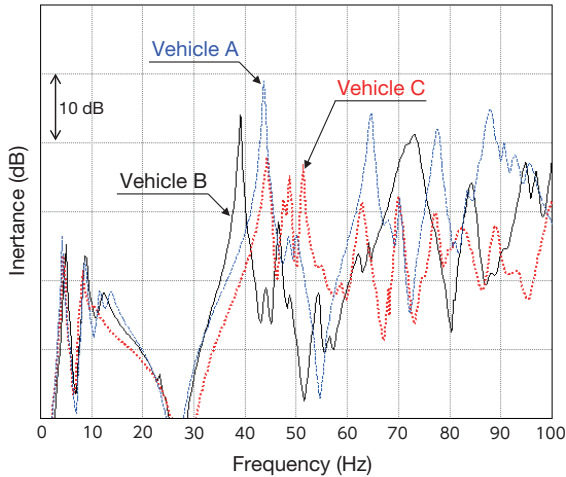


Fig. 11 Vibration Application Point Response Graph

The lowest natural frequency of vehicle C was raised to 44.3 Hz from 39.0 Hz in vehicle B. This also exceeds the lowest natural frequency of vehicle A (43.8 Hz).

5.2 Weight and inertial characteristics

Actual measurements also showed virtually no change in weight. The center of gravity shifted 10 mm to the rear and 12 mm in the downward direction of the vehicle, which is in line with the targeted change.

5.3 Driving evaluation

Fig. 12 shows the results of a subjective evaluation. The evaluation showed that the dynamic performance of vehicle C improved from the level of vehicle B to close to that of vehicle A.

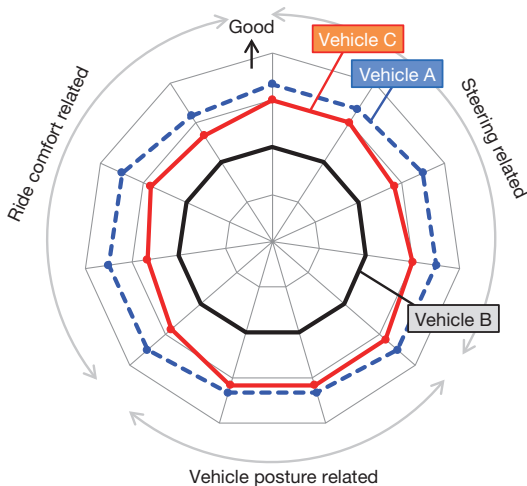


Fig. 12 Subjective Evaluation Graph

6. Conclusion

This study regarded the BIW as a single component and focused on its inertial and vibration characteristics. Then, a CAE-based design approach was applied to the BIW as a whole to realize a lightweight and highly rigid BIW design method considering inertial and vibration characteristics.

Original Paper

K. Daigaku et al. "Lightweight and High Stiffness BIW Design Method Considering Inertia Specification and Natural Frequency." *Proceedings of the JSAE Annual Congress (Autumn)* (2019).

Back Number Index



Vol. 57 No. 2 (2011)
Special Feature:
Next-Generation Electric Storage
and its Applications



Vol. 58 No. 1 (2012)
Special Feature:
Japanese Originality



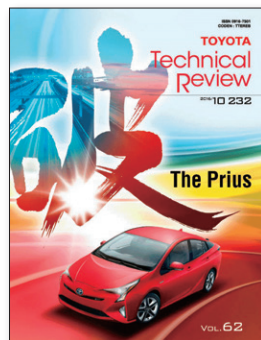
Vol. 59 (2013)
Special Feature:
Production Engineering



Vol. 60 (2014)
Special Feature: Powertrain



Vol. 61 (2015)
Special Feature 1: The Mirai FCV
Special Feature 2: ITS and
Advanced Driving Support Systems



Vol. 62 (2016)
Special Feature: The Prius



Vol. 63 (2017)
Challenging and Innovative
Technological Development



Vol. 64 (2018)
Special Feature:
TNGA Powertrains



Vol. 65 (2019)
Special Feature:
The Battery Technologies of the Future
- Fuel Cells and Storage Batteries



Vol. 66 (2021)
Special Feature:
Contrasts in Value and Manufacturing
-The Second-Generation Mirai and
New GR Yaris-

Back number (printed version) price:
¥2,800 (excluding tax)

Distributor: Ohmsha, Ltd.

Tel: 81-3-3233-0641

https://www.ohmsha.co.jp/magazine/partners_magazine.htm

Thank you for reading the *Toyota Technical Review* (TTR).

We are continuing to face incredible difficulties in our daily lives as the sudden outbreak of the novel coronavirus COVID-19 shows no sign of coming to an end.

Volume 66 of the TTR, which was published at the end of 2020, was originally intended to include a special feature about the mobility solutions developed for the Olympic and Paralympic Games Tokyo 2020. However, the pandemic forced the postponement of the Games and prompted a change in the content of the publication.

With the Games being held a year later than planned, we are delighted to finally bring you our special feature on mobility solutions in volume 67.

Toyota developed approximately ten mobility solutions and robots for the Games to help transport people around the Athletes' Village and perform other functions.

We particularly believe that mobility goes beyond cars. Mobility is about overcoming challenges and making dreams come true, something that might be possible if we can realize mobility for everyone in society. Therefore, rather than being a sponsor responsible simply for providing vehicles, as has been the case in previous games, we actively took on the challenge of providing comprehensive mobility solutions for the Games as the first ever worldwide mobility partner.

Although this edition of the TTR features detailed descriptions of technical elements in the planning and development of each mobility solution, the core aspects of these developments incorporated concepts focusing on sustainability, mobility for all, and the Toyota Production System (TPS).

I hope that this TTR will provide valuable and interesting insights into how these concepts were realized in the results of these development projects.

Finally, I'd like to extend my sincere gratitude to everyone who helped edit and publish this edition of the TTR during the incredibly busy period of the coronavirus pandemic.

I hope to continue creating useful, informative, and interesting content for your reading pleasure.

(Publisher: Kohigashi)

TOYOTA Technical Review Vol. 67

©2022 TOYOTA MOTOR CORPORATION
(All rights reserved)

Publisher's Office	R&D and Engineering Management Div. TOYOTA MOTOR CORPORATION 1 Toyota-cho, Toyota, Aichi, 471-8572 Japan 81-565-28-2121 (Operator)
Publisher	Tetsuya Kohigashi
Planning	Jun Toyama
Editor	Shingo Kato Technical Administration Dept., Toyota Office TOYOTA ENTERPRISE INC.
Printer	Shintec Hozumi Co., Ltd. 5-3-1 Neuramachi, Miyoshi, Aichi, 470-0217 Japan
Published	March 8, 2022



TOYOTA
Technical
Review

Vol.67

2022/ **3** 237